الجمهورية الجزائرية الديمقراطية الشعبية
People's Democratic Republic OF Algeria
وزارة التعليم العالي و البحث العلمي
MINISTRY OF HIGHER EDUCATION AND SCIENTIFIC RESEARCH
جامعة الشهيد الشيخ العربي التبسي-تبسة
Echahid Cheikh Larbi Tebessi University-Tebessa
كلية العلوم و التكنولوجيا

Department of Electrical Engineering

A Master's Thesis

presented to obtain the diploma of Academic Master in Electrical Engineering

Discipline: Science and Technology

Specialty: Industrial electrical engineering

Title

COMPARATIVE STUDY OF CONTROL STRATEGIES FOR PWM RECTIFIER BASED ON PI CONTROLLER APPLIED TO BATTERY CHARGING

Presented and defended by:

- **Dris Idris**

Under jury members:

– **DJEDDI Abdelghani**	**Presedent**	**MCA**
– **BOUKADOUM Aziz**	**Supervisor**	**MCA**
– **MOUSSA Mohamed Amine**	**Examinator**	**MCB**

2023/2024


بسم الله الرحمن الرحيم

Acknowlegement

First and foremost, we would like to express our gratitude to Allah the Almighty for granting us knowledge and countless blessings.

We extend our sincere appreciation to our supervisor, **Dr. BOUKADOUM Aziz**, for his unwavering guidance, assistance, and support throughout the project. His consistent presence and assistance were invaluable to us, and we acknowledge that this project would not have been possible without his expertise and encouragement.

We also wish to thank the President of the jury and all the members for graciously agreeing to be part of the examining committee. We are grateful for their commitment in dedicating their time and effort to thoroughly assess and evaluate our project amidst their busy schedules.

Last but certainly not least, we are indebted to our parents for their unwavering encouragement, guidance, and unconditional support, both emotionally and financially, throughout our educational journey. May Allah bless them abundantly for their sacrifices and love.

الإهداء

الحمدُ للهِ الذي أنشأ وبرا، وخلق الماء والثرى، وأبدع كل شيء وذرا، {الرَّحْمَنُ عَلَى الْعَرْشِ اسْتَوَى}، له الحمد حمداً طيباً يملأ السموات العلا، وصلاةً وسلاماً على من بكى على أمته، المبعوث في أم القرى، صلى الله وسلم على الحبيب المصطفى أما بعد، فإننا طلبنا العلم لوجه الله تعالى، ولا نريد بذلك إلا وجه الله، وذلك فضل الله يؤتيه من يشاء، إذ قال تعالى: {يَرْفَعِ اللَّهُ الَّذِينَ آمَنُوا مِنكُمْ وَالَّذِينَ أُوتُوا الْعِلْمَ دَرَجَاتٍ}. نسأل الله أن يرفعنا بذلك في الدنيا والآخرة، كما رفع مقامنا في الدنيا إنما طلبنا العلم لوجه الله تعالى، ثم لنسعد والدينا وأساتذتنا وكل عزيز على القلب ، نسأل الله أن يجعل هذا العمل خالصاً لوجهه الكريم، وأن ينفعنا به في الدنيا والآخرة ،الشكر والعرفان لمن لا أحصيه فضلًا وتقديرًا، لمن شجعني ودعمني، وإن لم أقدر على منحه من الثناء الوفير، فهو في القلب ملكًا متوجًا وأغلى رفيقًا

إلى أمي العزيزة، التي علمتني كيف يتحرك القلم بين يدي، وكانت حريصة على تعليمي منذ نعومة أظافري. لقد كنتِ السند والأمل، والمصدر الذي أستمد منه قوتي وإلهامي. لا تكفي كلمات الشكر لتوفيكِ حقكِ، فقد كنتِ النور الذي أضاء دربي، والداعم الذي لم يتوانى عن تقديم العون والنصيحة، شكراً لكِ من أعماق قلبي، فقد كنتِ دائمًا الحضن الدافئ الذي أعود إليه بعد كل تحدٍ وصعوبة وإليك أهدي هذه الابيات التي تعبر عن مدى حبي وتقديري:

الأمُّ مَدرسةٌ إذا أعددتَها أعددتَ شعبًا طيبَ الأعراقِ

الأمُّ روضٌ إن تعهده الحيا بالريّ أورقَ أيما إيراقِ

إلى أبي العزيز، الذي أجد أثره في كل صغيرة وكبيرة. شكرًا لك ليس فقط على ما قدمت من دعم وإرشاد، بل شكرًا لأنك كنت وستظل أبي. لقد كنتَ دومًا الجدار الذي أستند إليه، والصوت الذي يرشدني بنصائحه السديدة. أسعدك الله دهورًا وألبسك من تقواه نورًا، فقد منحتني القوة والعزيمة لأواصل المسير وأحقق أحلامي وفيك أهدي هذه الأبيات التي تعبر عن مدى حبي وتقديري :

كنتُ في كل عتبات الحياة أرى ظلّه يحميني من الألم

في كفوفه تجدُ الأمان والحنان وفي قلبه يعيش الحلم والكرم

هذا النجاح أهديه إلى أمي وأبي، فهو ثمرة تعبكم وتضحياتكم. أنتم النجوم التي أنارت طريقي، والبوصلة التي وجهتني نحو تحقيق هدفي. شكراً لكم من القلب، هذا الإنجاز هو بفضلكم، وأنتم سبب فخري وسعادتي

وإلى كل من أحبهم قلبي ونسيهم قلمي من أقارب وأعزاء على القلب و إلى أساتذتي وأهل الفضل عليا الذين غمروني بالحب والتقدير والنصيحة والتوجيه والإرشاد إلى كل هؤلاء أهديهم هذا العمل المتواضع سائلا الله العلي القدير أن ينفعنا به ويمدنا بتوفيقه

دريس إدريس

e_a, e_b, e_c	The line-to-neutral voltages of the three-phase power supply network (V).
E_m	The amplitude of the network voltages (V).
E	The effective phase voltage of the network (V).
e_d, e_q	The line-to-neutral voltages of the power supply network in the (d,q) reference frame (V).
e_a, e_b, e_c	The line-to-neutral voltages of the power supply network in the (a,b,c) reference frame (V).
V_d, V_q	The reference voltages in the (d,q) reference frame (V).
V_a, V_b, V_c	The reference voltages in the (a,b,c) reference frame (V).
I_{sa}, I_{sb}, I_{sc}	The line current of the three-phase power supply network (A).
I_q, I_d	The line currents in the (d,q) reference frame (A).
i_α, i_β	The components of the line current vector in the stationary (α,β) reference frame.
I_a, I_b, I_c	The line current in the (a,b,c) reference frame (A).
L_s	Total inductance of the network-rectifier line with PWM (H).
R_s	Resistance of the network-rectifier line with PWM (Ω).
R_{ch}	Resistance of the load (Ω).
L_{ch}	Inductance of the load (H).
C	DC bus capacitor (F).
V_a, V_b, V_c	The single-phase voltages at the input of the PWM rectifier (V).
$v_{s\alpha}, v_{s\beta}$	The components of the line voltage vector in the stationary (α,β) reference frame.
I_{ch}	Current in the load (A).
I_c	Current in the capacitor (A).
V_{dc}	DC bus voltage (V).
V_{dc_ref}	Reference DC bus voltage (V).
I_{dc}	Active current required to charge the DC bus (A).
I_{max}	The maximum amplitude of source currents (A).
E_{max}	The maximum amplitude of source voltages (V).
$i_a(t), i_b(t), i_c(t)$	Instantaneous reference currents.
S_a, S_b, S_c	Switching states of the PWM rectifier switches.
S_q, S_d	Switching states of the rectifier in the (d,q) reference frame.

S_a, S_b, S_c	Switching states of the rectifier in the (a,b,c) reference frame.
T	Period (s).
T_e	Sampling period (s).
v_p	Amplitude of the carrier voltage for PWM control (V).
v_{ref}	Amplitude of the reference voltage for PWM control (V).
S	Apparent power (VA).
P	Active power or real power (W).
Q	Reactive power or imaginary power (VAR).
p_{ref}	Reference active power.
q_{ref}	Reference reactive power.
D	The distorting power due to current harmonics (W).
d_p, d_q	Errors of active and reactive powers.
K_P	Proportional gain of the regulator.
K_i	Integral gain of the regulator.
Δ_p, Δ_q	Variation of instantaneous active and reactive powers.
Δ_i	Current variation.
Δ_v	Variation in the connection filter voltage.
α	Angle of the reference voltage vector.
k_p	Proportional parameter.
k_i	Integral parameter.
$\hat{P}$	Instantaneous active power (W).
$\hat{q}$	Instantaneous reactive power (VAR).
f	Fundamental frequency (Hz).
ω	Angular frequency (rad).
θ	The angle between sectors.
$\emptyset$	The estimated flux.
T_{b0}	The time constant of the open-loop system.
t	The time (s).
d, q	Park reference axis.
T_r	Electrical time constant of the impedance (R,L) with (T_r=L⁄R).
f_r	Tuning frequency.

P^*	Reference active power (W).
q^*	Reference reactive power (VAR).

Abbreviation

Acronym	**Meaning**
SAPF	Series Active Power Filter
PAPF	Parallel Active Power Filter
THD	Total Harmonic Distortion
UPQC	Unified Power Quality Conditioner
PI	Proportional-Integral (PI) Controller
AC-DC	Alternative -Continuous Conversion
IGBT	Insulated Gate Bipolar Transistor.
MOSFET	Metal Oxide Semiconductor Field Effect Transistor
GTO	Gate Turn Off Thyristors
PLL	Phase Locked Loop
PWM	Pulse Width Modulation PWM
DPC	Direct Power Control

List of Tables

List of Figures:

Index :

GENERAL INTRODUCTION

Power quality is a very important concept, covering both the quality of power supply and transmission lines, and the quality of the voltage and currents waveforms. Nowadays, improving power quality on electrical distribution networks is becoming a major challenge for both electrical network managers and electrical power operators.

Under normal operating conditions, electrical power quality is mainly reduced to the quality of the voltage waveform. The main phenomena problems that can affect the quality of the voltage waveform are:

- *Voltage dips of short or long time;*
- *System unbalance;*
- *Harmonic distortion;*

The main characteristic parameters of a three-phase system are:

- The frequency, which must be equal to the fundamental frequency of the electrical network at 50 Hz
- The amplitude of the three phases, so all three phases have the same amplitude,
- The waveform voltages and currents should be sinusoidal,
- The symmetry of the system characterized by the equality of the same amplitude and their relative phase shifts.

The use of power electronics equipment such as rectifiers, choppers, inverters in electrical systems caused harmonic distortion. These converters are considered as nonlinear loads; they absorb non-sinusoidal currents and consume some time reactive power, these phenomena could, on one hand, damage the electrical appliances connected to them through over voltages, overheating, and device damage, and on the other hand, lead to inefficient energy utilization with excessive losses in energy transmission lines. On one hand, standards for harmonic distortion impose maximum limits on the total harmonic distortion (THD) of electrical quantities characterizing the power supply.

For this reason, new topologies of static converters such as PWM rectifiers, cascaded rectifiers, matrix converters, etc. have been developed. They offer a better solution for reducing harmonic disturbances and improving power quality. In this thesis, we focus on studying a PWM rectifier.

The PWM rectifier, as a static converter, acts as a rectifier with the advantage of absorbing sinusoidal input currents with a unity power factor and allowing the output to produce an adjustable DC voltage. However, it has the disadvantages of a diode rectifier as a

unidirectional power flow converter, low power factor, and input current distortion (presence of harmonics).Therefore, the PWM rectifier is an increasingly popular solution used in industrial applications and offers the following advantages:

- *bidirectional Power*
- *Low harmonic distortion of the grid current.*
- *Unit power factor.*
- *Control of the DC bus voltage.*
- *Reduction in the size of the DC bus capacitor voltage*

Several control strategies for PWM rectifiers have been proposed, such as hysteresis control, Direct Power Control (DPC), etc. While these control strategies aim to achieve the same objectives, such as unity power factor correction, nearly sinusoidal input current, and adjustable of DC bus voltage.

The main objective of this thesis is to study the various control strategies of a PWM rectifier with the aim of improving its performances Take good control of it and use it to charge the battery .

The first chapter provides an in-depth exploration of electrical power quality, highlighting various disturbances that can compromise it. The discussion commences with an examination of harmonics, elucidating their origins, characteristics, and the adverse effects they impose on the electrical grid and connected loads. Special attention is given to harmonic distortion stemming from diode rectifiers, alongside an overview of relevant standards and regulations governing harmonic pollution. It concludes with an overview of the various proposed solutions for harmonic compensation, encompassing both traditional and modern approaches.

Moving on to the second chapter, it delves into the control strategies employed in PWM rectifiers, which play a pivotal role in ensuring efficient energy conversion and harmonic mitigation. The chapter provides insights into the operating principles and modeling techniques of PWM rectifiers, focusing on strategies such as hysteresis control and pulse-width modulation (PWM). Through comprehensive simulation results, the efficacy of these control strategies in regulating output voltage, compensating for harmonic currents, and achieving unity power factor is demonstrated.

Turning to the third chapter, classic Direct Power Control (DPC) techniques for PWM rectifiers are thoroughly investigated. The discussion revolves around the principles of DPC-based hysteresis control, emphasizing its ability to accurately estimate active and reactive power components. Simulation results are presented to illustrate the performance of classic

DPC control in optimizing the operation of PWM rectifiers, ensuring stable and efficient power conversion under varying load conditions.

Chapter IV explores the application of advanced control strategies, including Direct Power Control (DPC), in electric vehicle (EV) charging systems. The chapter highlights the pivotal role of these control methodologies in enhancing the precision and stability of the charging process, thereby ensuring optimal energy transfer efficiency from the grid to the vehicle's battery system. Through comprehensive case studies and simulation analyses, the effectiveness of these control strategies in optimizing battery charging performance is demonstrated, underscoring their significance in advancing EV technology.

CHAPTER I

PERTURBATION OF ELECTRICAL NETWORKS AND DIFFERENT TYPES OF COMPENSATION

CHAPTER I

PERTURBATION OF ELECTRICAL NETWORKS AND DIFFERENT TYPES OF COMPENSATION

1. Introduction

The significant presence of static converters in electrical installations has considerably contributed to the improvement of performance and reliability of these equipment's. Due to their nonlinear nature, these converters are the main cause of the deterioration of electrical network [1].In this chapter, we discuss electrical energy quality, its degradation and its consequences. Additionally, we present the disturbances that affect voltage and current in electrical networks, along with their origins, consequences, and solutions for remediation. We will then propose passive and active power filter solutions for compensating harmonic distortion.

2. Quality of Electrical Energy

The quality of electrical energy is a broad concept that encompasses both the quality of electrical energy supply in terms of power and the quality of voltage and current waveforms. There are different phenomena that can affect voltage and currents waveforms quality, such as voltage sags, over voltages, outages, imbalances, and rapid variations, including transient over voltages, flicker, and harmonic distortion. Conversely, current quality reflects the ability of loads to operate without disturbing or reducing the efficiency of the power system [2].

- Frequency.
- Amplitude of the three voltages and currents.
- Waveform, which should be as sinusoidal.
- Symmetry of the three-phase system.

3. Degradation of Voltage Quality

Disturbances that degrade voltage quality can result from [3]:

- Faults in the electrical network.
- Short circuits.
- Atmospheric causes such as :lightning, frost, storms, etc..
- Material causes such as: aging of insulation, etc..
- Human causes (mis operations, third-party work, etc.).
- Disturbing installations.
  - ✓ Arc furnaces.
  - ✓ Welding machines.

- ✓ Variable speed drives (static converters).
- ✓ All applications of power electronics, such as televisions, fluorescent lighting, starting or switching of appliances, etc.

4. Different types of electrical disturbances

Electrical disturbances affecting one of the four voltage parameters listed above may manifest as different types of disturbances of electrical origin such as: a dip or a voltage cut, a voltage fluctuation, an unbalanced of the three-phase voltage system, a variation in frequency, and the presence of harmonics distortion, … etc[4].

4.1.Voltage Dip or Voltage Cut-Off

A voltage dip is a decrease in the effective value of the voltage to a value between 10 and 90% of the nominal voltage and a duration ranging from 10 ms to a few seconds. Voltage dips are caused by natural phenomena such as lightning or faults in the installation or distribution system [5, 6]. See Figure (1.1) and (1.2).

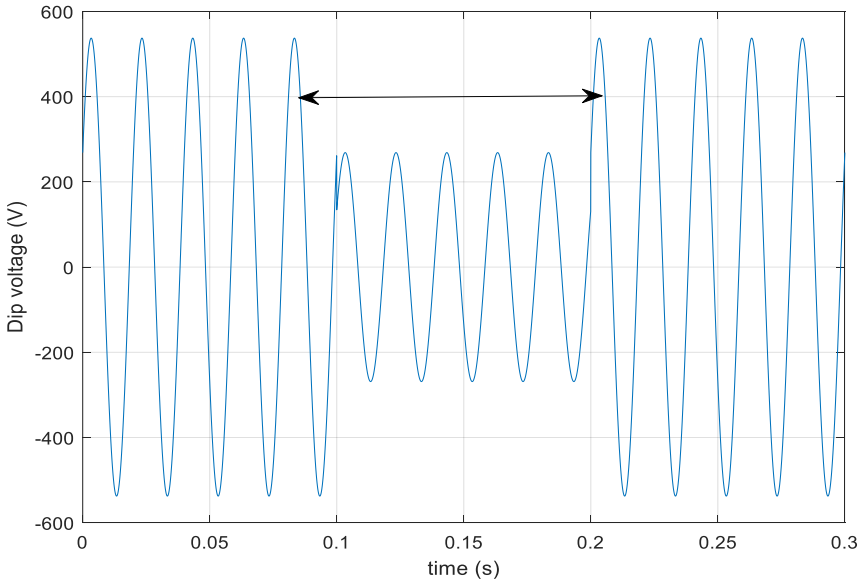

Figure 1.1 Dip voltage

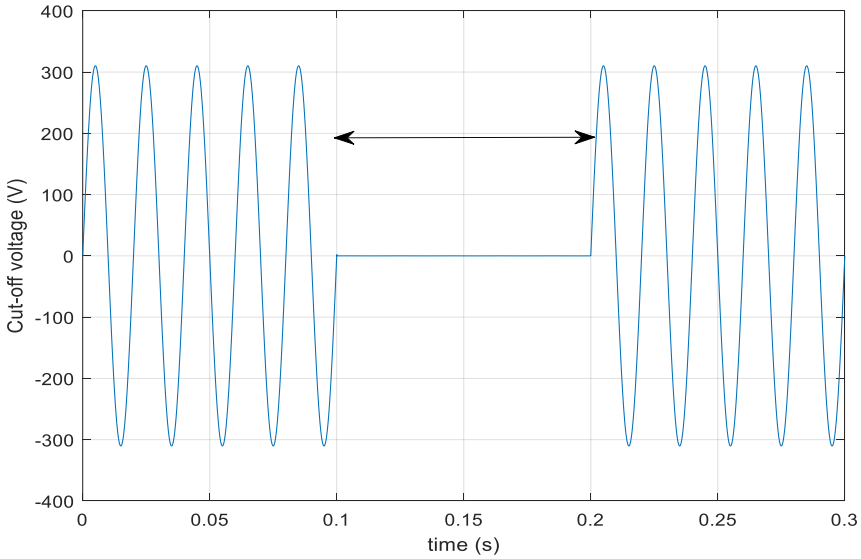

Figure 1.2 Cut-off voltage

4.2. Voltage fluctuations and spikes

Voltage fluctuations are periodic or erratic variations in the voltage envelope. These are sudden variations in the amplitude of the voltage located in a band of 10% and occur over a time interval of a few hundredths of a second [5].

They are in particular due to the propagation on the lines of the network of important calling currents. The main source of these currents is the operation of devices whose power consumption varies rapidly, such as arc furnaces and welding machines. These fluctuations result in variations in intensity, visible at the level of lighting causing a perceptible visual gene for a variation of 1% of the voltage. This flickering phenomenon is called flicker voltage [6].

The voltage bump is an increase in voltage above the nominal voltage for a period of 0.5 cycle to 60 s. It is characterized by its amplitude and duration. It may cause heating and destruction of components, See Figure (1.3).

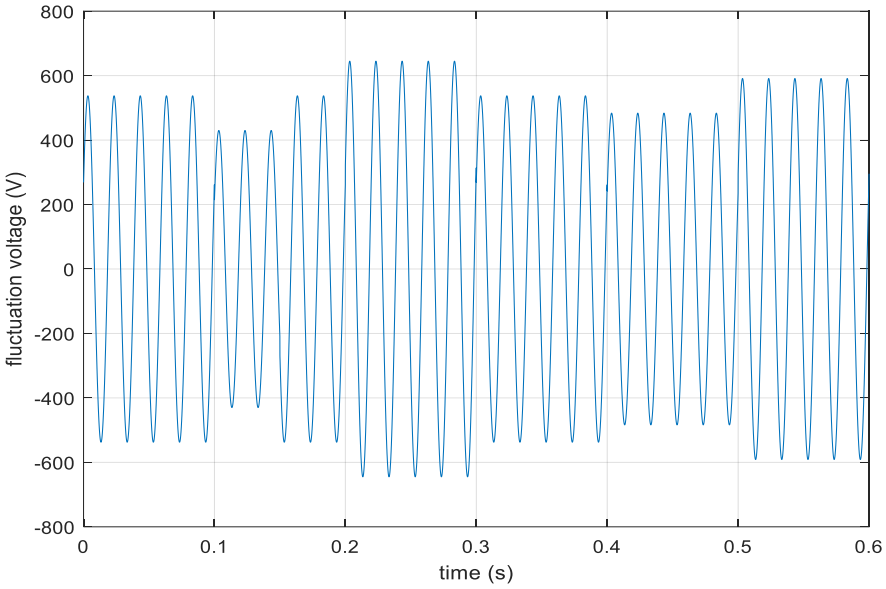

Figure 1.3 fluctuations Voltage

4.3. Unbalanced Three Phase Voltage System

Three quantities of the same nature and of the same pulsation form a balanced three-phase system when they have the same amplitude and when they are out of phase of 120 between them. When the quantities do not check these phase and amplitude conditions [7]. We speak of an unbalanced three-phase system which is well demonstrated in Figure (1.4)

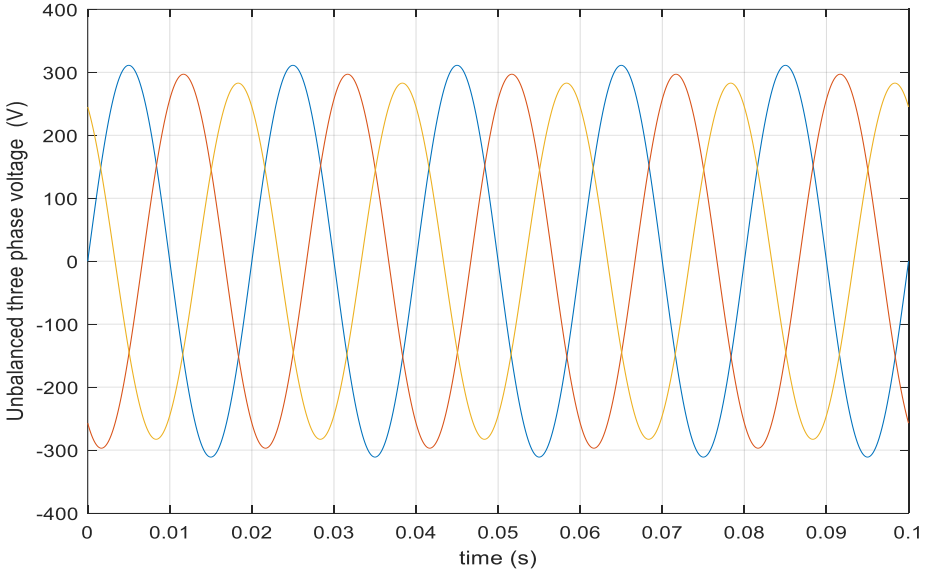

Figure 1.4 unbalanced three-phase Voltage systems

4.4. Frequency variation:

A significant variation in the frequency of the network may occur on the networks of users not interconnected or powered by an autonomous thermal source at the level of distribution or transmission networks [5], this frequency variation is very rare and is present only in exceptional circumstances, as in the case of some serious network defects. Under normal operating conditions, the mean value of the fundamental frequency shall be within the range 50 Hz 1% shown in Figure (1.5).

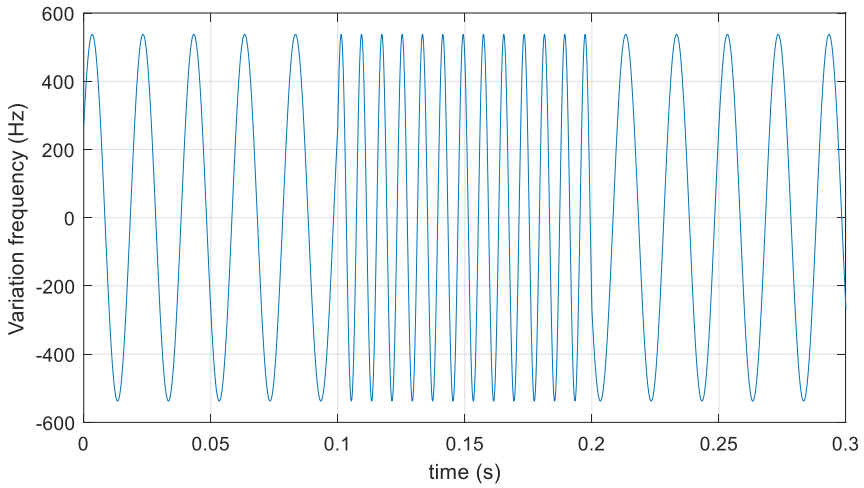

Figure 1.5 Frequency variation

4.5. Harmonic distortion

The harmonics are a superposition on the fundamental wave at 50 Hz, of waves also sinusoidal but of whole multiple frequencies of that of the fundamental. Figure (1.6) shows the superposition of the third harmonic and a fundamental current at frequency 50 Hz.

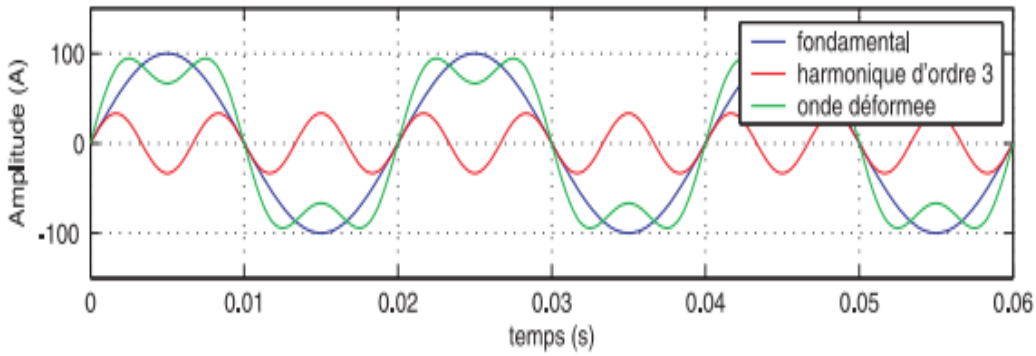

Figure 1.6 Harmonic distortion

5. Study of harmonic disturbances

The main source of the harmonics distortion in electrical networks is the presence of power electronics equipment.

The vast majority of harmonic sources are:

❖ **Industrial loads**

✓ Power electronics equipment: rectifier, inverters,..etc.

✓ Loads using electric arc: welding machine, lighting (fluorescent tube), arc furnace.

❖ **domestic loads**

✓ Equipped with converters or switch-mode power supplies: microwave oven, computer, printer, television, induction cooker...etc.

5.1. Spectral representation analysis (THD)

A distorted signal typically consists of multiple harmonics. This signal is often represented in the form of a spectrum

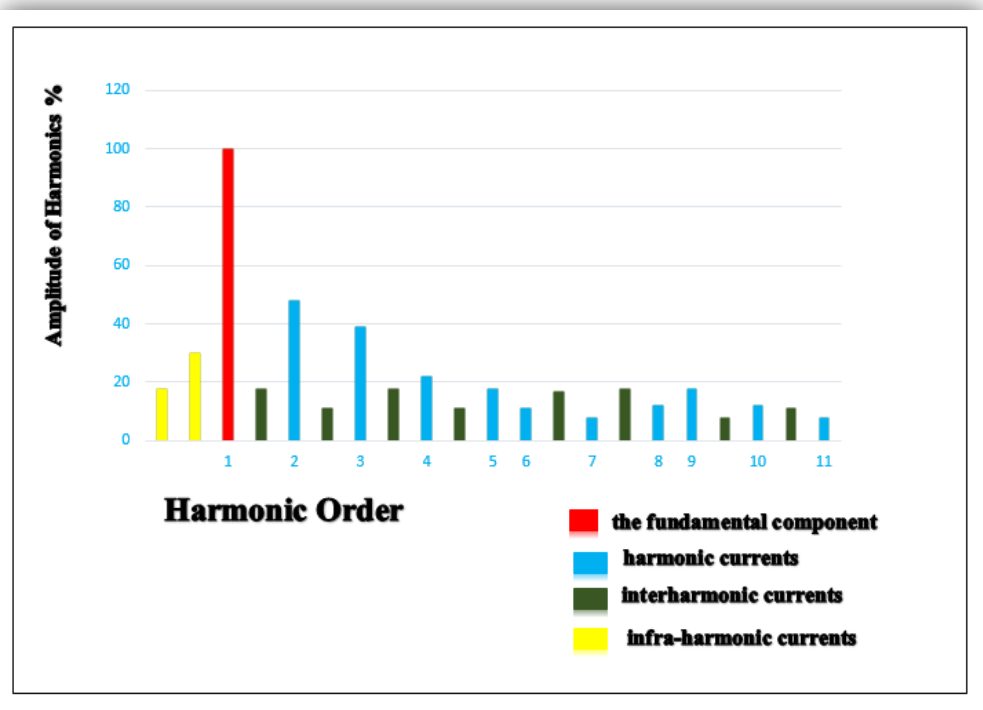

Figure 1.7 harmonics spectrum analysis

5.2. Consequences of harmonics distortion

Many effects of harmonics distortion on electrical installations and their equipment can be cited:

✓ Heating equipment (cables.....);

✓ Malfunctioning of electrical equipment;

✓ Problems of resonance;

✓ Degradation of the accuracy of measuring devices;

✓ Induced disturbances on communication lines, including electromagnetic radiation.

5.3. Characteristics of harmonics

5.3.1. Total Harmonic Distortion (THD) ratio:

The harmonic distortion rate (THD) is used to assess the difference between the actual waveform and the sine waveform for a current or voltage. It is given by the ratio between the effective value of harmonics and that of the fundamental. It is defined by:

$$\mathrm{THD}(\%) = 100\sqrt{\frac{\sum_{n=2}^{\infty} y_n^2}{y_1^2}} \quad (1.1)$$

With

y_1:Root mean square (RMS) value of the fundamental current or voltage

y_n:RMS values of the various harmonic components current or voltage

5.3.2. The powers

The active and reactive powers for the fundamental frequency defined respectively:

$$\begin{cases} P = V_1 I_1 \cos\varphi_1 \\ Q = V_1 I_1 \sin\varphi_1 \end{cases} \quad (1.2)$$

The expression of the power factor can be expressed in the following form:

$$F_p = \frac{P}{S} = \frac{P}{\sqrt{(P^2+Q^2+D^2)}} \quad (1.3)$$

This last equation shows that in non-sinusoidal regimes, harmonics create a distorting power that reduces the power factor. To estimate the contribution of harmonics in the power balance, the distorting power D is defined as:

$$D = mV_1\sqrt{\sum_{n=2}^{\infty} Y_n^2} \quad (1.4)$$

With :

m: is the number of phases.

5.3.3. Standards concerning harmonic disturbances

The widely recognized organization as the conservator of electrical quality standards is the IEC (International Electro technical Commission), based in Geneva. The IEC has defined a series of standards, called electromagnetic compatibility (EMC) standards, to address electrical quality.

The IEC 61000 series considers harmonics and inter-harmonics as electromagnetic phenomena caused by low frequencies. A widely used alternative to the IEC standard is the IEEE 519-1992 recommendation, which provides practical guidelines on harmonics.

5.3.4. IEC 61000

Among the sections of the IEC 61000 standard (considered a European standard) that are of interest to us are IEC 61000-2-2, IEC 61000-3-2, and IEC 61000-3-4.

IEC 61000-2-2 :defines the compatibility levels of harmonic voltages on low-voltage public networks (Table 1.1). This standard aims to protect equipment connected to a distorted low-voltage network.

Translated from French (technical) to English (technical):

IEC 61000-3-2: defines emission limits for harmonic currents from equipment consuming current less than or equal to 16 A per phase. This concerns domestic appliances. This limitation of the scope is very restrictive in most industrial applications.

This standard classifies devices into four groups or classes, with equipment ranging from 75 W to 600 W.

- Class A: All balanced three-phase equipment not included in classes (B, C, and D).
- Class B: Portable tools.
- Class C: Lighting equipment, including regulating devices.
- Class D: Microcomputers and televisions.

The limits of harmonic currents in standard IEC 61000-3-2 are provided in Table 1.2. It is interesting to note that these limits are expressed in absolute values and not relative to the fundamental. This implies that equipment with low power can meet the standard with a very high Total Harmonic Distortion Index (THD_I).

Odd harmonics not multiples of 3		*Odd harmonics multiples of 3*		*Even harmonics*	
Harmonic order H	Harmonic voltage %	Harmonic order H	Harmonic voltage %	Harmonic order h	Harmonic voltage %
5	6	3	5	2	2
7	5	9	1.5	4	1
11	3.5	15	0.3	6	0.5
13	3	21	0.2	8	0.5
17	2	>21	0.2	10	0.5
19	1.5			12	0.2
23	1.5			>12	0.2
25	1.5				
>25	0.2+0.5*25/h				

Table 1.1: Compatibility levels for individual harmonic voltages on low-voltage networks (IEC 61000-2-2).

Harmonics *(h)*	*Class A* *(A)*	*ClassB* *(A)*	*ClassC* *Ih/I1%*	*ClassD* *(mA/W)*
Odd harmonics				
3	2.30	3.45	30 xF_p	3.4
5	1.14	1.71	10	1.9
7	0.77	1.155	7	1.0
9	0.40	0.60	5	0.5
11	0.33	0.495	3	0.35
13	0.21	0.315	3	0.296
$15 \leq h \leq 39$	*0.15 x15/h*	0.225 x15/h	3	3.85/h
Even harmonics				
2	1.08	1.62	2	-
4	0.43	0.645	-	-
6	0.30	0.45	-	-
$8 \leq h \leq 40$	0.23 x8/h	0.345 x8/h	-	-
□F_p□ :Power factor				

Table 1.2: Limits of harmonic current components (IEC 61000-3-2).

- **The EN 50160 standard** specifies the characteristics of the voltage supplied by low-voltage public networks.

- **The IEEE 519 standard** (Recommended Practices and Requirements for Harmonic Control in Electric Power Systems - USA) aims to limit the impact of nonlinear loads both between the energy distributor and the customer (mutual commitment to limit harmonics).[8]

6. Types of loads

6.1. Linear Load

If a linear load is powered by a sinusoidal voltage, the current flowing through this load is also sinusoidal [9].

Figure 1.8 Linear load.

Figures (1.9) and (1.10) respectively show the load current and its spectrum harmonic analysis in the case of a linear load (RL load) powered by a sinusoidal three-phase source. In

this case, it is noted that the current waveforms are purely sinusoidal, with only the presence of the fundamental frequency at 50 Hz.

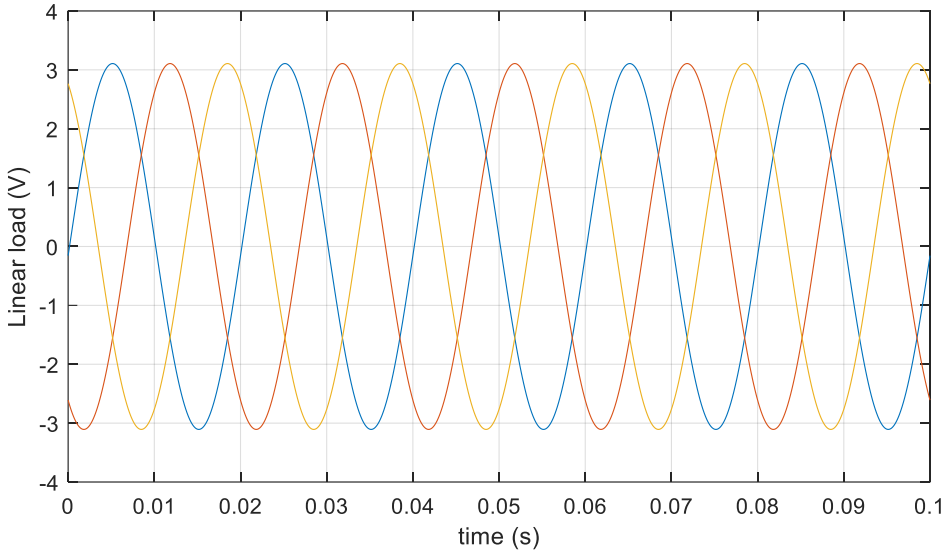

Figure 1.9: linear load currents

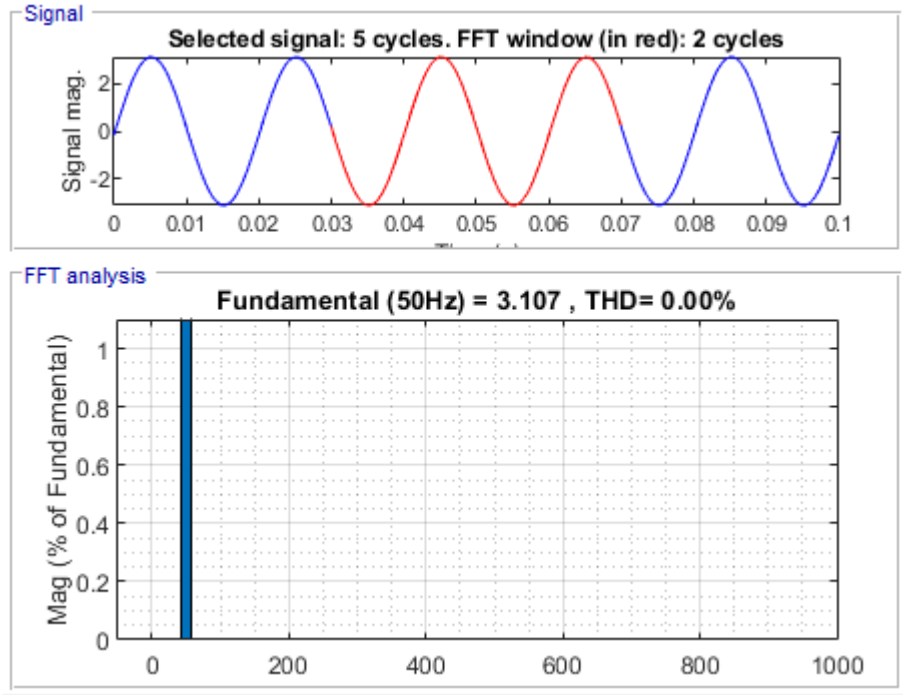

Figure 1.10 Spectrum harmonic analysis of current in a linear load.

6.2. Nonlinear Load

If a sinusoidal voltage powers a nonlinear load, the current flowing through the load is no sinusoidal waveforms. It contains both a fundamental component and harmonic components [10].

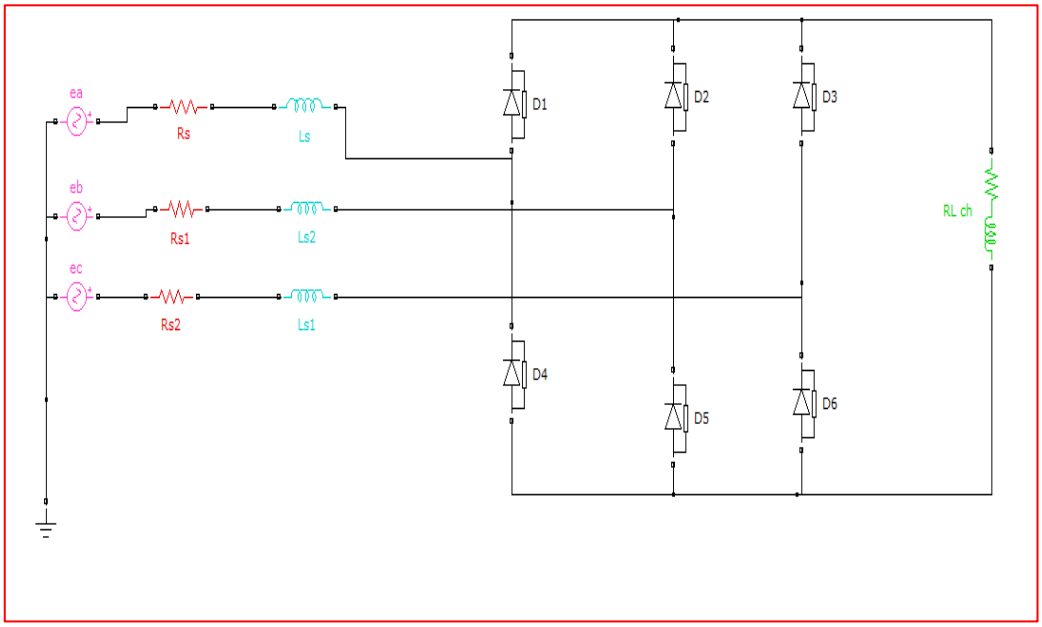

Figure 1.11: Nonlinear load

Figure (1.12) and (1.13) represent the current and its harmonic spectrum for a nonlinear load. In this case, the nonlinear load generates rectangular currents towards the network containing harmonics of order 6k ± 1 with k: being a natural number, such that odd harmonics not multiples of three, namely h_5,h_7,h_{11},h_{13} h_{17},h_{19},h_{23},h_{25} , which cause deformation in the shape of the three phase currents (I_{sa},I_{sb},I_{sc}),affecting the quality of energy in the network. The network is characterized by a THD equal to 30.84%.

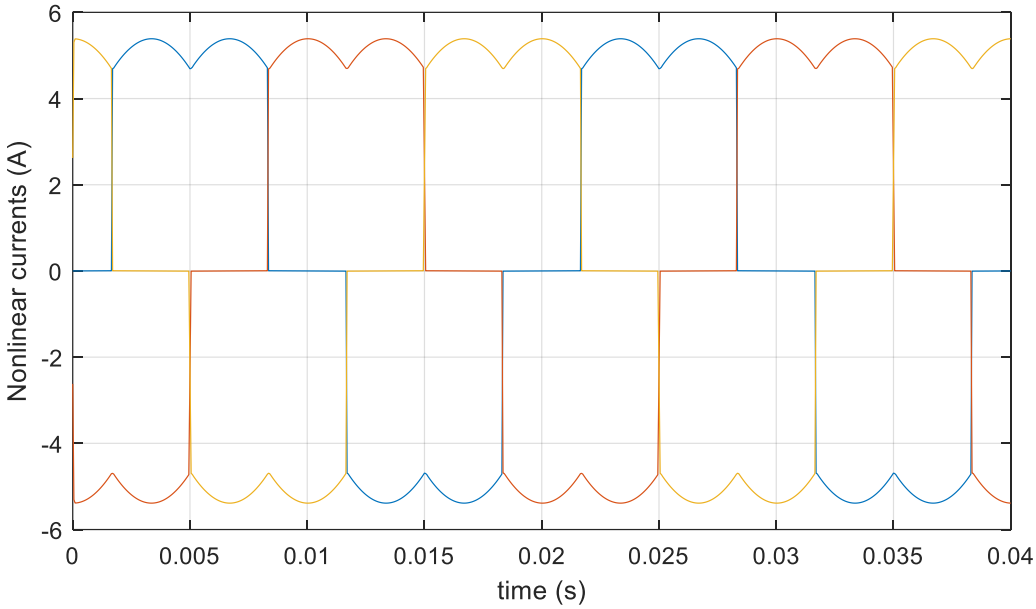

Figure 1.12 Current of a nonlinear load.

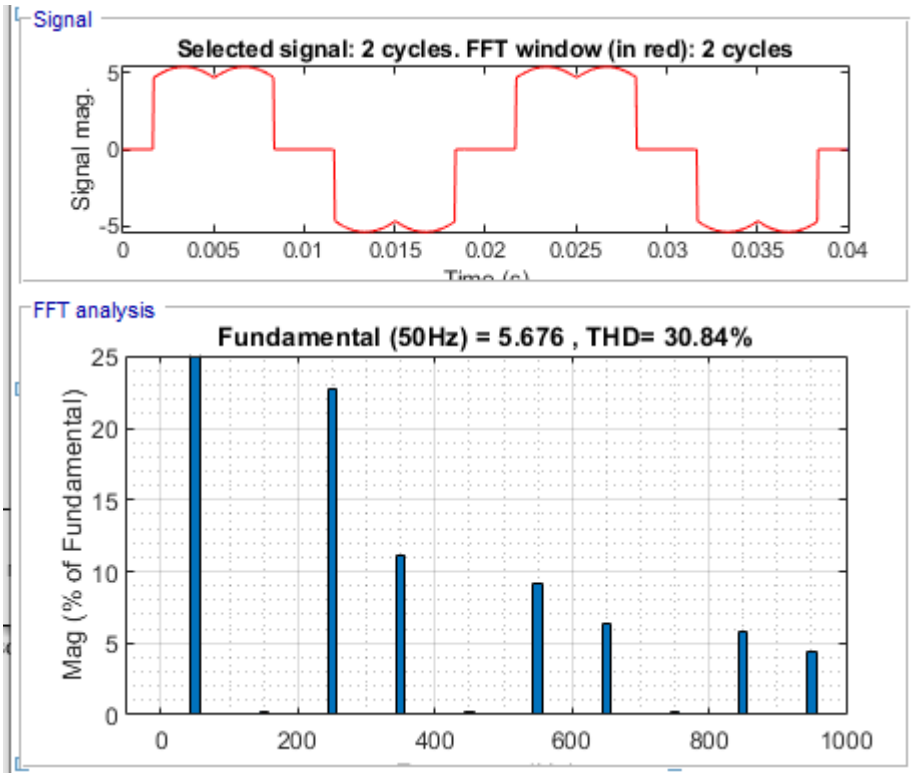

Figure 1.13 Spectrum harmonics analysis of the current in a nonlinear load.

7.Solutions of harmonics distortion

Several solutions based on harmonic filtering have been considered to limit the propagation of harmonics in the electrical network. The most classical and widely used solution in the industry involves the use of passive filters. Later, to overcome the limitations of passive

filters, active filters were designed and commercialized. In recent years, the combination of passive and active filters, called hybrid active filters, has become increasingly popular due to its advantages over passive or active filters.

7.1. Passive Filtering

There are two types of passive filters :

7.1.1. Resonant Filter

It consists of a series RLC circuit tuned to a specific frequency. This filter is highly selective [10]. Figure (1.14) shows the connection diagram of the filter and the evolution of their impedance as a function of frequency. The filter has equivalent impedance Z_{eq} given by:

$$Z_{eq}(w) = \frac{1-LCw^2+jRCw}{jCw} \quad (1.5)$$

With: $w = 2\pi f$

$$f_r = \frac{1}{2\pi\sqrt{LC}} \quad (1.6)$$

7.1.2. Damped Filter

This filter presents low impedance over a wide frequency range. It is much less selective and reduces harmonics above their tuning ranks. Figure (1.14) depicts the connection diagram of a damped filter and the evolution of its impedance as a function of the harmonic rank. This filter has poorer performance than the resonant filter. However, the consequences of a variation in capacitance or frequency are very limited.

The filter has equivalent impedance $\mathbf{Z_{eq}}$ given by [10]:

$$Z_{eq}(w) = \frac{1-LCw^2+j\frac{L}{R}w}{-\frac{L}{R}Cw^2+jCw} \quad (1.7)$$

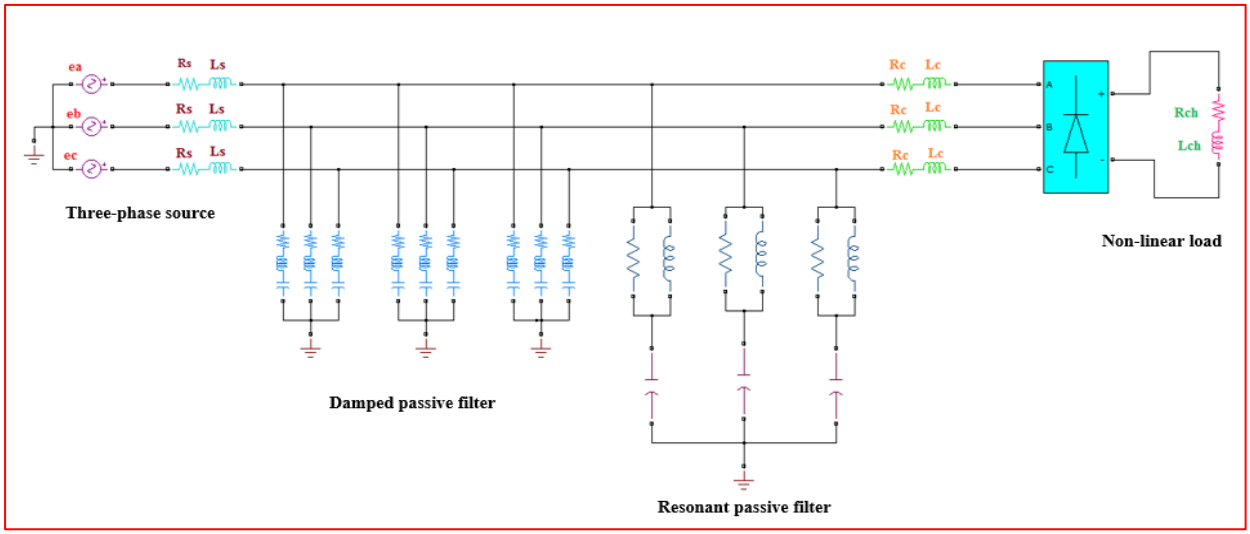

Figure 1.14 Resonant and damped filters connected to the network

7.2. Active power Filters

Two main reasons led to the design of a new, modern, and efficient filtering structure called an active filter. The first reason is due to the inherent disadvantages of traditional pollution control solutions that no longer meet the evolving demands of loads and electrical networks. The second reason follows the emergence of new semiconductor components, such as GTO thyristors and IGBT transistors. The purpose of these filters is to generate either currents or voltages harmonics in order to compensate for disturbances responsible for the degradation of the performance of electrical equipment and installations. Three possible topologies of active filters are mentioned:

7.2.1. Parallel Active Filter (PAF)

The shunt active power filter is a current generator designed to compensate for all disturbances caused by harmonic currents, imbalances, and reactive power. It is connected in parallel to the distribution network as shown in Figure (1.15).

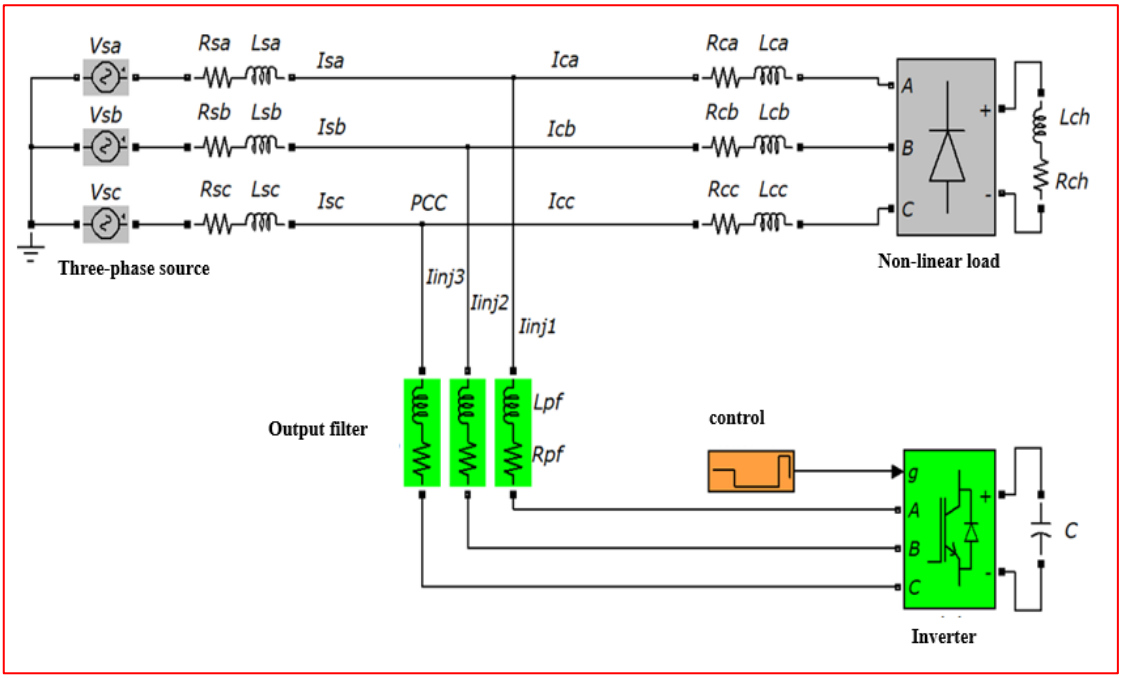

Figure 1.15 Parallel active power filter (PAPF)

7.2.2. Series Active power Filter (SAPF)

The series active filter is connected in series with the network as shown in Figure (1.16). It behaves like a voltage source that generates harmonic voltages whose sum with the network voltage is a sinusoidal waveform.

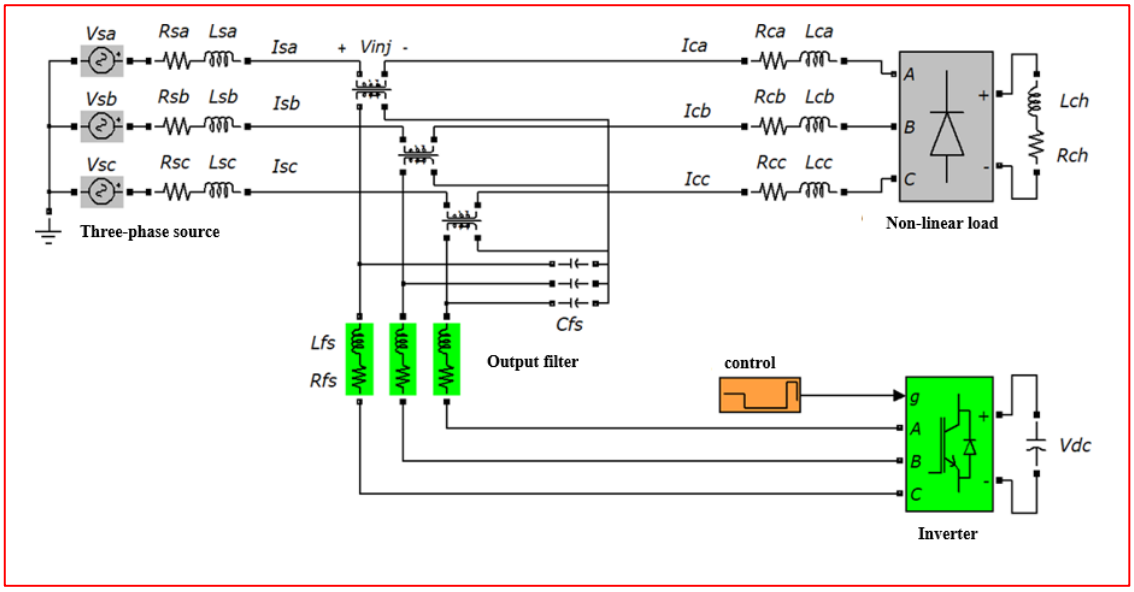

Figure 1.16 Series active power filter (SAF)

7.2.3. Unified Power Quality Conditioner (UPQC)

It is the combination of two series and shunt active power filters that allows compensating for all disturbances in current and voltage harmonics as shown in Figure (1.17).

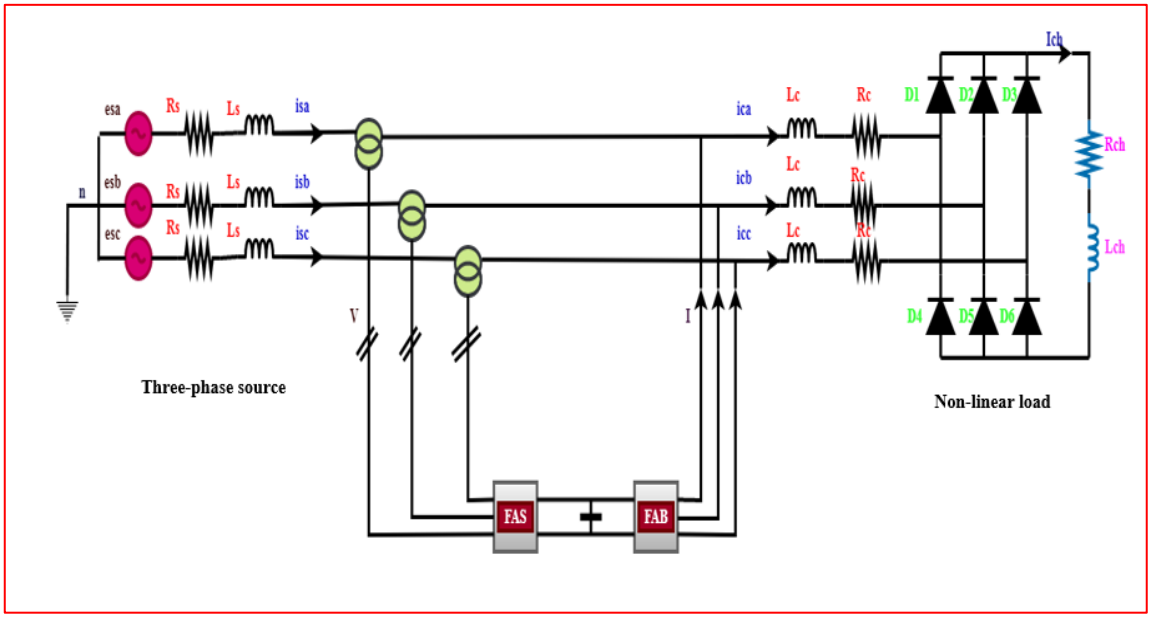

Figure 1.17 Combination of parallel and series active filter (UPQC).

7.2.4. Hybrid Filters

Several configurations have been presented in the literature, the most studied of which are [10]:

- ✓ Series Active Filter with Parallel Passive Filters
- ✓ Series Active Filters connected in series with Parallel Passive Filters
- ✓ Parallel Active Filter with Parallel Passive Filter

8. Modern Solutions for Harmonic Pollution:

The principle of these converters consists of using a transformer with different couplings between the primaries and secondaries (Y/Y and Y/D or D/D and D/Y), or a three-winding transformer with the two secondary windings phased 30° apart. Each of these secondaries powers a Greinacher bridge rectifier. The considered poly-phase diode rectifiers have 6, 9, 12, 15, 18, 21, 24 phases, which produce at the output a DC voltage with ripples at a frequency equal to 12, 18, and 24, 30, 36, 42, 48 times the supply frequency [10]

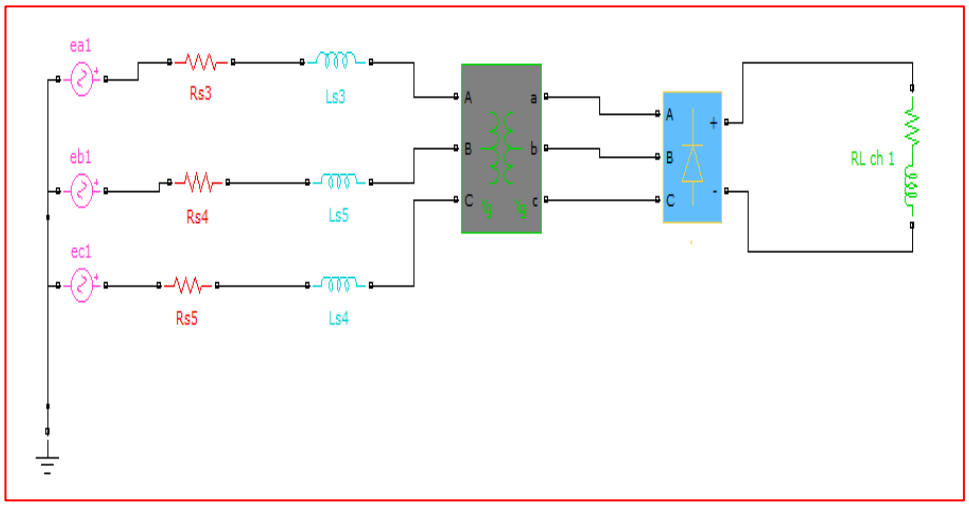

Figure 1.18 06-pulse rectifier.

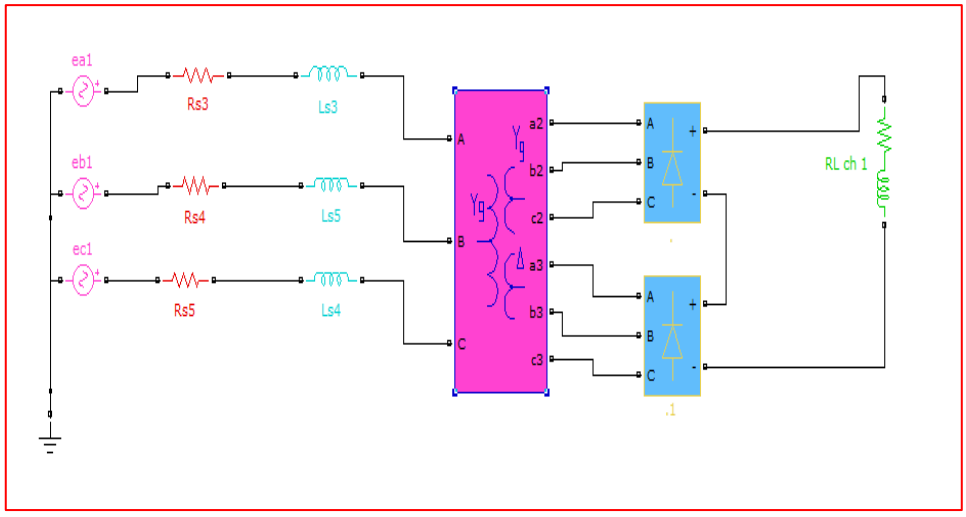

Figure 1.19 12-pulse rectifier.

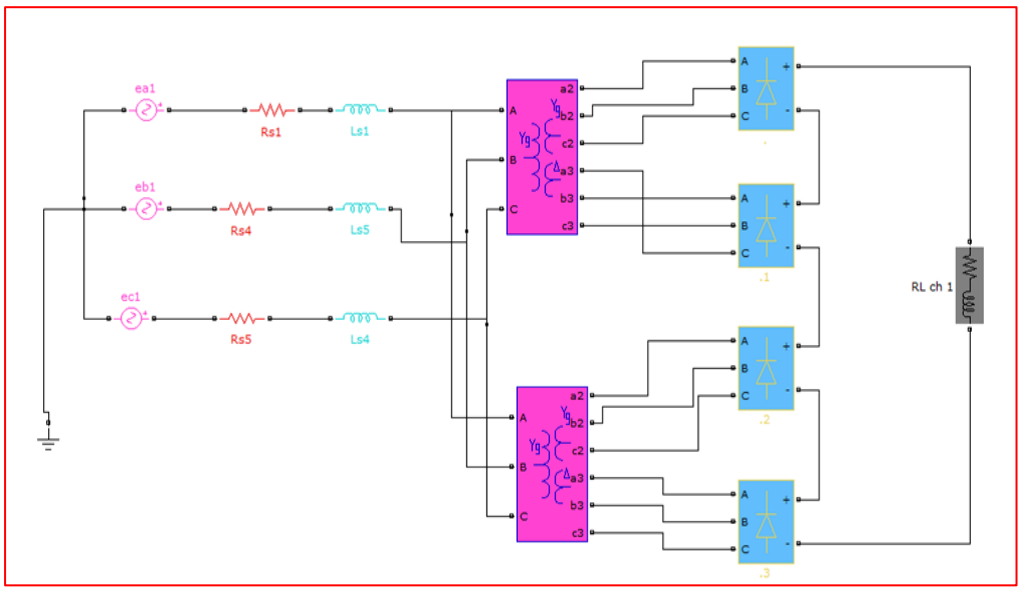

Figure 1.20 24-pulse rectifier.

8.1. PWM Rectifiers

The principle of operation of PWM rectifier comprises of maintaining the DC voltage across the capacitor as constant and it is done by means of feedback of output voltage as shown in Figure.21. The reference voltage given to the control loop should able to block the conduction of diodes so that the converter works in unity power factor and absorbs sinusoidal currents. It also allows control of active and reactive power flow in both directions [11].

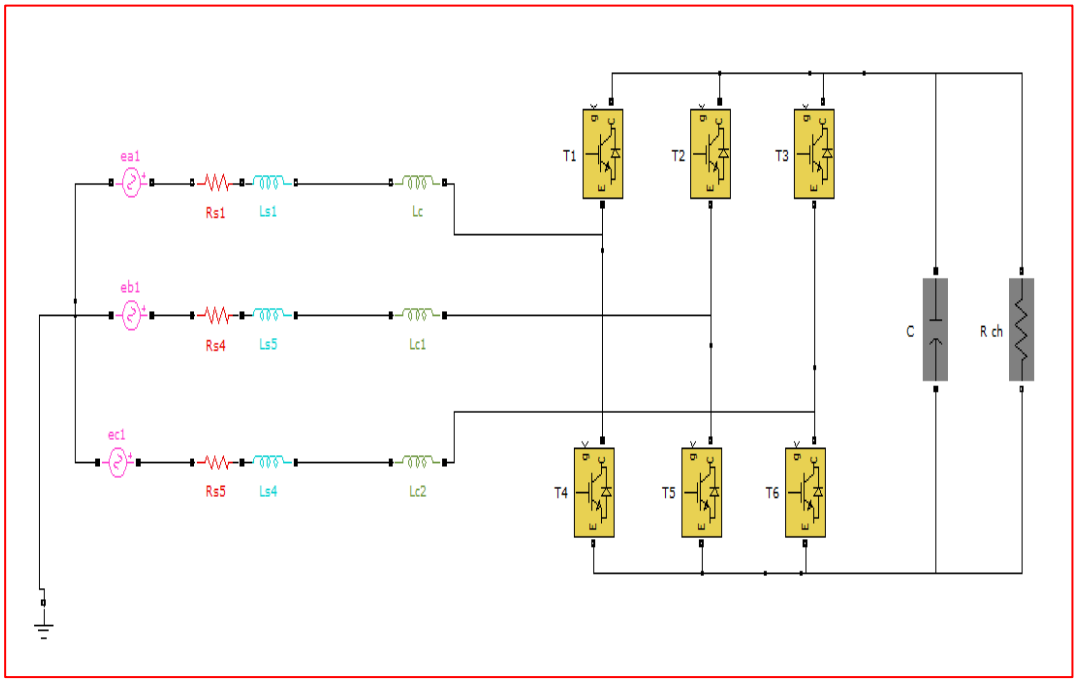

Figure 1.21 PWM Rectifier.

9. Conclusion:

In this chapter, we have discussed the various disturbances that affect the electrical network and consequently degrade the quality of the voltage and current waveforms. After identifying the origins and harmful consequences of harmonics, we have emphasized on harmonics produced by static converters, particularly natural commutation rectifiers (diode bridges). At the end of the chapter, we have presented passive and active power filter solutions to mitigate harmonic disturbances. The PWM rectifier is one of the modern solutions that have been developed with great concern. This type of converter will be the subject of the upcoming chapters.

CHAPTER II

MODELLING AND SIMULATION OF PWM RECTIFIER USING HYSTERESIS BAND CURRENT CONTROL

CHAPTER II

MODELLING AND SIMULATION OF PWM RECTIFIER USING HYSTERESIS BAND CURRENT CONTROL

1. Introduction

The PWM rectifiers aim to deliver a continuous voltage from an alternating current network. This conversion type must ensure sinusoidal current absorption on the source side and regulate the DC capacitor voltages according to its reference.

Currently, the PWM rectifier is the most widespread static converter, integrated into numerous industrial applications, especially in harmonic pollution mitigation systems. It therefore requires an appropriate control strategy. Its topology is ideal for operation in all installations, allowing for output voltage regulation, compensation of harmonic currents and reactive power consumption at the grid, and operation with unity power factor.

This chapter is dedicated to the study of the PWM rectifier using different strategies control. In this study, we will discuss its operating principle modelling in the (a, b, c) and (d, q) reference frames, and its different strategies control such as hysteresis, PWM controls. Simulation results are presented and discussed.

2. PWM Rectifier

The PWM rectifiers can adapt to changes in load and the electrical grid parameters without modifying the installations. These rectifiers are applied in several domains, such as battery charging, electric drives for machines, renewable energies, and electric vehicle charging. General topology of the three-phase voltage-sourced PWM rectifier (VSR) is show Figure (2.1).

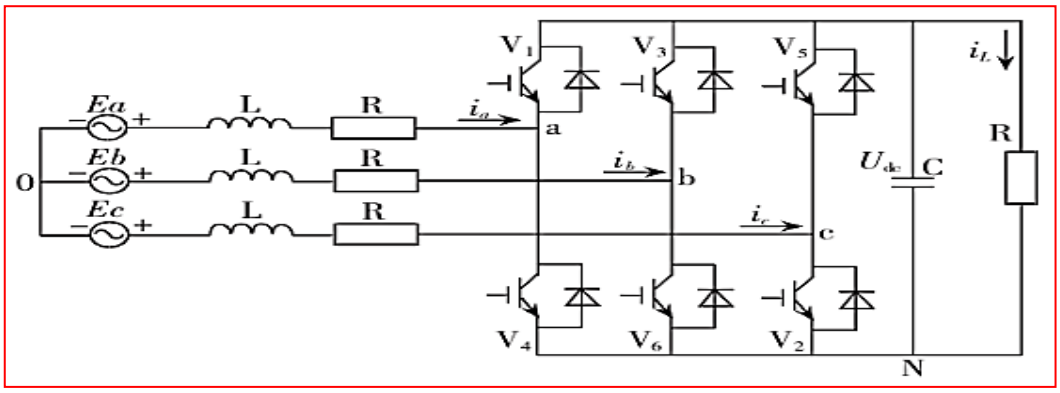

Figure 2.1 Topology of the three-phase voltage-sourced PWM

3. Type of PWM rectifier

Two structures can be distinguished for PWM rectifier

- *Three-phase PWM rectifier current.*
- *Three-phase PWM rectifier Voltage.*

3.1 PWM rectifier current

The topology of the current PWM rectifier is illustrated in Figure (2.2). It allows for the conversion of energy between an AC voltage source and a DC current receiver. The switches are unidirectional in current, but bidirectional in voltage [3]. The use of PWM control technique leads to sinusoidal AC current with controlled harmonic pollution. This structure is often equipped with a second-order LC filter on the AC side [9].To power the input of the rectifier with a current source, an additional inductance is added between the grid and the rectifier. In the operation of the current PWM rectifier, the AC grid determines the voltage value at the converter's input.

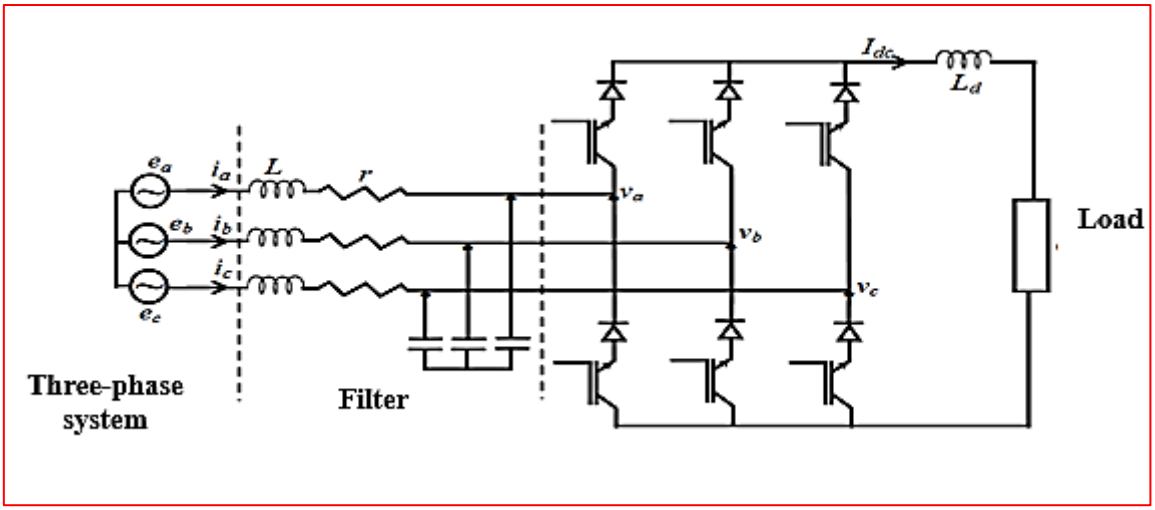

Figure 2.2 Topology of a current PWM rectifier

3.2 PWM Rectifier Voltage

A voltage source PWM rectifier is simply a voltage inverter used in reverse to produce a DC voltage from an AC grid, but with sinusoidal current absorption and unity power factor. It is powered by a sinusoidal voltage source and supplies a DC current load. Therefore, it has the structure of a current inverter [12]. The voltage source PWM rectifier can operate as a voltage dropper. It can also be directly used to supply a variable voltage to a DC current load [12]. Figure (2.3) illustrates the principle of a PWM rectifier. Each switch consists of an IGBT and a diode in anti-parallel. This switch is unidirectional in voltage and bidirectional in current. Thus, this converter, by its structure, is reversible in current, and can therefore instantaneously control the waveform of the currents drawn from the grid [13].It has the advantage of

supplying a load with DC from an AC grid, with the absorbed current being sinusoidal and possibly in phase with the corresponding grid voltage. This PWM rectifier enables achieving a power factor very close to unity and adjustable via the control of its switches [12]. In the following work, we focus on studying this type of converter.

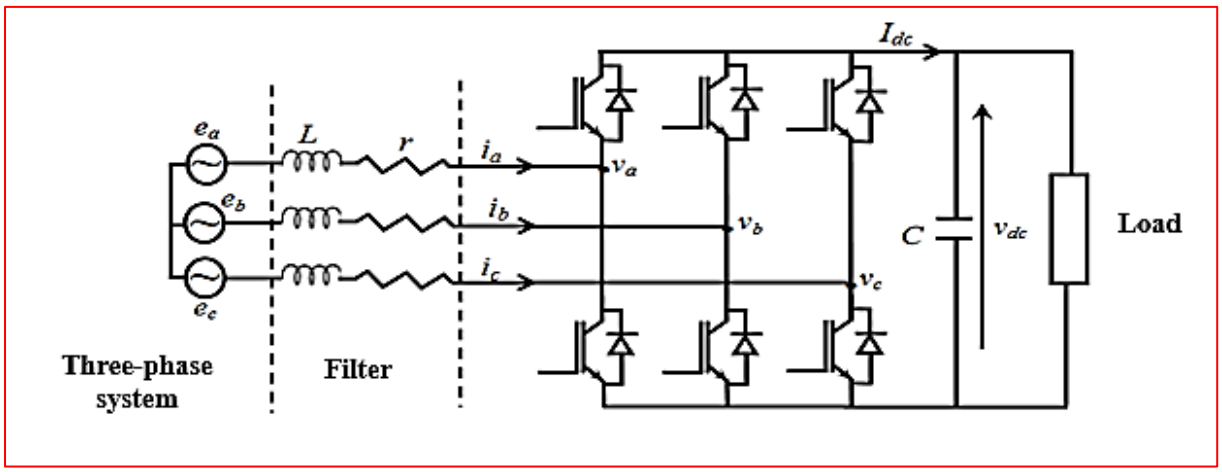

Figure 2.3 Topology of a three-phase voltage PWM rectifier

4. Constitution of a Voltage PWM Rectifier

The PWM rectifier consists of six power switching (transistors and anti-parallel diodes). All these elements are considered as ideal switches. The arm is a two-position switch that allows obtaining two voltage levels at the output [14], See figure (2.4).

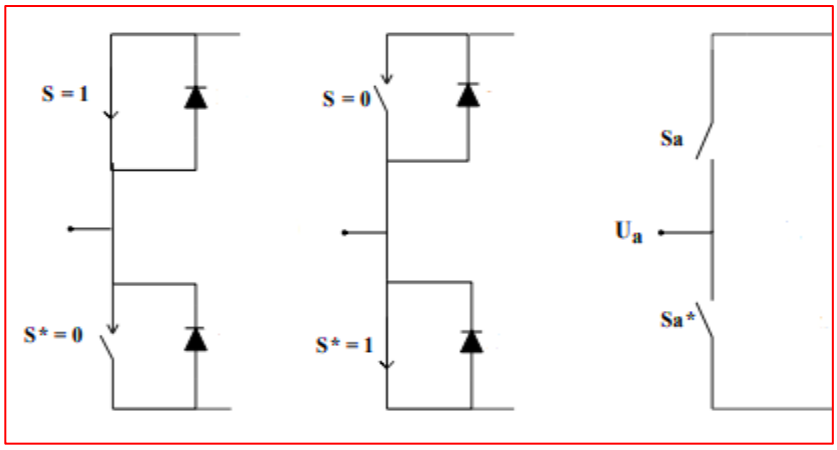

Figure 2.4 Diagram of the arm of PWM rectifier

5. Principles operating of PWM rectifier

The voltage rectifier operates by maintaining the DC bus voltage at a desired reference value using closed-loop control, as shown in Figure (2.5). To accomplish this task, the DC bus voltage $V_{dc}$is measured and compared with a reference.V_{dc-ref}The error signal produced from this comparison is used to switch the six rectifier switches. In this way, power can flow in both directions depending on the conditions of the DC bus voltageV_{dc}measured across the capacitor [15,16].

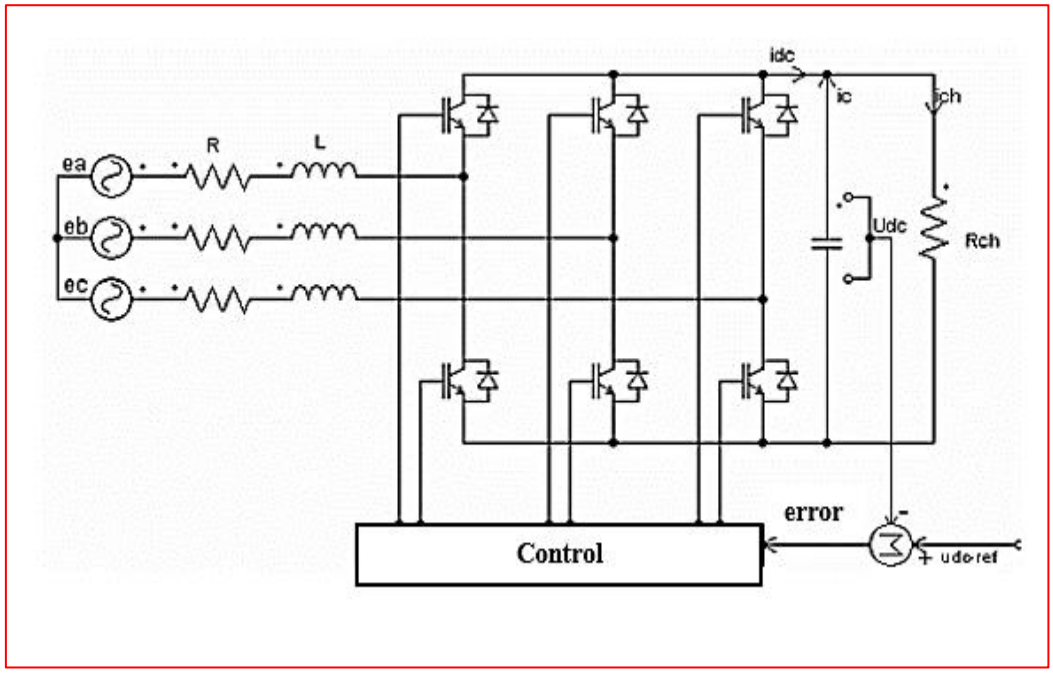

Figure 2.5 Basic topology of a voltage rectifier

The PWM rectifier converter is reversible, meaning that during rectifier operation, the charging current $i_{ch}$is positive, the capacitor C is discharged, and the error signal instructs the control block to draw more power from the AC source. The control block draws power from the AC source by producing an appropriate PWM signal for the six switches. In this way, more current flows from the AC source to the DC side, and the capacitor voltage is replenished.

6. Modeling of the PWM rectifier

The modelling of the PWM rectifier requires modelling of the:

- Source block
- Input passive filter
- block Converter
- Load
- Technique Control

6.1. Source block

The source block consists of three purely sinusoidal three-phase electromotive forces (f.é.m.) in series with a resistance $R_s$and an inductance $L_s$on each phase. The network is assumed to be perfectly balanced. The impedances of the three phases are identical [12].

We have:

$$\begin{cases} e_a = E_m cos\omega t \\ e_b = E_m \cos(\omega t - \frac{2\pi}{3}) \\ e_c = E_m \cos(\omega t + \frac{2\pi}{3}) \end{cases} \quad (2.1)$$

where: V_a, V_b, V_c are the line-to-neutral voltages.

The system of differential equations giving the current in each phase [12] is as follows:

$$\frac{d}{dt}\begin{bmatrix} i_a \\ i_b \\ i_c \end{bmatrix} = \begin{bmatrix} -\frac{R_s}{L_s} & 0 & 0 \\ 0 & -\frac{R_s}{L_s} & 0 \\ 0 & 0 & -\frac{R_s}{L_s} \end{bmatrix}\begin{bmatrix} i_a \\ i_b \\ i_c \end{bmatrix} + \frac{1}{L_s}\begin{bmatrix} e_a - v_a \\ e_b - v_b \\ e_c - v_c \end{bmatrix} \quad (2.2)$$

6.2. Converter block

The converter is an inverter operated as a controlled rectifier with an adjustable output DC voltage, as shown in Figure (2.6). The IGBTs and diodes comprising the bridge are assumed to be ideal. Switching is assumed instantaneous, and losses due to conduction and switching are neglected.

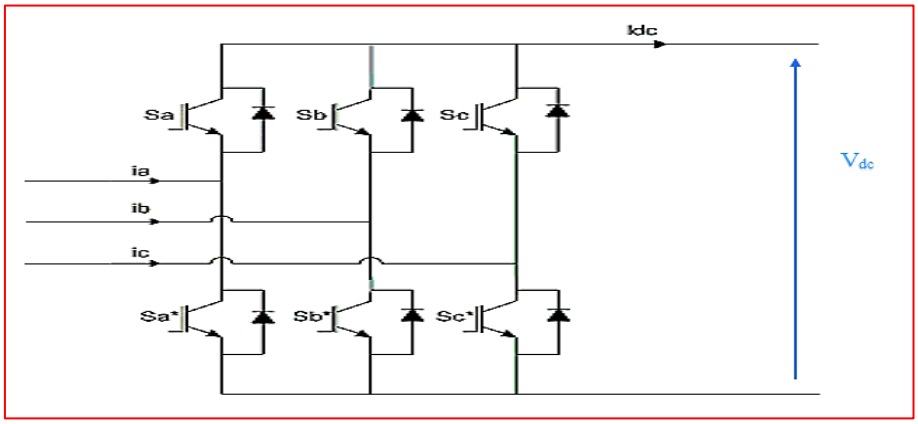

Figure 2.6 Structure topology of AC/DC converter

By knowing the state of each switch, we can define the connection matrix of the converter. We can then deduce the expression of the input quantities as a function of the output quantities [17].

The input voltages of the rectifier as a function of the output voltage and the states of the switches are given by the system:

$$\begin{bmatrix} V_a \\ V_b \\ V_c \end{bmatrix} = \frac{1}{3}\begin{bmatrix} 2 & -1 & -1 \\ -1 & 2 & -1 \\ -1 & -1 & 2 \end{bmatrix}\begin{bmatrix} S_a \\ S_b \\ S_c \end{bmatrix}[V_{dc}] \quad (2.3)$$

Similarly, the output current I_{rd} can be expressed in terms of the input currents by the relationship:

$$i_{dc} = [S_a \quad S_b \quad S_c] \begin{bmatrix} i_a \\ i_b \\ i_c \end{bmatrix} \tag{2.4}$$

6.3.Load block

This block is composed of a capacitance C in parallel with a resistance R_d and an inductance L_d.

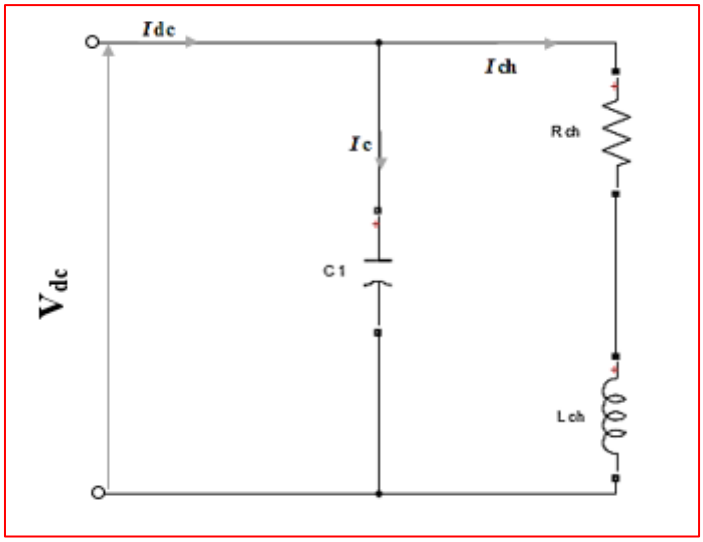

Figure 2.7 Diagram on the load side

The voltage V_{dc} across the load terminals is given by the following equation:

$$\begin{cases} \frac{dv_{dc}}{dt} = \frac{i_{dc} - i_{ch}}{c} \\ \frac{di_{ch}}{dt} = \frac{v_{dc} - R_{ch} i_{ch}}{L_{ch}} \end{cases} \tag{2.5}$$

7. Equation for the PWM rectifier-load association:

The equations giving the input current and output voltage of the converter are as follows:

$$\begin{cases} \frac{di_a}{dt} = \frac{e_a - R_s i_a - V_a}{L_s} \\ \frac{di_b}{dt} = \frac{e_b - R_s i_b - V_b}{L_s} \\ \frac{di_c}{dt} = \frac{e_c - R_s i_c - V_c}{L_s} \\ \frac{dv_c}{dt} = \frac{i_{dc} - i_{ch}}{C} \end{cases} \tag{2.6}$$

Where:

i_{ch} : is the current absorbed by the load

For a resistive load R_d

$$i_{ch} = \frac{V_{dc}}{R_d} \tag{2.7}$$

For a resistive-inductive load (R_d, L_d)

$$\frac{di_{ch}}{dt} = \frac{V_{dc} - R_d i_{ch}}{L_d} \tag{2.8}$$

For an active load (R_d, L_d, E):

$$\frac{di_{ch}}{dt} = \frac{V_{dc} - R_d i_{ch} - E}{L_d} \quad (2.9)$$

8. Mathematical Model of three phase PWM Rectifier

8.1 Model in the (a, b, c) reference frame

The equation of phase voltage of the three-phase rectifier is given by the following system:

$$\begin{bmatrix} e_a \\ e_b \\ e_c \end{bmatrix} = R \begin{bmatrix} i_a \\ i_b \\ i_c \end{bmatrix} + L \frac{d}{dt} \begin{bmatrix} i_a \\ i_b \\ i_c \end{bmatrix} + \begin{bmatrix} V_a \\ V_b \\ V_c \end{bmatrix} \quad (2.10)$$

The voltages V_{abc} upstream of the rectifier are as follows:

$$v_n = V_{dc}(S_n - \frac{1}{3}\sum_{n=0}^{c} S_n) \quad (2.11)$$

With: n=1, 2, 3

Furthermore, we can express the current of the DC bus as follows:

$$C \frac{dV_{dc}}{dt} = i_c \quad (2.12)$$

The current through the capacitor is then:

$$i_c = i_{dc} - i_{ch} \quad (2.13)$$

$$C \frac{dV_{dc}}{dt} = S_a i_a + S_b i_b + S_c i_c \quad (2.14)$$

Therefore, for the alternating side of the rectifier, we can write:

$$\begin{cases} L \frac{di_a}{dt} + R i_a = e_a - V_{dc}(S_a - \frac{1}{3}\sum_{n=a}^{c} S_n) = e_a - v_{dc}(S_a - \frac{1}{3}(S_a + S_b + S_c)) \\ L \frac{di_b}{dt} + R i_b = e_b - V_{dc}\left(S_b - \frac{1}{3}\sum_{n=a}^{c} S_n\right) = e_b - v_{dc}(S_b - \frac{1}{3}(S_a + S_b + S_c)) \\ L \frac{di_c}{dt} + R i_c = e_c - V_{dc}\left(S_c - \frac{1}{3}\sum_{n=a}^{c} S_n\right) = e_c - v_{dc}(S_c - \frac{1}{3}(S_a + S_b + S_c)) \end{cases} \quad (2.15)$$

Where:

e_a, e_b, e_c:Grid voltage;

i_a, i_b, i_c:Line currents;

S_a, S_b, S_c:Switch states.

The combination of equations allows us to draw the three-phase functional diagram in the (a, b, c) reference frame given by Figure (2.9).

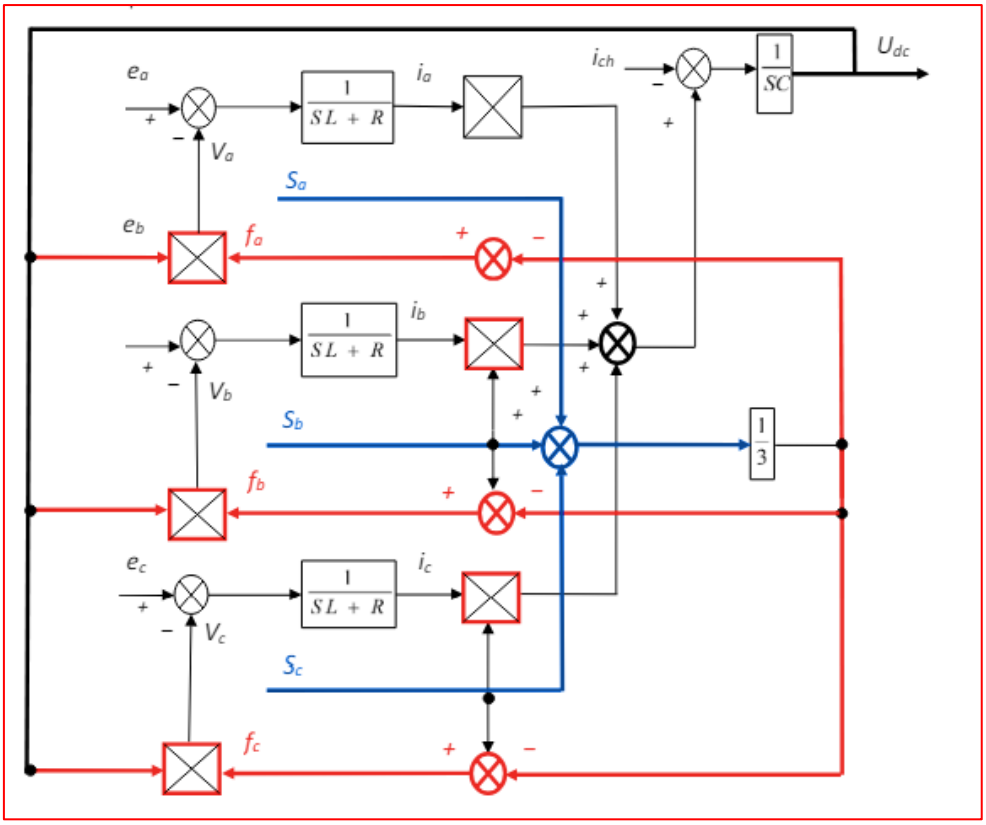

Figure 2.8 Diagram bloc of a PWM rectifier in the (a, b, c) reference frame

8.2. Model in the (d, q) reference frame

The PWM rectifier can also be modelled in a rotating (d, q) reference frame linked to the rotating field, using the Park transformation (see appendix) of each quantity. The resulting voltage equations are [18]:

$$\begin{cases} e_d = Ri_d + L\frac{di_d}{dt} - \omega Li_q + v_d \\ e_q = Ri_q + L\frac{di_q}{dt} + \omega Li_d + v_q \end{cases} \quad (2.16)$$

The voltage equations in the rotating (d, q) reference frame are obtained using the Park transformation according to the following methodology:

We have

$$e_{abc} = Ri_{abc} + L\frac{d}{dt}i_{abc} + V_{abc} \quad (2.17)$$

On the other hand, we write the modified direct Park transformation.Haut du formulaire

$$\begin{cases} [e_{abc}] = [P(\theta)]^{-1}[e_{odq}] \\ [i_{abc}] = [P(\theta)]^{-1}[i_{odq}] \\ [v_{abc}] = [P(\theta)]^{-1}[v_{odq}] \end{cases} \quad (2.18)$$

We replace (2.17) in the three-phase equation (2.18), as follows:

$$[P(\theta)]^{-1}[e_{odq}] = R[P(\theta)]^{-1}[i_{odq}] + L\frac{d}{dt}([P(\theta)]^{-1}[i_{odq}]) + [P(\theta)^{-1}][v_{odq}] \quad (2.19)$$

Multiplying both sides of equality (2.19) by P(θ), we then obtain equation (2.20):

$$[e_{odq}] = R[i_{odq}] + [P(\theta)]L\frac{d[P(\theta)]^{-1}}{dt}[i_{odq}] + L\frac{d[i_{odq}]}{dt} + [v_{odq}] \quad (2.20)$$

Knowing that we can demonstrate that:

$$\begin{cases} \frac{d}{dt}[P(\theta)]^{-1} = \frac{d\theta}{dt}\frac{d[P(\theta)]^{-1}}{dt} \\ [P(\theta)]\frac{d[P(\theta)]^{-1}}{dt} = \frac{d\theta}{dt}\begin{bmatrix}0 & 0 & 0\\ 0 & 0 & -1\\ 0 & 1 & 0\end{bmatrix} \end{cases} \quad (2.21)$$

Replacing equation (2.21) in equation (2.20), we will have equation (2.22):

$$\begin{cases} [e_{odq}] = R[i_{odq}] + L\frac{d\theta}{dt}\begin{bmatrix}0 & 0 & 0\\ 0 & 0 & -1\\ 0 & 1 & 0\end{bmatrix}[i_{odq}] + L\frac{d}{dt}[i_{odq}] + [v_{odq}] \\ \begin{bmatrix}e_o\\ e_d\\ e_q\end{bmatrix} = R\begin{bmatrix}i_o\\ i_d\\ i_q\end{bmatrix} + L\frac{d\theta}{dt}\begin{bmatrix}0 & 0 & 0\\ 0 & 0 & -1\\ 0 & 1 & 0\end{bmatrix}\begin{bmatrix}i_o\\ i_d\\ i_q\end{bmatrix} + L\frac{d}{dt}\begin{bmatrix}i_o\\ i_d\\ i_q\end{bmatrix} + \begin{bmatrix}v_o\\ v_d\\ v_q\end{bmatrix} \end{cases} \quad (2.22)$$

After expansion, we arrive at the equations in the d-q Park reference frame, taking into consideration the homopolar component.

$$\begin{cases} e_o = Ri_o + L\frac{di_o}{dt} + v_o \\ e_d = Ri_d - L\frac{d\theta}{dt}i_q + L\frac{di_d}{dt} + v_d \\ e_q = Ri_q + L\frac{d\theta}{dt}i_d + L\frac{di_q}{dt} + v_q \end{cases} \quad (2.23)$$

We know that

$$:\frac{d\theta}{dt} = \omega \quad (2.24)$$

Finally, we deduce the three equations (2.25), which allow us to develop our functional diagram of the PWM rectifier in the d-q reference frame.

$$\frac{dV_{dc}}{dt}\begin{cases} e_d = Ri_d + L\frac{di_d}{dt} - \omega Li_q + v_d \\ e_q = Ri_q + L\frac{di_q}{dt} + \omega Li_d + v_q \\ C = S_d i_d + S_q i_q - i_{ch} \end{cases} \quad (2.25)$$

The functional diagram is therefore as follows:

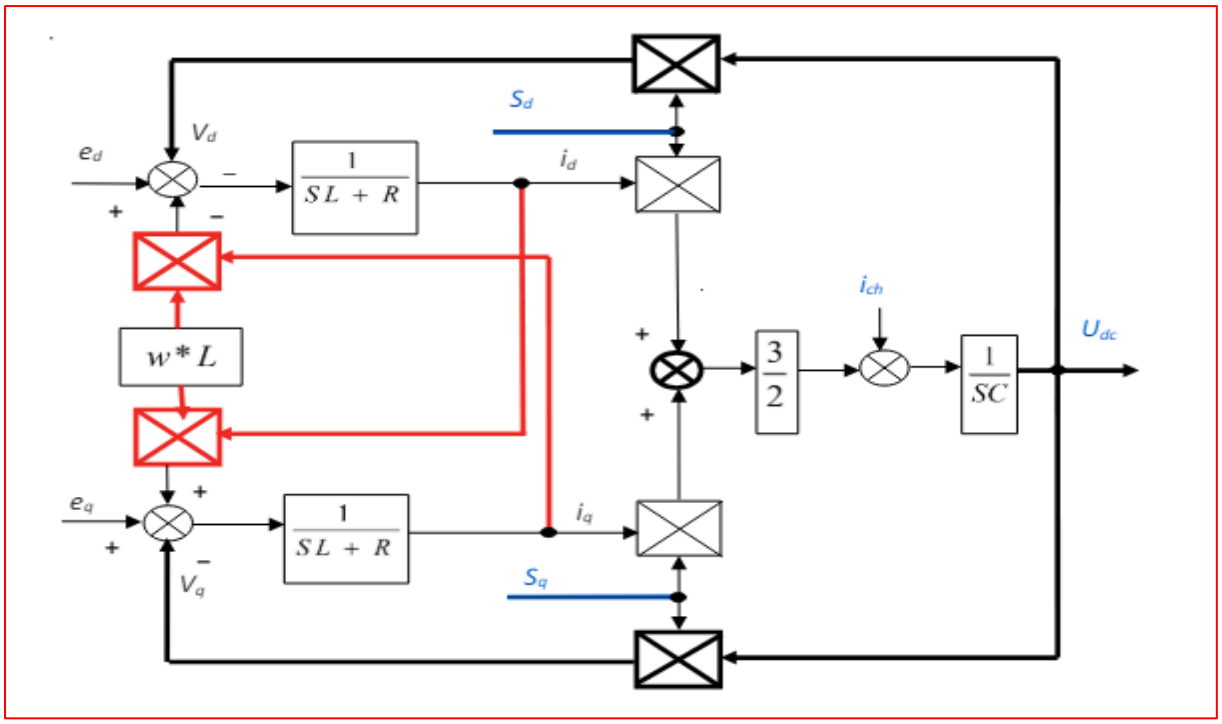

Figure 2.9 Diagram bloc of a PWM rectifier in the rotating (d, q) reference frame

9. Method for estimating reference currents:

9.1. Current control of a PWM rectifier:

The DC voltage$V_{dc}$is measured and compared to a reference (V_{dc_ref},)and the resulting error signal is used to generate a reference current(i_{ref}) . This reference has a sinusoidal waveform similar to the source with an amplitudeI_{max}, evaluated by the DC bus voltage controller according to equation [9,19]:

$$I_{max} = G.(V_{dc} - V_{dc\_ref}) \quad (2.26)$$

Where

G: is a controller consisting of a proportional term and an integral term.

The control in Figure (2.10) involves measuring the instantaneous currents (i_{abc}) and forcing them to follow the reference currents (i_{ref}.). Once an error occurs, PWM control is generated using a hysteresis regulator to switch the switches [8].

The overall structure for estimating reference currents of a voltage PWM rectifier bridge is presented in Figure (2.10). This method involves using a peak detector for the amplitude (peak) of the three source voltages.

$$\begin{cases} e_{sa}(t) = E_{max}\sin(\omega t) \\ e_{sb}(t) = E_{max}\sin(\omega t - \frac{2\pi}{3}) \\ e_{sc}(t) = E_{max}\sin(\omega t - \frac{4\pi}{3}) \end{cases} \quad (2.27)$$

The extraction of the amplitude of the three voltages is expressed by the following relation:

$$E_{max} = \sqrt{2/3\,(e_{sa}^2 + e_{sb}^2 + e_{sc}^2)} \quad (2.28)$$

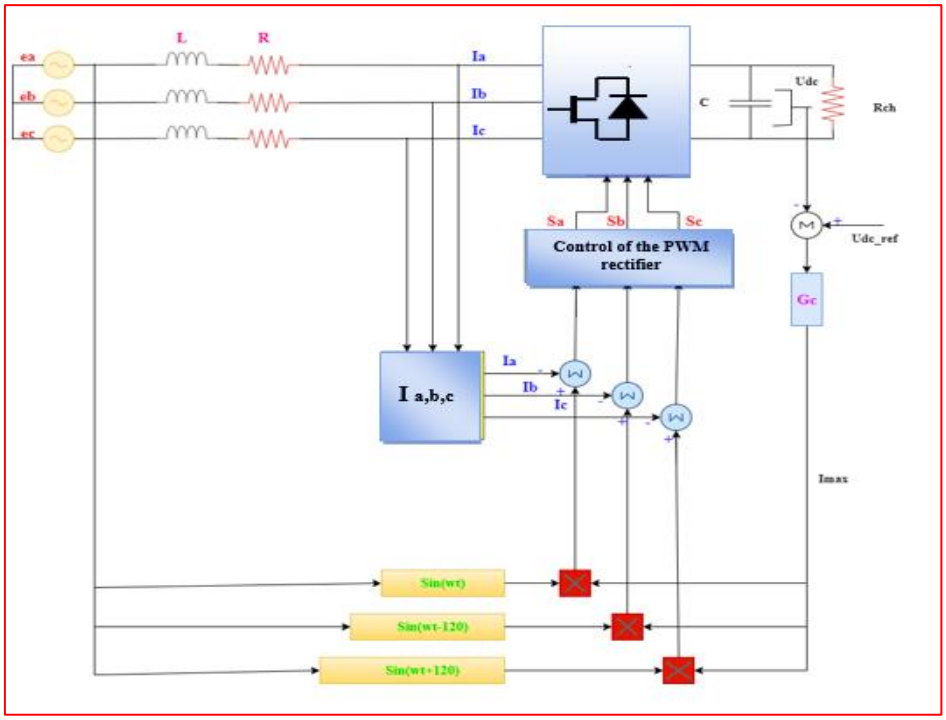

Figure 2.10 Control of the PWM rectifier

9.2. Estimation of the Source Reference Current and Regulation of the DC bus Voltage

The variation in the output voltage of the PWM rectifier is mainly due to conduction losses, switching losses, the presence of smoothing inductors, and load variations [20]. To mitigate these variations, a regulation loop for the DC bus voltage is provided to maintain the voltage equal to its reference value by controlling the charging and discharging process of the capacitor. Indeed, the DC voltage V_{dc} is measured and compared to a reference voltage. The result of this comparison (voltage error) is applied to this regulator to obtain the magnitude, and subsequently the three instantaneous reference currents [21, 19].

Various methods have been proposed by the authors to determine the reference currents. In our work, the method used consists of using a detector peak. The amplitude of the source currents is generated by a regulation loop of the DC bus voltage of the PWM rectifier using PI controller.

The instantaneous reference currents isa*, isb*, isc* are calculated from the multiplication of three unit sines (sin(ωt), sin(ωt+2π/3), sin(ωt+4π/3)) by the value reference current peak of the Ism source. The three unit sines are obtained from the division of three network voltages by their amplitude V_{sm}.

From the method of peak detector, V_{sm} is obtained using this equation:

$$V_{sm} = \sqrt{2/3\,(v_{sa}^2 + v_{sb}^2 + v_{sc}^2)} \quad (2.29)$$

9.3. PLL system

Indeed, this peak detector method requires that the network voltage must be healthy (sinusoidal and balanced), otherwise it is not applicable. Since the network voltage is often disturbed and/or distorted, and in order to generalize the application of this method identification that we have adopted at any type of voltage, the use of the loop at phase locking (phase-locked-loop PLL) is essential for the synthesis of the three unit sinuses [19].

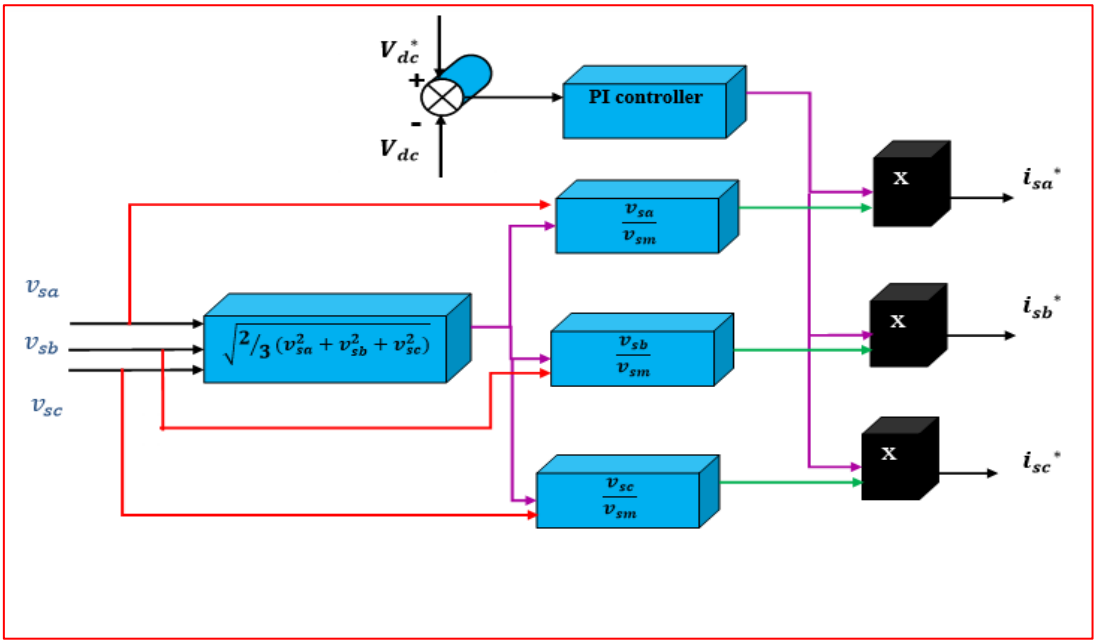

Figure 2.11 Scheme for calculating source reference currents with PI Controller

.94. PI Controller

The Proportional Integral (PI) controller used for adjusting the currents of the PWM rectifier, and the DC bus voltageV_{dc}, is simple and quick to implement while offering acceptable performance. The parameters of this PI controller are determined based on the relationship between the power absorbed by the capacitor and the voltage across its terminals [17]. Figure (2.12) illustrates the schematic of the continuous voltage regulation loop.

To determine the parameters of the PI regulator, we follow the development following mathematics: The relationship between the power absorbed by the capacitor and the voltage across this is written [22]:

$$P_{dc} = \frac{d}{dt}\left(\frac{1}{2}C_{dc}.V_{dc}^2\right) = C_{dc}.V_{dc}^* \frac{dV_{dc}}{dt} \quad (2.30)$$

By neglecting losses in the inverter and eliminating the disturbance due to current load, the relationship between the instantaneous power at the filter input and the power absorbed by the capacitor is given by:

$$P_{dc} = \frac{3}{2} V_{sm} I_{sm} = V_{dc} V_{dc}^{*} C_{dc} S \quad (2.31)$$

The transfer function of the PI controller can be expressed as:

$$k_p + \frac{k_i}{S} = \frac{1+\tau P}{T_i P}$$

(2.32)

After calculation, the closed-loop transfer function of the overall system is given by:

$$F(P) = \frac{\omega_0^2 (1+\tau)}{P^2 + 2\varepsilon_0 \omega_0 P + \omega_0 P} \quad (2.33)$$

with :

$$\begin{cases} \omega_0 = \sqrt{\frac{2}{C_{dc} T_i}} \\ \varepsilon_0 = \frac{\tau}{\sqrt{2 C_{dc} T_i}} \\ k_P = \frac{\tau}{T_i} \\ k_i = \frac{1}{T_i} \end{cases} \quad (2.34)$$

To achieve a good compromise between dynamic and static performance, we will choose a value of the critical damping coefficient ξc between 0.4 and 0.8. There quality of regulation will also depend on the choice of the cut-off pulse. This must be high enough to ensure good dynamics in transient conditions.

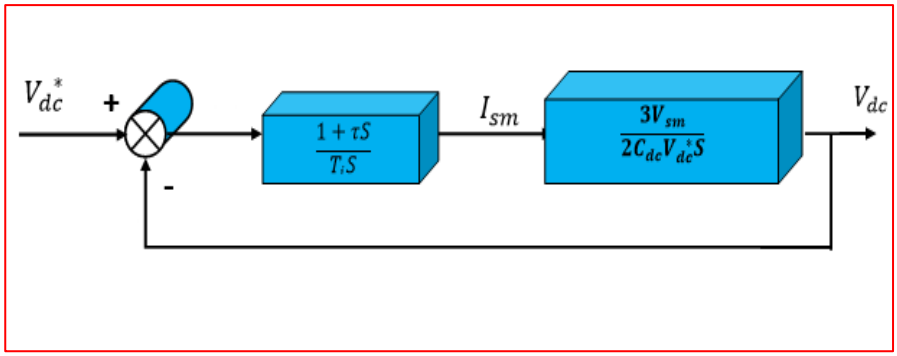

Figure 2.12 Represents the PI controller used for regulating the DC bus voltage of a PWM rectifier

10. Control Strategies of PWM rectifier

Research on PWM rectifiers has grown rapidly over the last few years. These converters have become an area of research attractive and of great interest, for their various industrial and domestic applications and advantages they offer, namely: the possibility of energy regeneration, control of the voltage of the DC bus over a wide range, the absorption of sinusoidal currents on the power network, and the possibility of operation with a power factor close to of the unit.

The performance of the PWM rectifier and in particular the reduction in the THD of the source current are certainly linked to the performance of the generation of references current, but also depend on the control strategy of the voltage inverter (pursuit current references). Two types of static converter controls are mainly implemented [23]:

- ❖ Hysteresis control.
- ❖ PWM control.

10.1 Hysteresis control

In this chapter, we study hysteresis control, since it is commonly used. This current control by hysteresis consists of maintaining the current in a band enveloping its reference. Each violation of this band gives an order to switching to switches.

Figure (2.13) illustrates the principle of current control by two-level fixed-band hysteresis. The difference between the reference current and that measured is applied to the input of a hysteresis comparator H whose output provides the order of control of the corresponding arm of inverter.

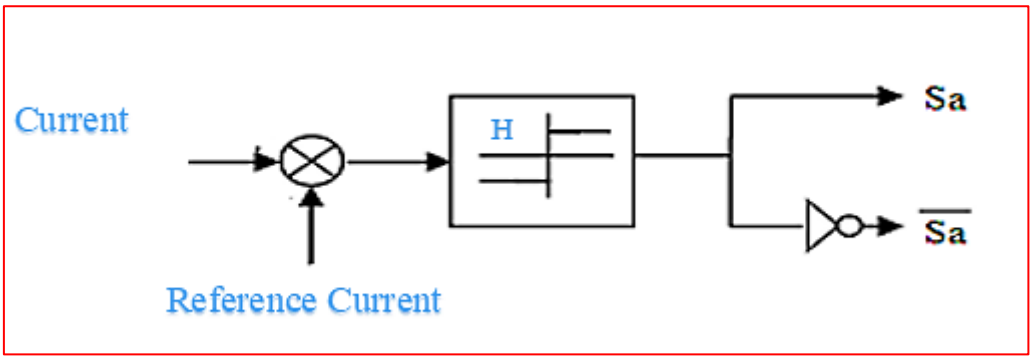

Figure 2.13 Principle of fixed-band hysteresis control

The principle of hysteresis control consists of keeping each of the generated currents within a band [24]. The difference between the current and its reference is compared to a fixed-width band H called the hysteresis band. This method ensures the control of the switching frequency of the switches by acting on H. Each violation of this band results in a switching command for the switches [25]. Figures (2.14) illustrate this principle.

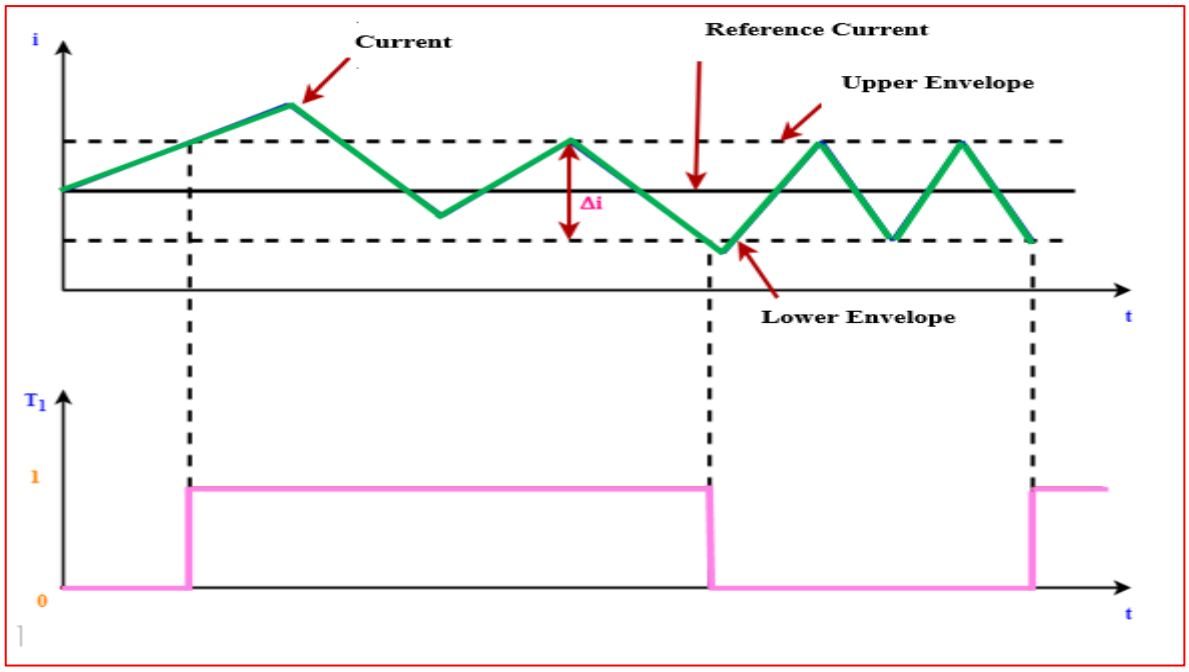

Figure 2.14 Principle of hysteresis control.

Let be the difference between the reference current and the measured actual line current defined by :

$$\varepsilon_k = I^*_{ref} - I_{mes} \tag{2.35}$$

The control commands for the switches are then determined as follows:

$$Si : \begin{cases} \varepsilon_k \geq \Delta_i \ \text{ so } \ B_{k1} = 1 \\ \varepsilon_k \leq -\Delta_i \ \text{ so } \ B_{k1} = 0 \end{cases} \tag{2.36}$$

k=1, 2,3

If not, the control of the switch remains unchanged.Δ_i is being the width of the hysteresis band.

10.2 Sinusoidal PWM (SPWM) Control

SPWM is one of the most popular and simple methods utilized in power inverter and motor control fields. Its main features can be summarized as sine-triangle wave comparison.As shown in (Figure 2.15), a sine wave (modulated wave, magenta) is compared with a triangle wave (carrier wave, green) and when the instantaneous value of the triangle wave is less than that of the sine wave, the SPWM output signal (orange) is in high level (1).Otherwise it is turned into the low level (0). The level switching edge is produced at every moment the sine wave intersects the triangle wave. Thus the different crossing positions result in variable duty cycle of the output waveform.

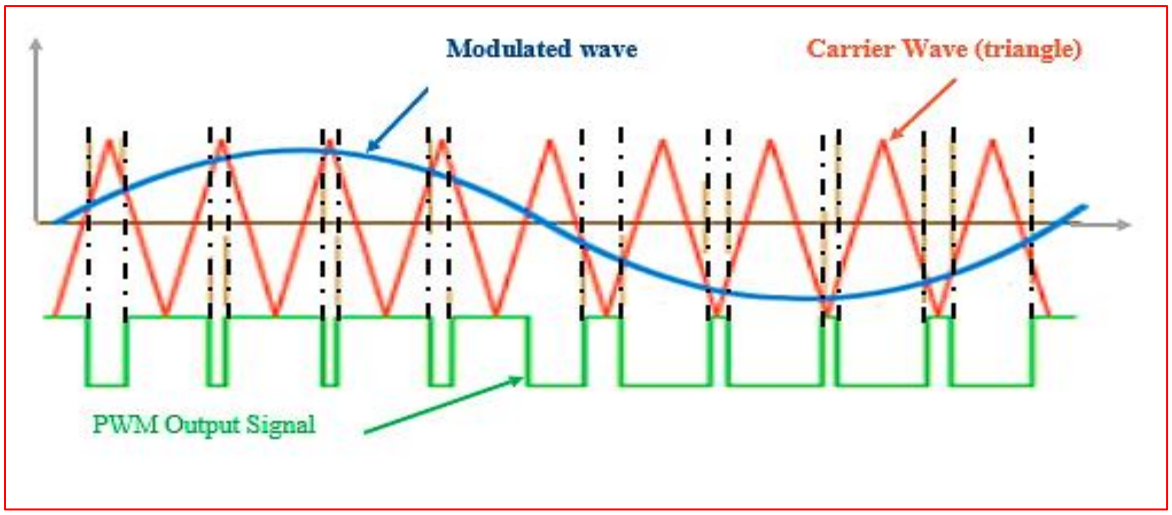

Figure 2.15 SPWM Waveform Generation

In terms of the basic principle of SPWM illustrated above, it's easy to implement using analogy circuit (Figure 2.16). Sine and triangle waves are respectively generated by specially designed circuits and then fed to the properly selected comparator which can output the desired SPWM signal.

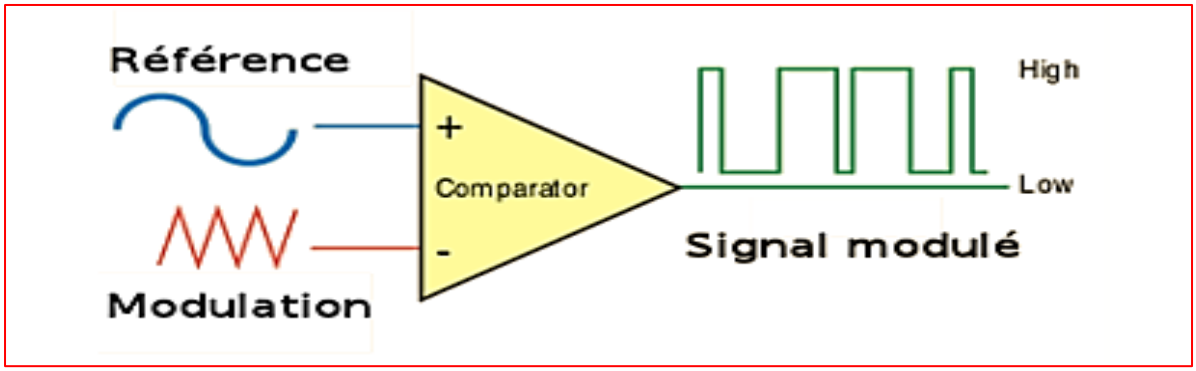

Figure 2.16 Analog Scheme for SPWM Implementation

The operating mode is very simple:

If: $V_{ref} > V_p$: the upper switch of the bridge arm conducts;

If: $V_{ref} < V_p$: the lower switch of the bridge arm conducts;

The principal method of SPWM is illustrated in Figure (2.17)

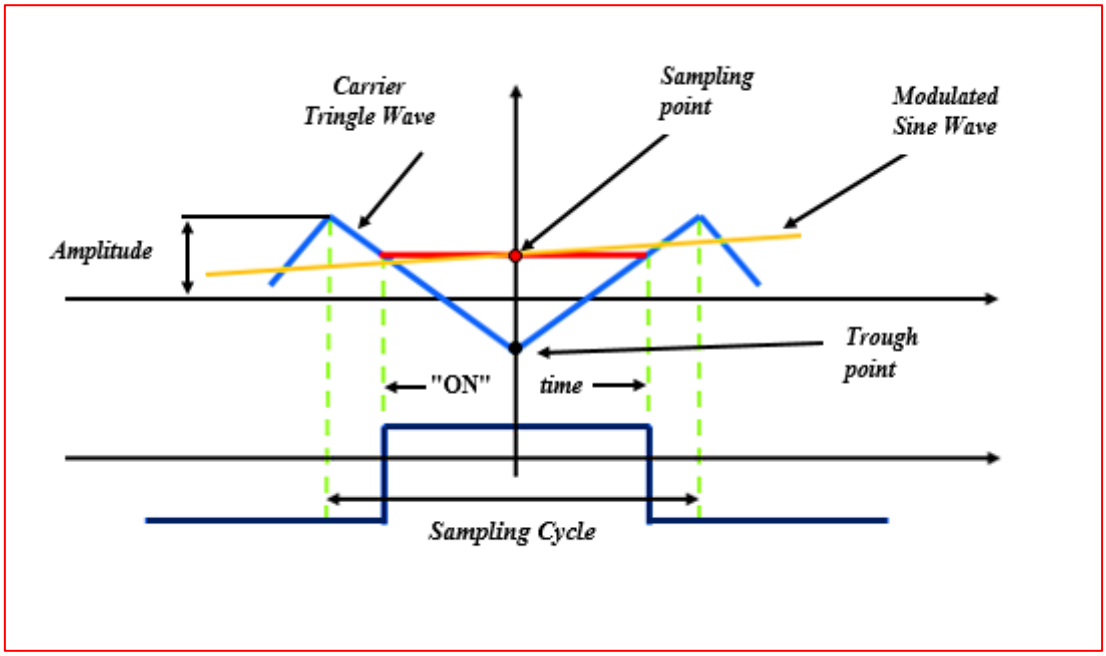

Figure 2.17 Symmetric Regular Sampled Method

11. Simulation

In this section, we present the various results obtained from simulation. These results were obtained for a conventional setup using a PI controller for the DC bus voltage regulation using hysteresis band current control. The simulation parameters used are presented in Table (2.1).

parameters	***Values***
Input voltage phase to phase (rms)	380V
Input filtre	0.1Ω, 0.1e-3 H
coupling inductance	0.5 H
Capacitive load	500e-6 μF
Load	100Ω, 3e-3 H

Table 2.1 System parameter of Simulation bloc of PWM rectifier using hysteresis control

The simulation bloc of a PWM rectifier using hysteresis banc current control connected to the grid under MATLAB/Simulink environment is presented in figure (2.18)

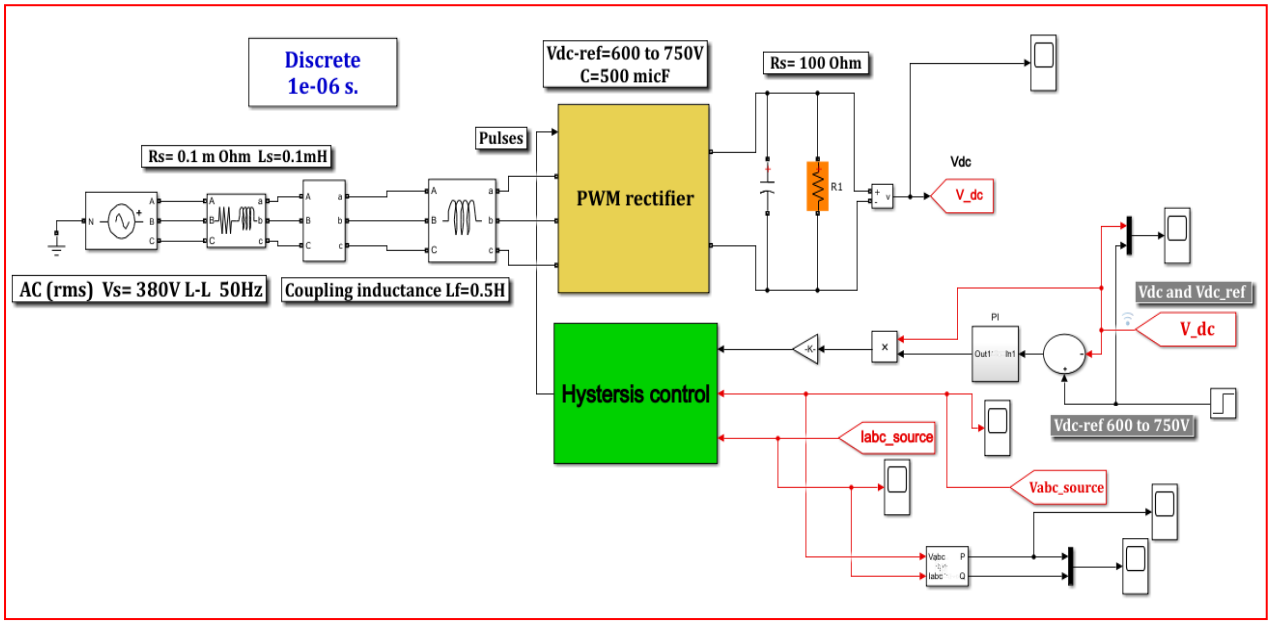

Figure 2.18 Simulation bloc of PWM rectifier using hysteresis control

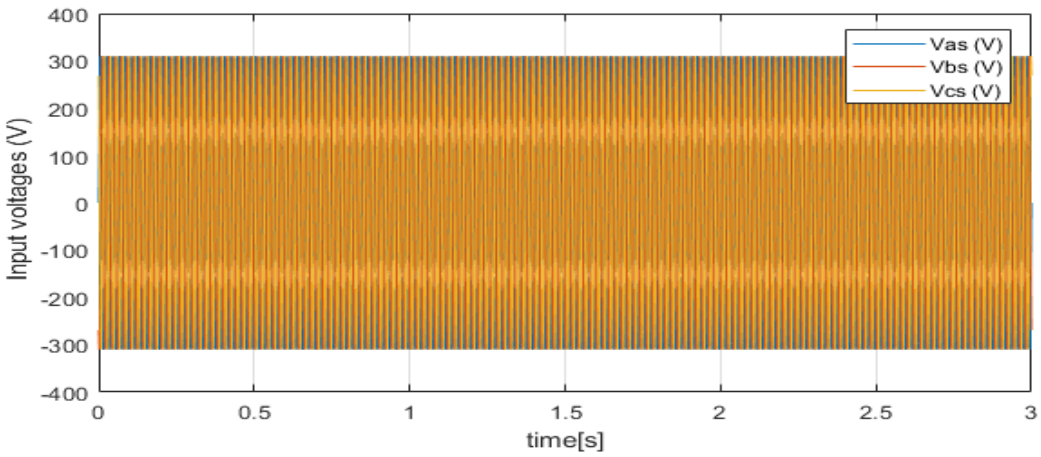

(a) Input voltage

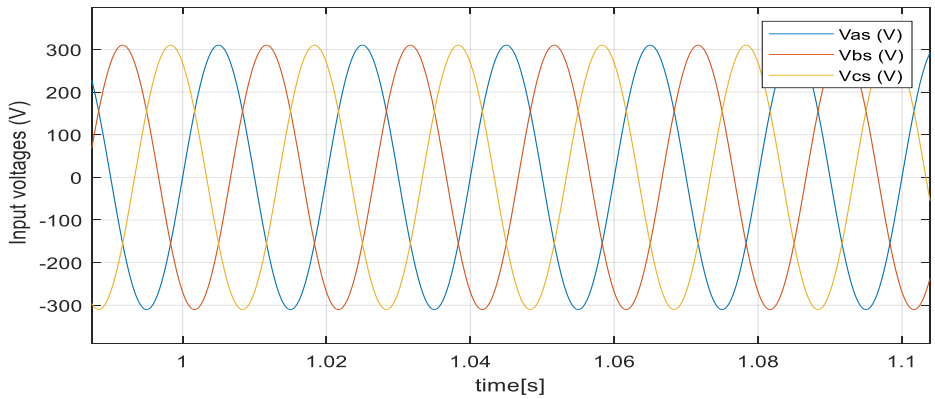

(b) Zoom of the input voltage

Figure 2.19 Input voltages

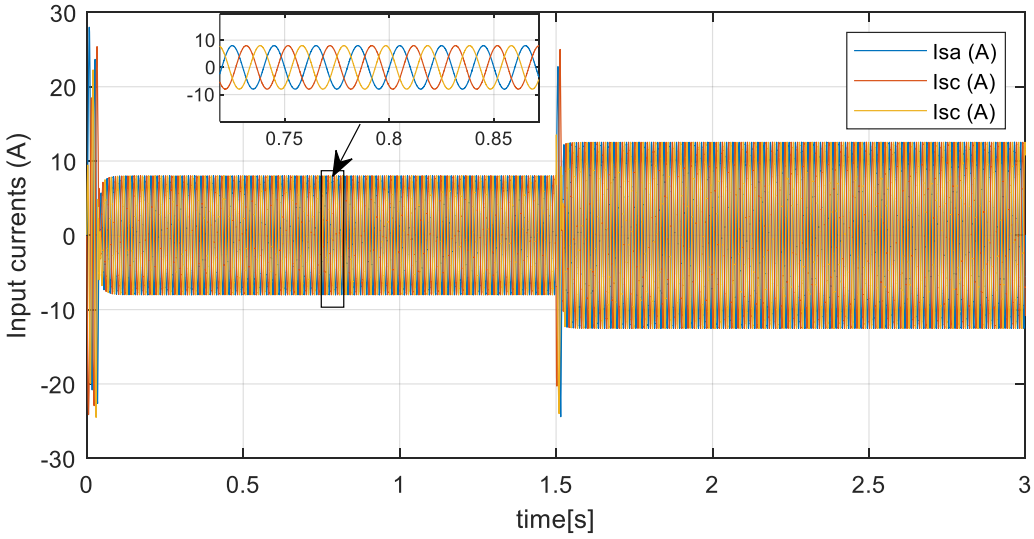

Figure 2.20 Input currents

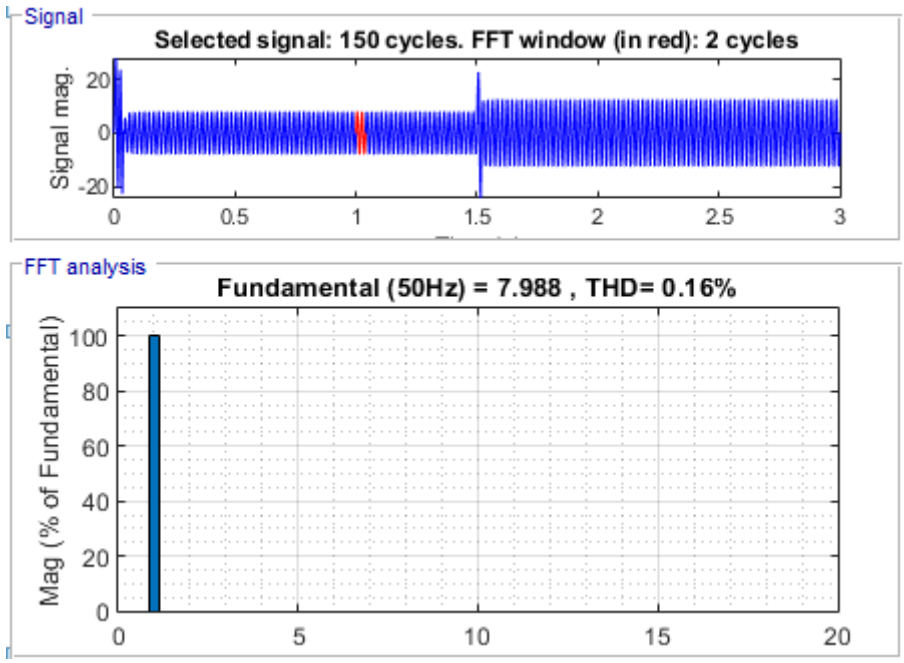

Figure 2.21 Spectrum harmonic of input currents

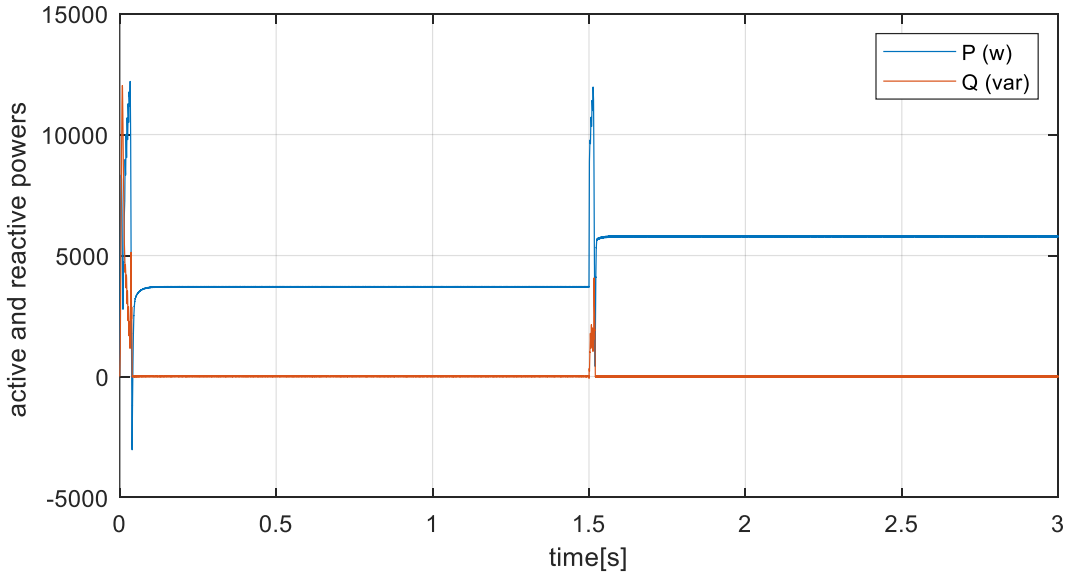

Figure 2.22 Active and reactive powers

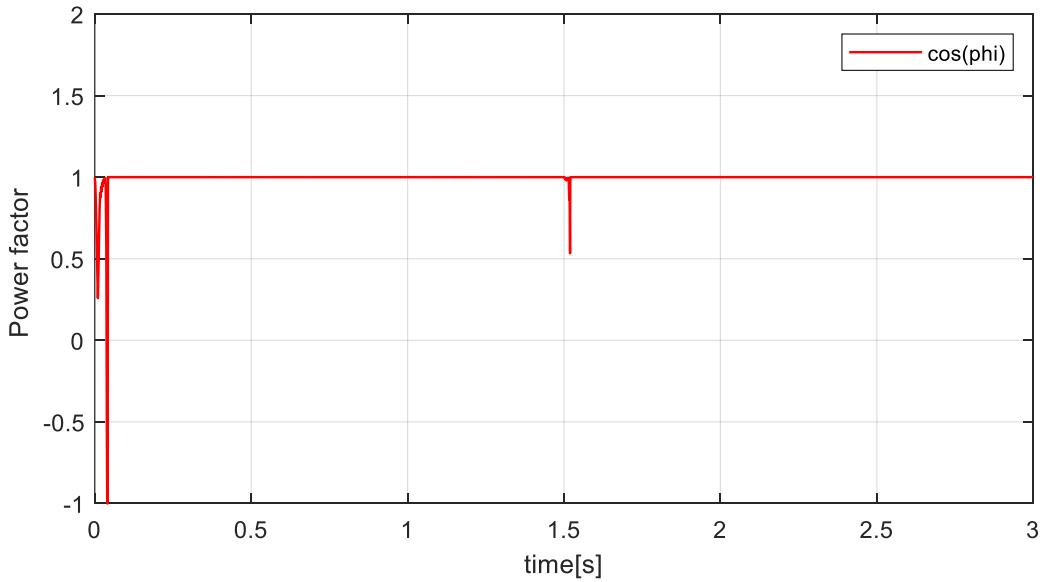

Figure 2.23 Power factor at unity

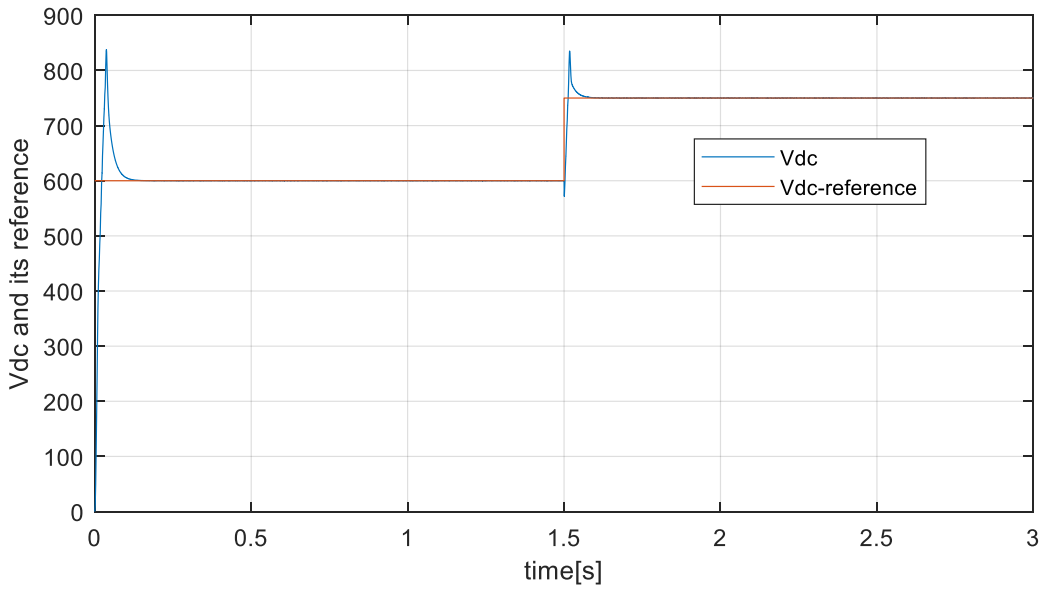

Figure 2.24 DC voltage and its reference

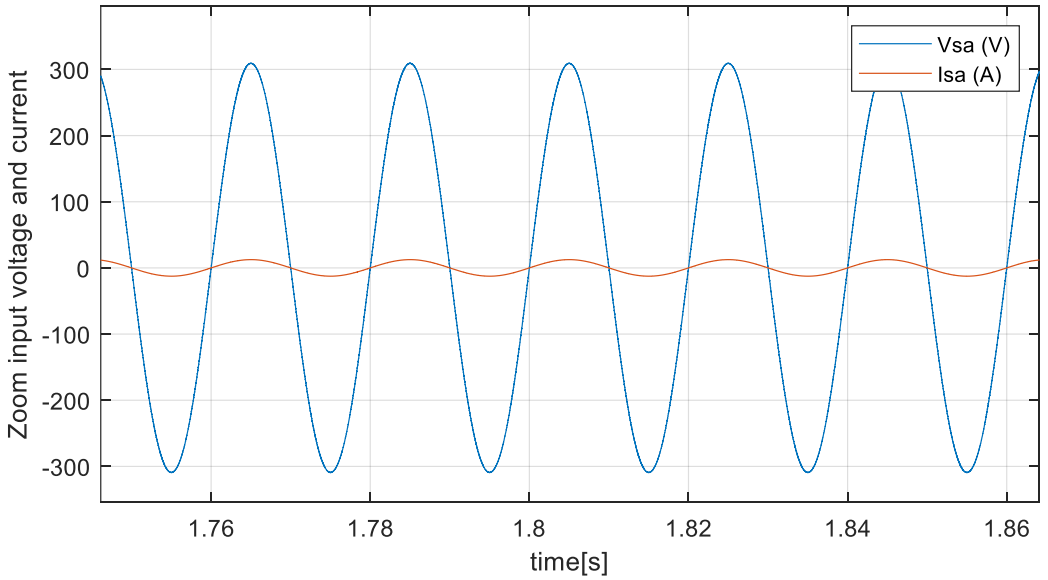

Figure 2.25 The waveform of the source voltage and current per phase.

The bloc simulation of PWM rectifier in Figure (2.18) is controlled by hysteresis band current, with the bandwidth set such that $\Delta_i = 0.01A$. The results from Figure (2.19) and Figure (2.20) show the waveforms of the input voltage and the input currents. We observe that the shapes of the input voltage and current for all three phases are purely sinusoidal. Figure (2.21) illustrates that the current total harmonic distortion (THD) is very low, at 0.16%. Figure (2.22) demonstrates the presence of active power, while reactive power is completely absent, resulting in a unity power factor shown in Figure (2.23). Figures (2.24) represent the

DC bus voltage, which stabilizes close to its reference between 600V and 750V at 1.5s. The phase difference between the current and the ideal voltage is completely nullified, as shown in Figure (2.25). This justifies that the PWM rectifier with Hysteresis control achieves good performance.

12. Conclusion:

In this chapter, we discussed the basic structure of a two-level PWM rectifier. Subsequently, our study focused on the analysis of the voltage PWM rectifier, its operating principle, and its modeling. We proposed the controls strategies control for the rectifier: hysteresis band current control is presented. This technique is applied to the PWM rectifier based on PI controller. The obtained results are effective and high-performing.

CHAPTER III

DIRECT POWER CONTROL OF PWM RECTIFIER

Chapter III

DIRECT POWER CONTROL OF PWM RECTIFIER

1. Introduction

In this chapter, we will study the classic DPC control based on hysteresis control of a PWM rectifier. For classic DPC control, we will develop the estimation of the two control variables, which are active and reactive power. Finally, we will present simulation results that highlight the performance of classic DPC control of a PWM rectifier.

2. Operation principle of classic DPC

The principle of classic DPC involves selecting a sequence of switching commands (S_a, S_b, S_c) for the semiconductors constituting the PWM rectifier, based on a switching table. The selection is made based on digitized errors,S_P and S_q, between the references of active and reactive powers (P* and q*). The reference for active power is obtained by regulating the DC voltage using a PI controller. Meanwhile, to ensure unity power factor control and reactive power at zero, real values (P and Q) are provided by two-level hysteresis comparators, as well as the angular position of the grid voltage vector ($e_{\alpha\beta}$). For the latter, the α_β plane is divided into twelve (12) equal sectors of 30° each. Each of the control sequences (S_a, S_b, S_c) corresponds to a voltage vector at the input of the rectifier v_i [26] [27].

3. Direct Power Control (DPC)

The Direct Power Control (DPC) is based on the concept of direct torque control applied to electrical machines. The objective is to directly control the active and reactive power in a PWM rectifier, similar to the principle applied to control torque and flux in alternative machines [28]. Errors between the reference values of instantaneous active and reactive powers and their measurements are introduced into two hysteresis comparators. These comparators, along with a switching table and the sector value where the grid voltage is located, determine the switching state of the semiconductors. The DC bus voltage loop is regulated with a PI controller [29], ensuring the error between the measured (DC) voltage and its reference is controlled. Meanwhile, the reference reactive power is directly set to zero to absorb sinusoidal currents under a source voltage assumed to be sinusoidal, ensuring the rectifier operates with unity power factor [26].

The main idea of Direct Power Control (DPC), initially proposed by Ohnishi (1991) and further developed by Noguchi and Takahachi in 1998, is similar to the Direct Torque Control

(DTC) of asynchronous machines. Instead of controlling flux and torque, the instantaneous active (P) and reactive (Q) powers are chosen as the two quantities to be controlled, Figure 3.1 show general configuration of DPC based PWM rectifier.

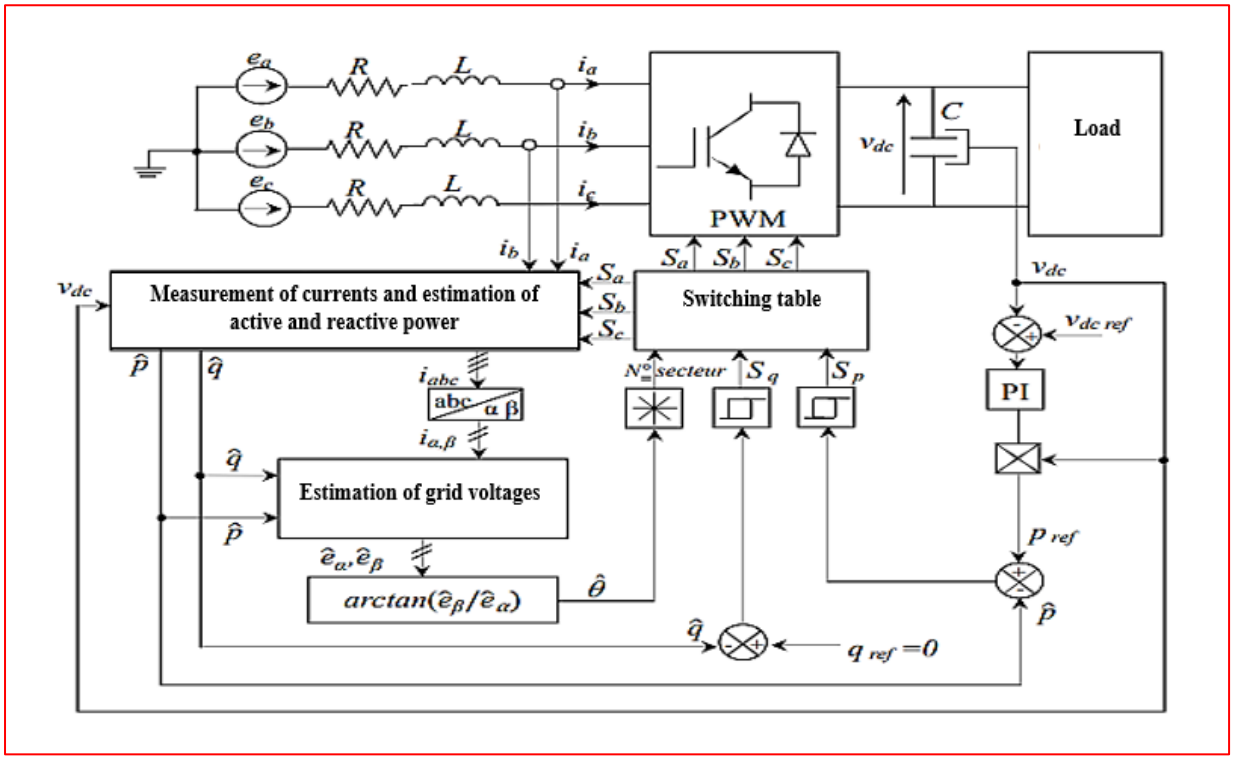

Figure 3.1: General configuration of DPC control

Figure (3.1) shows the overall configuration of sensor less Direct Power Control for a PWM rectifier. DPC involves selecting a control vector based on a commutation table. This table is built upon the digitized errors S_p, S_q of instantaneous active and reactive powers, provided by the two-level hysteresis controllers, as well as the angular position of the estimated voltage vector. Depending on this position value, the (α-β) plane is divided into twelve sectors, where each sector is associated with a logical state of the rectifier. The reference for active power is obtained by regulating the DC voltage using a PI controller. Meanwhile, to ensure unity power factor, reactive power control is maintained at zero [32].

4. Instantaneous active and reactive Powers Estimation

Instantaneous active power is defined as the scalar product of line currents and voltages, while reactive power is defined as the vector product between them [31]. The complex apparent power $\overline{S}$ can be expressed by the following expression [31]:

$$\overline{S} = P + jq \tag{3.1}$$

$$\overline{S} = e_a i_a + e_b i_b + e_c i_c + \frac{1}{\sqrt{3}}[(e_b - e_a)i_a + (e_c - e_a)i_b + (e_a - e_b)i_c] \tag{3.2}$$

However, expression (3.1) and (3.2) requires knowledge of the grid voltages. Therefore, it is necessary to express the powers in terms of other expressions independent of the grid voltages. Thus, the expressions that give the estimation of instantaneous active and reactive powers without measuring the grid voltages are as follows [31]:

$$\begin{aligned}\widehat{P} &= L\left(\frac{di_a}{dt}+\frac{di_b}{dt}+\frac{di_c}{dt}\right)+v_{dc}(S_a i_a+S_b i_b+S_c i_c)\\ \hat{q} &= \frac{1}{\sqrt{3}}\left[L\left(\frac{di_a}{dt}i_c-\frac{di_c}{dt}i_a\right)-v_{dc}(S_a(i_b-i_c)+S_b(i_c-i_a)+S_c(i_a-i_b)\right]\end{aligned} \quad (3.3)$$

The first part of both expressions represents the power in the line inductances. It is worth noting here that the internal resistances of these inductances are neglected because the active power dissipated in these resistances is indeed much lower compared to the power involved. However, the second part represents the output power of the rectifier. It can be seen that both equations (.33) are functions of the states of the switches S_a, S_b, S_c, and also the knowledge of the line inductance L is necessary to perform power estimation.

5. Estimation of Grid Voltage

The calculation of the sector number is based on knowledge of the voltage vector position, so estimating the line voltage is essential. The following expression gives the line currents ia, ib, ic in stationary α-β coordinates:

$$\begin{bmatrix} i_\alpha \\ i_\beta \end{bmatrix} = \sqrt{\frac{2}{3}}\begin{bmatrix} 1 & -\frac{1}{2} & -\frac{1}{2} \\ 0 & -\frac{\sqrt{3}}{2} & -\frac{\sqrt{3}}{2} \end{bmatrix}\begin{bmatrix} i_a \\ i_b \\ i_c \end{bmatrix} \quad (3.4)$$

The active power can be written in the following form:

$$\widehat{P} = \bar{e}_{(abc)}\bar{i}_{(abc)} = e_\alpha i_\alpha + e_\beta i_\beta \quad (3.5)$$

Similarly, reactive power can be written as follows:

$$\hat{q} = \bar{e}_{(abc)}\bar{i}_{(abc)} = e_\beta i_\alpha - e_\alpha i_\beta \quad (3.6)$$

We can write equations (3.5) and (3.6) in matrix form as follows:

$$\begin{bmatrix} \widehat{P} \\ \hat{q} \end{bmatrix} = \begin{bmatrix} e_\alpha & e_\beta \\ e_\beta & -e_\alpha \end{bmatrix}\begin{bmatrix} i_\alpha \\ i_\beta \end{bmatrix} \quad (3.7)$$

The voltage can be estimated by the following equation:

$$\begin{bmatrix} \hat{e}_\alpha \\ \hat{e}_\beta \end{bmatrix} = \frac{1}{(i_\alpha^2+i_\beta^2)}\begin{bmatrix} i_\alpha & -i_\beta \\ i_\beta & i_\alpha \end{bmatrix}\begin{bmatrix} \widehat{P} \\ \hat{q} \end{bmatrix} \quad (3.8)$$

If we denote the components $\hat{e}_\alpha$and $\hat{e}_\beta$as projections of the voltage vector $\hat{e}$onto the α and β axes respectively, then the three voltage vectors in the three-phase plane can be represented by a single voltage vector e^ in the two-phase α,β plane rotating with the angular frequency

$\omega = 2\pi$ f. in a circle of radiu s $\sqrt{\frac{3}{2}}E_m$, Figure (3.2):

Where

f: grid frequency.

E_m: amplitude of three-phase voltages.

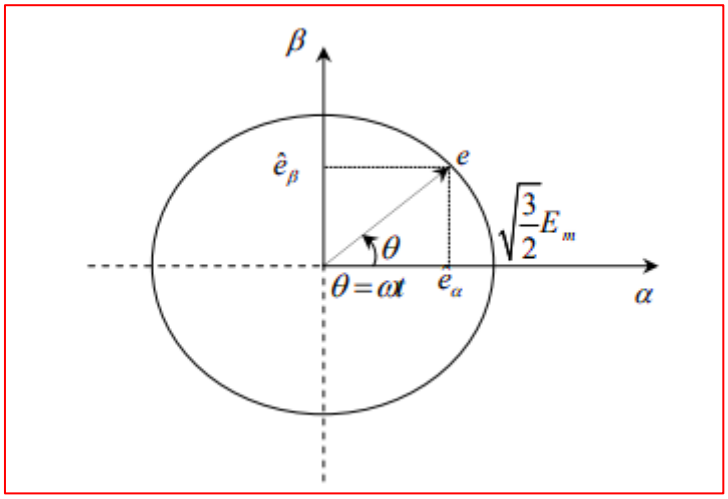

Figure 3.2: Estimated voltage vector in the (α,β) plane

6. Sector Determination

Knowledge of the sector of the estimated voltage is necessary to determine the optimal commutation states. To do this, the workspace (α, β) is divided into 12 sectors (Figure (3.3)), which can be determined by the following relationship [31]:

$$(n-2)\frac{\pi}{6} < \theta_n < (n-1)\frac{\pi}{6} \quad n = 1 \cdots\cdots 12, \tag{3.9}$$

Where: n is the sector number

The sector number is determined instantaneously by the position of the voltage vector given by:

$$\theta = \text{Arctg}(\frac{e_\beta}{e_\alpha}) \tag{3.10}$$

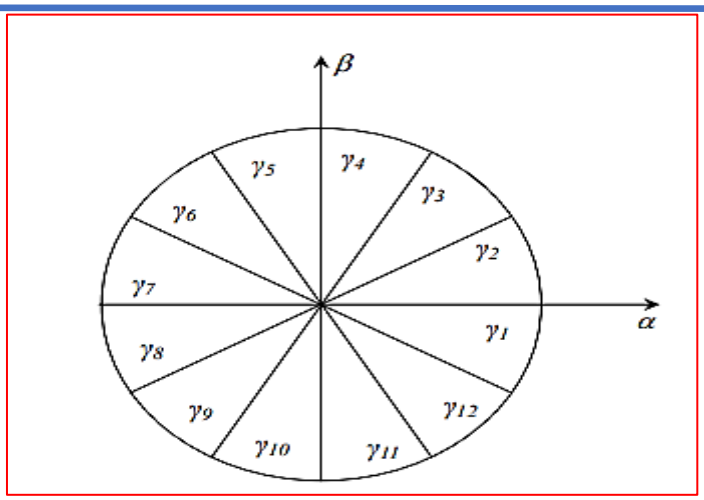

Figure 3.3: (α, β) Plane Divided into 12 Sectors

7. Hysteresis Controller

The simplicity of implementation of the two-level comparator is behind the choice of this type of controller. Additionally, energy considerations on the rectifier impose a limited number of switching. For the same control hysteresis width, the two-level comparator will require a lower number of switching [30].

The width of the hysteresis band of the hysteresis controllers has a considerable effect on the rectifier's performance. In particular, it affects harmonic current distortion and the average switching frequency of the rectifier. The controller proposed in classic DPC uses a two-level controller for active and reactive powers.

The outputs of the hysteresis controllers, given by the Boolean variables S_p and S_q, indicate upper or lower exceedances of power errors according to the following logic:

$$\begin{aligned} S_p = 1 \quad &\Leftrightarrow P_{ref} - \hat{P} > h_p \\ S_p = 0 \quad &\Leftrightarrow P_{ref} - \hat{P} < -h_p \\ S_q = 1 \quad &\Leftrightarrow q_{ref} - \hat{q} > h_p \\ S_q = 0 \quad &\Leftrightarrow q_{ref} - \hat{q} < -h_p \end{aligned} \tag{3.11}$$

Where h_p, h_q are the deviations of the two-level hysteresis controllers.

The digital error signals S_p and S_q, along with the working sector number, are the inputs to the commutation table, where the switching states S_a, S_b, and S_c of the PWM rectifier are stored.

8. Commutation Table

The digital error signals S_p and S_q, along with the working sector number, are the inputs to the commutation table, where the switching states S_a, S_b, and S_c of the PWM rectifier are stored.

The optimum switching state of the rectifier can be chosen at each commutation state based on the combination of the digital signals S_p, S_q, and the sector number. That is to say, the choice of the optimum switching state is made such that the error of the active power can be restricted within a hysteresis band of width 2hp, and similarly for the reactive power error, with a band of width 2hq.

The expression of the currents in theα, β reference frame is given by:

$$\frac{\mathrm{di}_\alpha}{\mathrm{dt}} = \frac{1}{L}(e_\alpha - u_{c\alpha} - Ri_\alpha) \tag{3.12}$$

$$\frac{di_\beta}{dt} = \frac{1}{L}\left(e_\beta - u_{c\beta} - Ri_\beta\right) \tag{3.13}$$

The line current vector $[i_\alpha i_\beta]^T$ can be controlled by the choice of appropriate voltage vector at the input of the rectifier. The change in line current depends on the grid voltage $e_{\alpha\beta}$, the chosen voltage vector at the input of the rectifier $u_{c\alpha\beta}$, and the measured currents $i_{\alpha\beta}$. The parameter R is practically neglected, which leads to a first approximation of equation (3.12) and (3.13) that can be adopted [33]. Therefore, equation (3.12) and (3.13) becomes:

$$\frac{\mathrm{di}_\alpha}{\mathrm{dt}} = \frac{1}{L}(e_\alpha - u_{c\alpha}) \tag{3.14}$$

$$\frac{di_\beta}{dt} = \frac{1}{L}\left(e_\beta - u_{c\beta}\right) \tag{3.15}$$

The derivatives of active and reactive powers in the α, β reference frame are given by:

$$\frac{dp}{\mathrm{dt}} = \frac{de_\alpha}{dt} i_\alpha + e_\alpha \frac{di_\alpha}{dt} + \frac{de_\beta}{dt} i_\beta + e_\beta \frac{di_\beta}{dt} \tag{3.16}$$

$$\frac{dq}{\mathrm{dt}} = \frac{de_\beta}{dt} i_\alpha + e_\beta \frac{di_\alpha}{dt} - \frac{de_\alpha}{dt} i_\beta - e_\alpha \frac{di_\beta}{dt} \tag{3.17}$$

If the switching frequency is sufficiently high, the change in grid voltage can be neglected [33]. The dynamics of active and reactive power can be given as follows:

$$\frac{dp}{\mathrm{dt}} = e_\alpha \frac{di_\alpha}{dt} + e_\beta \frac{di_\beta}{dt} \tag{3.18}$$

$$\frac{dq}{\mathrm{dt}} = e_\beta \frac{di_\alpha}{dt} - e_\alpha \frac{di_\beta}{dt} \tag{3.19}$$

By replacing equation (3.14 and 3.13) into (3.18 and 3.19) the dynamics of powers become:

$$\frac{dp}{\mathrm{dt}} = \frac{1}{L}\left(e_\alpha^2 + e_\beta^2\right) - \frac{1}{L}\left(e_\alpha . u_{c\alpha} + e_\beta . u_{c\beta}\right) \tag{3.20}$$

$$\frac{dq}{\mathrm{dt}} = \frac{1}{L}\left(e_\alpha . u_{c\beta} + e_\beta . u_{c\alpha}\right) \tag{3.21}$$

The term $\left(e_\alpha^2 + e_\beta^2\right)$ represents the square of the magnitude of the grid voltage in the (α,β) reference frame, so:

$$e_\alpha^2 + e_\beta^2 = \frac{3}{2}E_m^2 \tag{3.22}$$

Let's set:$E^2 = \frac{3}{2}{E_m}^2$and the voltages e_α and $e_\beta$are given by:

$$\left.\begin{matrix} e_\alpha = E\ cos(\theta) \\ e_\beta = E\ sin(\theta) \end{matrix}\right\}, \theta = \omega t \tag{3.23}$$

By replacing equation (3.23) into (3.20)and (3.21) we get:

$$\frac{dp_i}{dt} = \frac{1}{L}E^2 - \frac{1}{L}E\left(cos(\theta).u_{s\alpha i} + sin(\theta).u_{s\beta i}\right) \tag{3.24}$$

$$\frac{dq_i}{dt} = \frac{1}{L}E\left(cos(\theta).u_{s\beta i} + sin(\theta).u_{s\alpha i}\right) \tag{3.25}$$

The normalized expression of the dynamics of active and reactive powers can be given as follows:

$$\overleftarrow{\dot{p}_\iota} = \frac{\dot{p}_\iota}{\frac{1}{L}.E.\sqrt{\frac{2}{3}}V_{dc}} = \frac{E}{\sqrt{\frac{2}{3}}V_{dc}} - \left(cos(\theta).\bar{u}_{c\alpha i} + sin(\theta).\bar{u}_{c\beta i}\right) \tag{3.26}$$

$$\overleftarrow{\dot{q}_\iota} = \frac{\dot{q}_\iota}{\frac{1}{L}.E.\sqrt{\frac{2}{3}}V_{dc}} = \left(cos(\theta).\bar{u}_{c\beta i} + sin(\theta).\bar{u}_{c\alpha i}\right) \tag{3.27}$$

With:

$$\bar{u}_{c\alpha i} = \frac{u_{c\alpha i}}{\sqrt{\frac{2}{3}}V_{dc}}, \bar{u}_{c\beta i} = \frac{u_{c\beta i}}{\sqrt{\frac{2}{3}}V_{dc}} \tag{3.28}$$

From (3.27) (3.28), we can observe that the dynamics of reactive power are sinusoidal for all input voltage vectors of the rectifier. However, the dynamics of active power have a shifted sinusoidal waveform as shown in Figure (3.4).

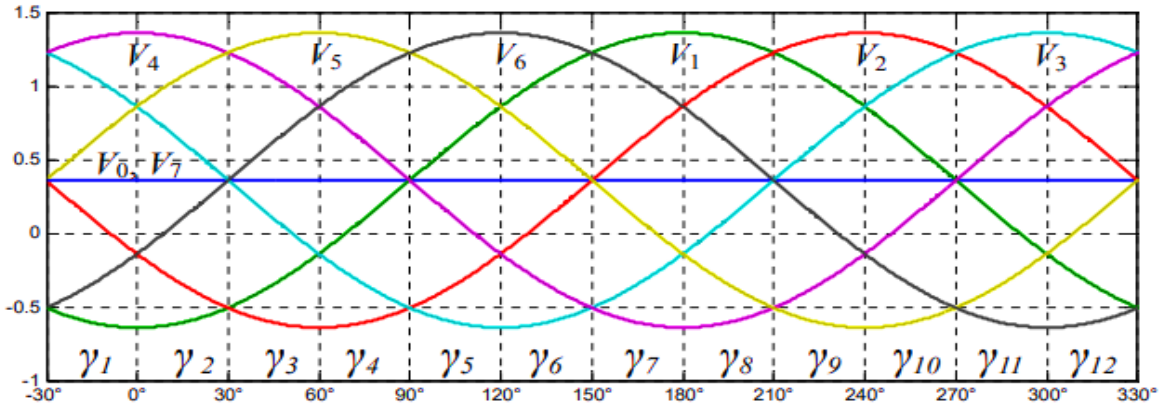

Figure 3.4 Derivative of active power in all sectors

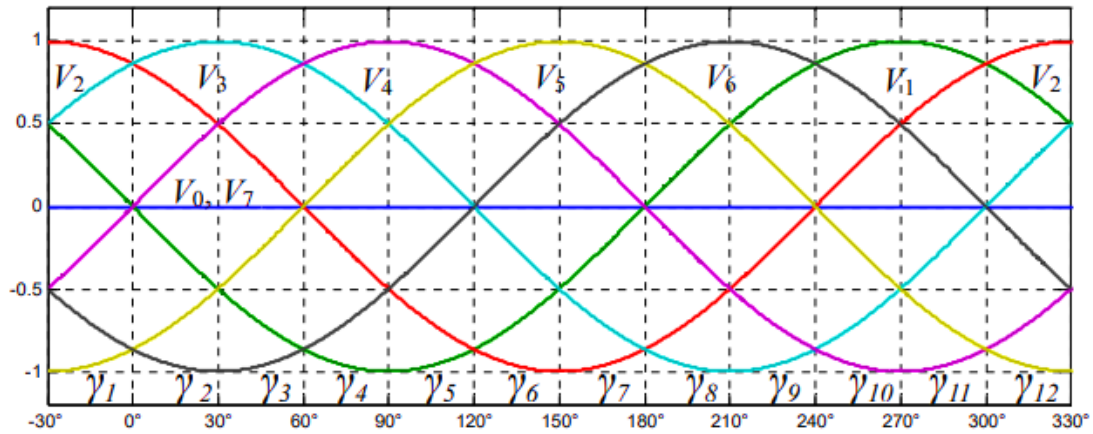

Figure 3.5 Derivative of reactive power in all sectors

The synthesis of the commutation table is based on the signs of the derivatives of active and reactive powers in each sector. For each sector, the change in reactive power is positive for three vectors, negative for three vectors, and zero for V_0, V_7. The sign of the change in active power is positive for four vectors, negative for two or three vectors. For example, for the first sector, the vectors that influence the sign of the change in active and reactive powers are summarized in Table (3.1).

$\overbrace{\dot{p}_\iota} > 0$	$\overbrace{\dot{p}_\iota} < 0$	$\overbrace{\dot{q}_\iota} > 0$	$\overbrace{\dot{q}_\iota} < 0$	$\overbrace{\dot{p}_\iota} = 0$
V_3 ,V_4,V_5,V_0	**V_1, V_6**	**V_1, V_2, V_3**	**V_4, V_5, V_6**	**V_0, V_7**

Table 3.1: Change in active and reactive powers in sector γ_1

For each combination of hysteresis output signals, S_p and S_q, the voltage vectors chosen for sector γ1 are shown in Table (3.2).

Secteur I		$\bar{q}_1$	
		$>0 \Leftrightarrow S_q = 1$	$<0 \Leftrightarrow S_q = 0$
$\bar{p}_1$	$>0 \Leftrightarrow S_p = 1$	V_3	V_4, V_5
	$<0 \Leftrightarrow S_p = 0$	V_1	V_6

Table 3.2: Voltage vectors chosen for sector γ1

For all sectors, the proposed commutation table is represented in Table (3.3).

S_p	S_q	γ_1	γ_2	γ_3	γ_4	γ_5	γ_6	γ_7	γ_8	γ_9	γ_{10}	γ_{11}	γ_{12}
1	**0**	V_7	V_7	V_1	V_0	V_2	V_7	V_3	V_0	V_4	V_7	V_5	V_0
	1	V_7	V_7	V_0	V_0	V_7	V_7	V_0	V_0	V_7	V_7	V_0	V_0
0	**0**	V_6	V_1	V_1	V_2	V_2	V_3	V_3	V_4	V_4	V_5	V_5	V_6
	1	V_1	V_2	V_2	V_3	V_3	V_4	V_4	V_5	V_5	V_6	V_6	V_1

Table 3.3: Commutation table of the adapted DPC

9. PI controlled DC voltage

The regulation of the DC voltage is ensured by a PI-type regulator. This regulator corrects the error between the measured DC voltage and its reference. The product of the reference DC current with the DC voltage gives the reference active power. The time equation of this controller is given as follows:

$$u(t) = k_p e(t) + k_i \int_0^t e(\tau)\, d\tau \tag{3.29}$$

Where:

$e(t)$, $u(t)$, k_p, k_i : respectively denote the error at time t, the generated control, and the gains of the controller.

The corresponding transfer function is given by:

$$R(s) = k_p + \frac{k_i}{s} \tag{3.30}$$

Where: s is the Laplace operator.

The following diagram represents the regulation of the DC voltage with a PI controller:

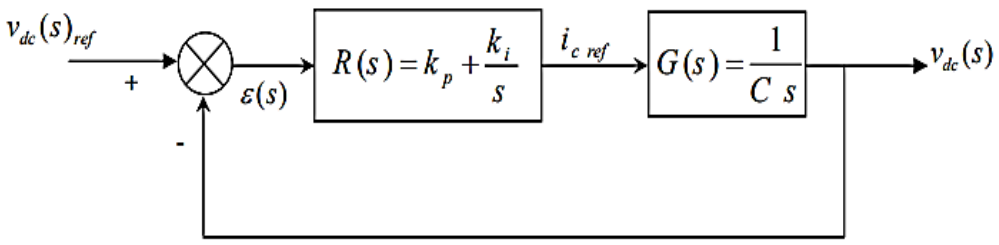

Figure 3.6 Regulation of DC voltage with a PI controller

The closed-loop transfer function is given by:

$$H(s) = \frac{R(s).G(s)}{1+R(s).G(s)} \tag{3.31}$$

We obtain:

$$H(s) = \frac{k_p.s+k_i}{C.S^2+k_p.s+k_i} \tag{3.32}$$

To control the system in closed-loop, it is necessary to choose the coefficients k_p and k_i well.

In this case, the pole placement method is used [33].

The transfer function of a second-order closed-loop system is characterized by:

$$F(s) = \frac{1}{S^2+2\xi\omega_n.s+{\omega_n}^2} \tag{3.33}$$

By analogy between expressions (3.32) and (3.33), we find:

$$k_p = 2.C.\xi\omega_n \tag{3.34}$$

$$k_i = C.{\omega_n}^2 \tag{3.35}$$

The reference DC current is expressed by:

$$I_{rd\ ref} = i_{c\ ref} + I_{ch} \tag{3.36}$$

Where:

- $I_{c\ ref}$: The reference current in the capacitor provided by the PI regulator of the voltage.

- I_{ch}: The measured charging current.

-$i_{rd\ ref}$: The reference DC current.

The product of the reference DC current with the DC voltage gives the reference active power (Figure (3.7)).

$$p_{ref} = V_{dc\ ref}.I_{rd\ ref} \tag{3.37}$$

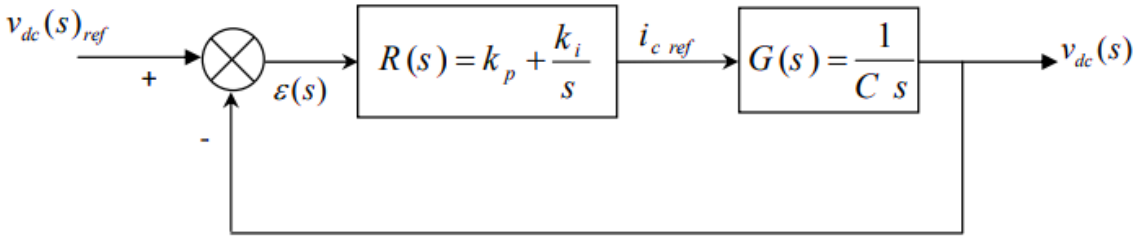

Figure 3.7 Calculation of the reference power

10. Simulation Results

The simulation results were conducted to:

- Confirm the theoretical study of DPC controlled PWM rectifier.
- Verify the dynamic performance of the proposed system

The parameters of the rectifier used in the simulation are presented in table 3.4:

Parameters	***Values***
Line resistance:	R = 0.25 Ω
Line inductance:	L = 10 mH
Capacitor:	C = 5 mF
Load: R_{ch}	R_{ch} = 100
Maximum network voltage amplitude E_m	E_m = 220 sqrt(2) V
Reference voltage: $V_{dc\ ref}$	$V_{dc\ ref}$ = 600 V to $V_{dc\ ref}$ = 750 V
Sampling frequency of the PI regulator:	f_e = 100 kHz
The parameters of the PI regulator and hysteresis regulators are:	
Bandwidth of the hysteresis regulators: h_p ,h_q	h_p = 1 W, h_q = 1 var
Parameters of the PI controller: kp, ki	kp= 0.176, ki=3.125

Table 3.4 System parameter of simulation bloc of a PWM rectifier using classic DPC

The simulation bloc of a PWM rectifier using classic DPC control connected to the grid under MATLAB/Simulink environment is presented in **Figure (3.8)**

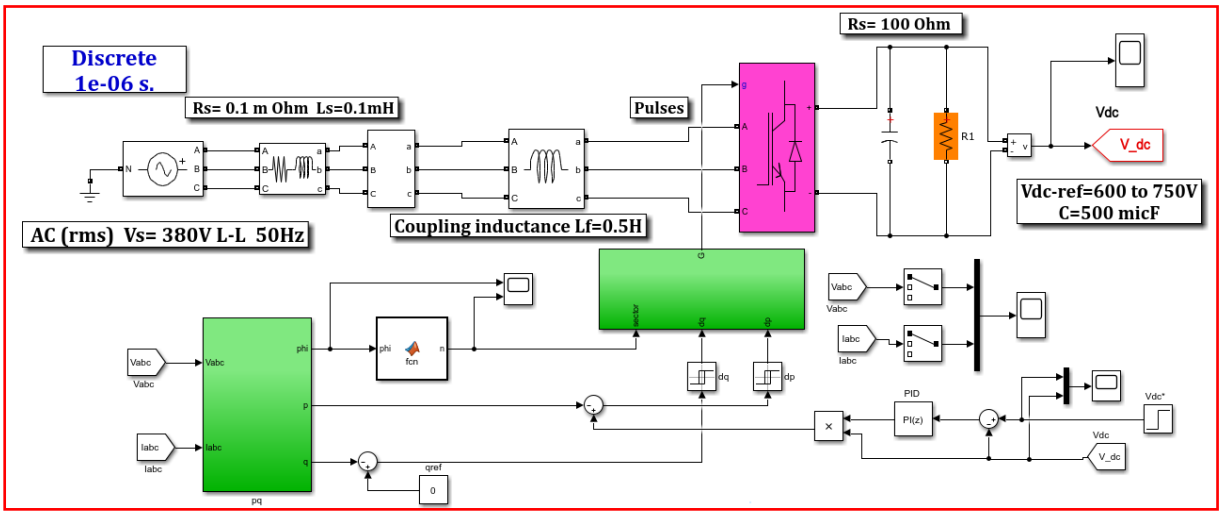

Figure 3.8 Simulation bloc of PWM rectifier using DPC control

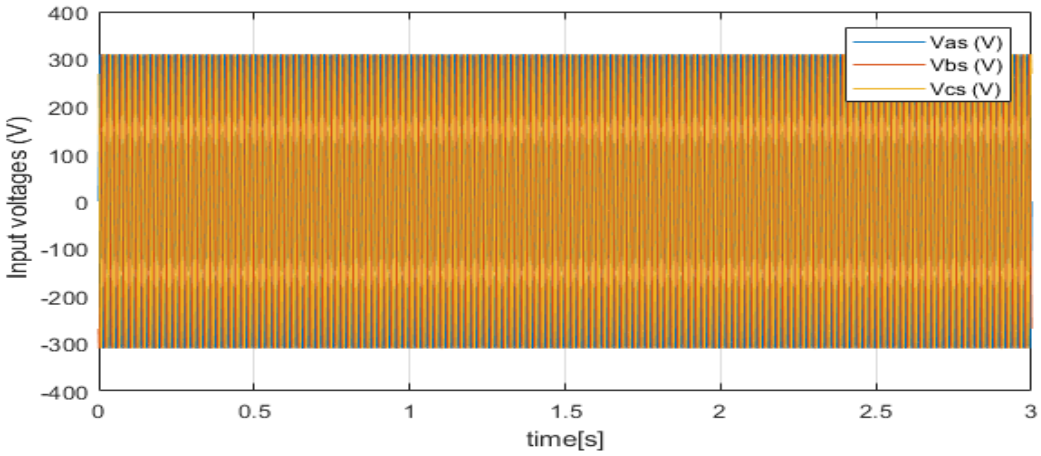

(a) Input voltage

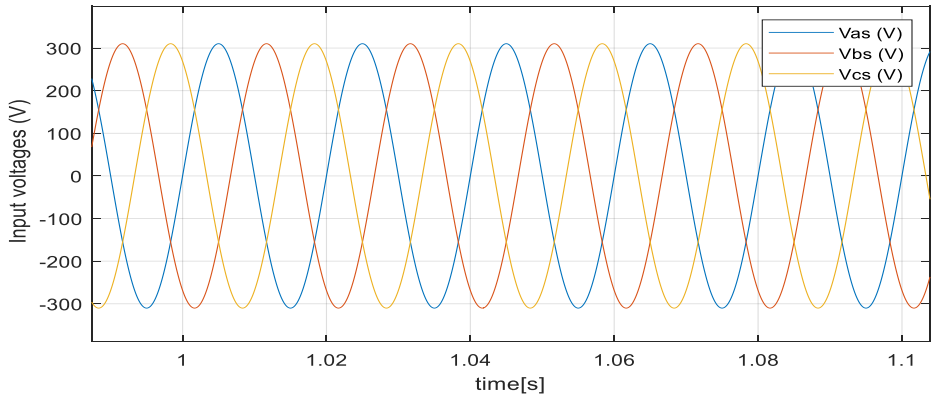

(b) Zoom of the input voltage

Figure 3.9 Input voltages

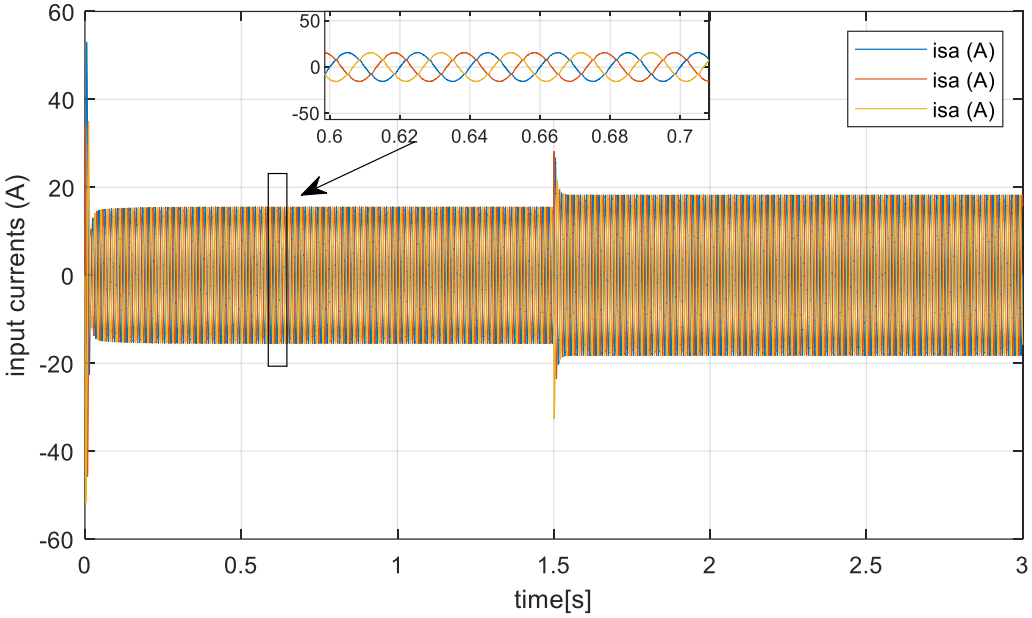

Figure 3.10 Input currents

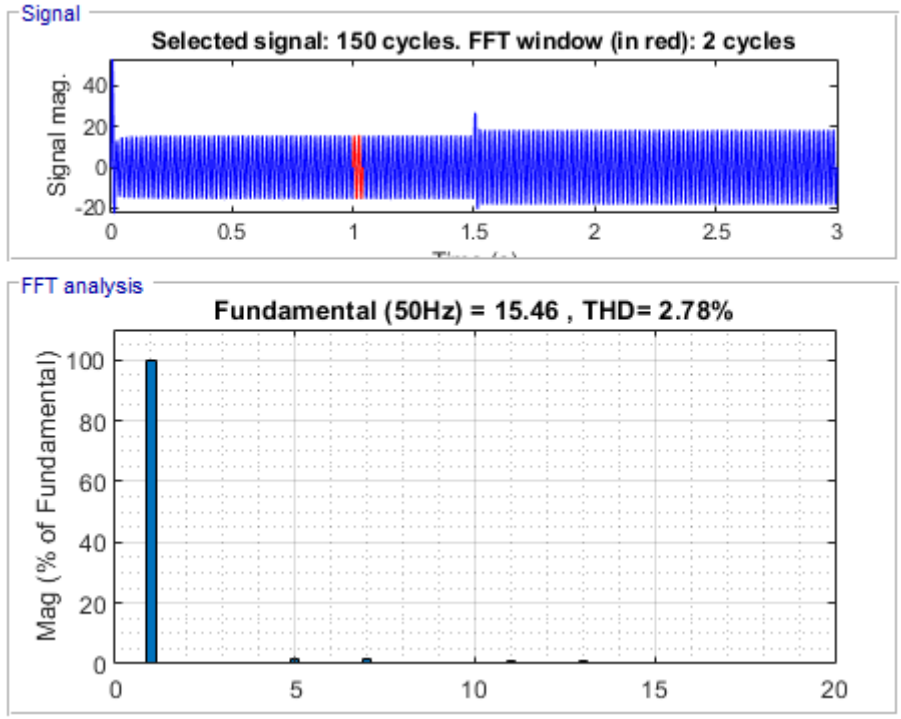

Figure 3.11 Spectrum harmonic of input currents

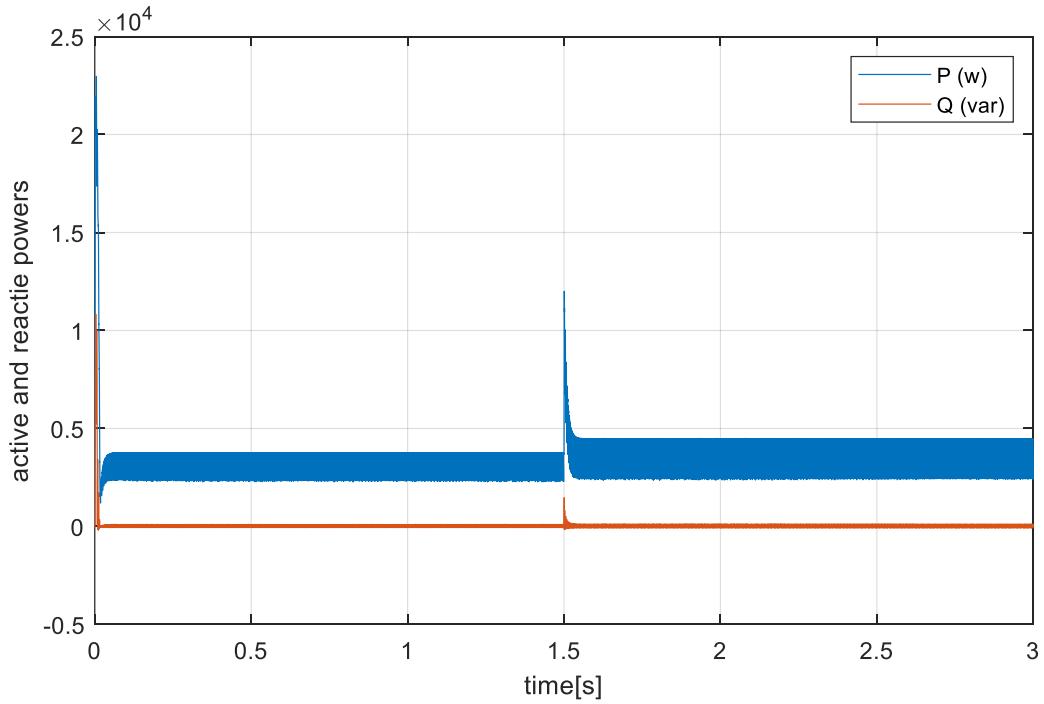

Figure 3.12 Active and reactive powers

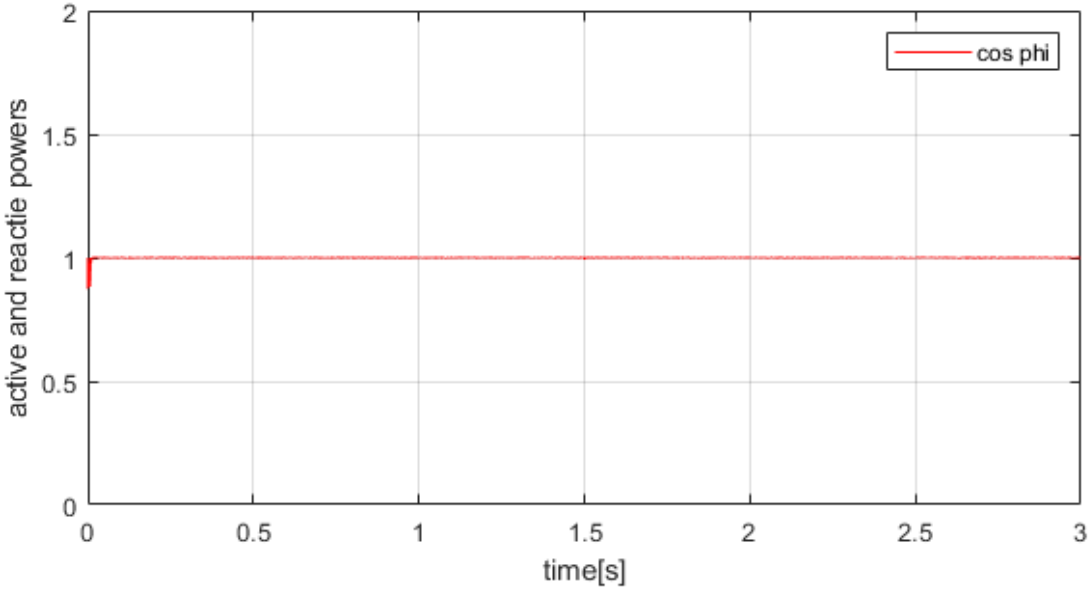

Figure 3.13 Power factor at unity

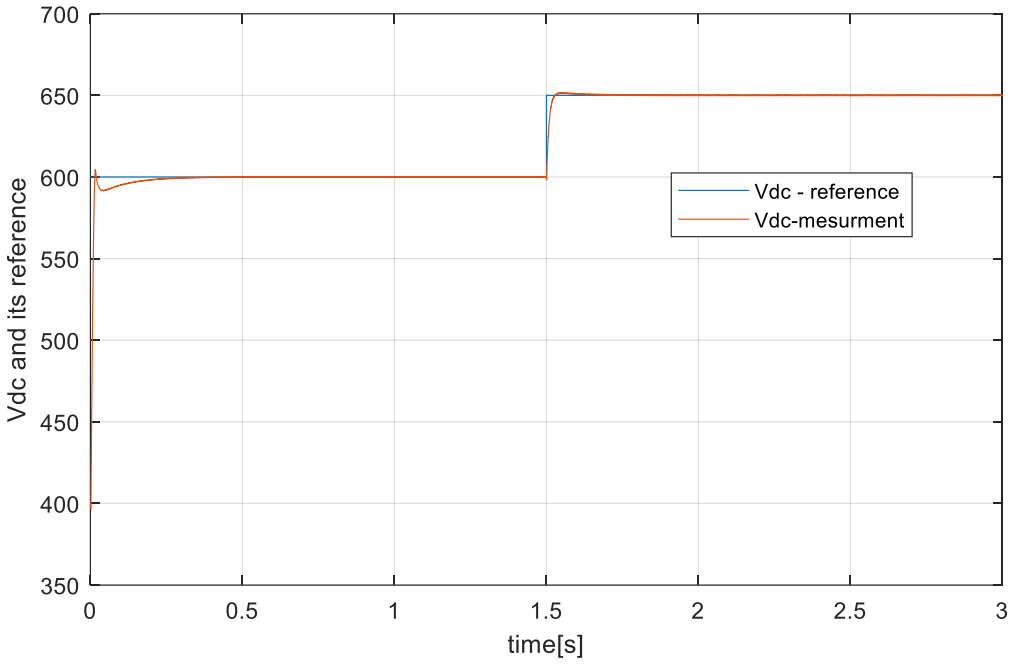

Figure 3.14 DC voltage and its reference

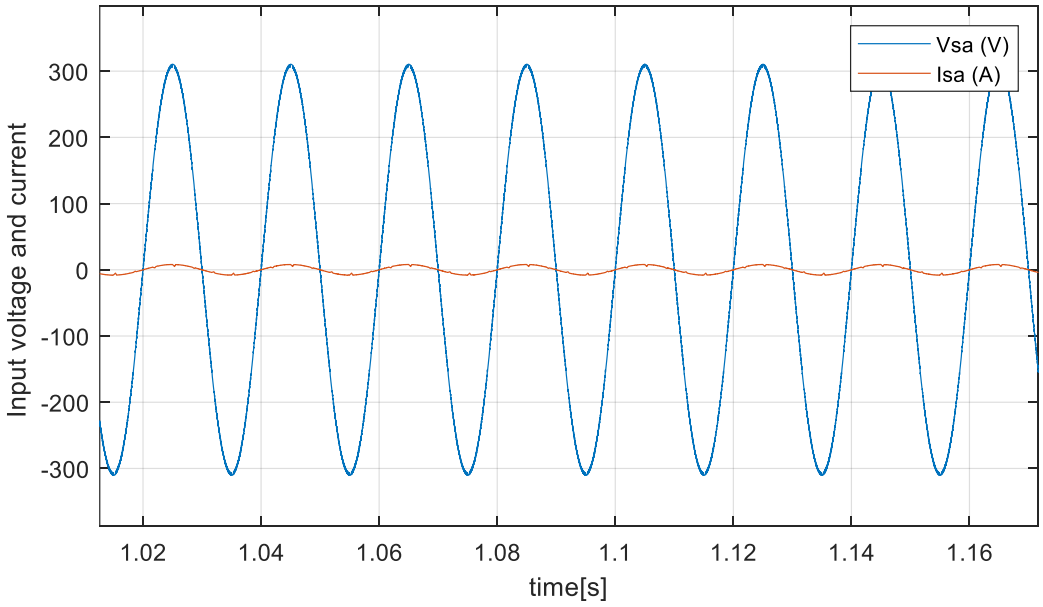

Figure 3.15 The waveform of the source voltage and current per phase.

The bloc simulation of PWM rectifier in Figure (3.8) is controlled by Direct Power Control (DPC), with the bandwidth set such that Δi=0.01A. The results from Figure (3.9) and Figure (3.10) show the waveforms of the input voltage and the input currents. We observe that the shapes of the input voltage and current for all three phases are purely sinusoidal. Figure (3.11) illustrates that the current total harmonic distortion (THD) is very low, at 2.78%. Figure (3.12) demonstrates the presence of active power, while reactive power is completely absent, resulting in a unity power factor shown in Figure (3.13). Figures (3.14) represent the DC bus voltage, which stabilizes close to its reference between 600V and 750V at 1.5s. The phase difference between the current and the ideal voltage is completely nullified, as shown in Figure (3.15). This justifies that the PWM rectifier with DPC control achieves good performance.

11. Comparison between control techniques of PWM rectifier

Figure 3.16 shows the comparison of the DC voltages using hysteresis and DPC controls. It is evident that all control techniques yield good results, with fast response times and low overshoot.

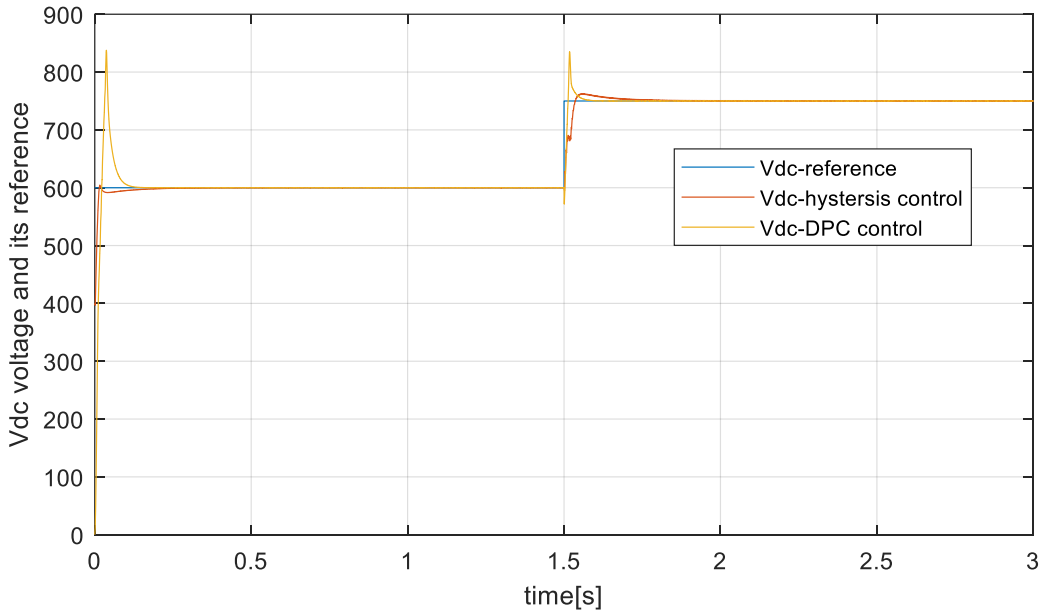

Figure 3.16 Comparison of Control Techniques.

In terms of Total Harmonic Distortion of the Current (THD_I)

Control Technique	THD_I Value
Hysteresis	0.16%
DPC control	2.78 %

Table 3.5 THD of Control Techniques.

12. Conclusion

In this chapter, we discussed the basic structure of a two-level PWM rectifier. Subsequently, our study focused on the analysis of the voltage PWM rectifier, its operating principle, and its modeling. We proposed control strategies for the rectifier, emphasizing the Direct Power Control (DPC) technique. This technique was analyzed in detail, and the results obtained demonstrated its high performance.

The DPC technique for the PWM rectifier was implemented and the results show that the current waveforms for all three phases are purely sinusoidal, resulting in a very low current total harmonic distortion (THD) of 2.78%. Additionally, the presence of active power and the complete absence of reactive power result in a unity power factor. The DC bus voltage stabilizes close to its reference value between 600V and 750V at 1.5 seconds, and there is no phase difference between the current and the ideal voltage. These results validate the effectiveness and high performance of the DPC technique in controlling the PWM rectifier.

In comparison, the hysteresis band current control technique was also applied to the PWM rectifier, and the simulation results for this technique are equally impressive. The current waveforms for all three phases remain purely sinusoidal, and the current THD is remarkably low at 0.16%. This is significantly better than the THD achieved with the DPC technique. Furthermore, the presence of active power and the complete absence of reactive power again result in a unity power factor. The DC bus voltage stabilizes close to its reference value between 600V and 750V at 1.5 seconds, and there is no phase difference between the current and the ideal voltage. These results demonstrate the superior performance of the hysteresis band current control technique in terms of THD.

In summary, both hysteresis band current control and Direct Power Control (DPC) are effective techniques for controlling PWM rectifiers, achieving low THD, unity power factor, and stable DC bus voltage. However, the hysteresis band current control exhibits a lower

THD value of 0.16%, making it slightly superior to DPC, which has a THD of 2.78%. Despite this, both techniques are highly acceptable and demonstrate high performance.

CHAPTER IV

STRATEGIES CONTROLS OF A PWM RECTIFIER BASED ON PI CONTROLLER APPLIED TO BATTERY CHARGING SYSTEM

CHAPTER IV

STRATEGIES CONTROLS OF A PWM RECTIFIER BASED ON PI CONTROLLER APPLIED TO BATTERY CHARGINGSYSTEM

1. Introduction

The advancement of electric vehicle (EV) technology is intricately linked to the development and optimization of efficient battery charging systems. In this context, the deployment of Direct Power Control (DPC) for Pulse Width Modulation (PWM) rectifiers, underpinned by PI controllers, has shown promising results in simulation studies as elucidated in chapter III. These control methodologies not only enhance the precision and stability of the charging process but also ensure optimal energy transfer efficiency from the grid to the vehicle's battery system.

In this chapter, we delve into the practical application of these control strategies in the charging process of a lithium-ion battery, a pivotal component in modern electrical vehicle.

2. Battery definition

Battery word was derived an old French word for “Baterie” which meant beating in terms of cannons when scientists were looking for energy storage in the 1700s. A battery can be a single or a group of electrochemical cell combination. An electrochemical cell converts the chemical energy in the electrical energy and essentially consists of three components, Cathode, Anode and Electrolyte, this type of accumulator battery has good performance at high temperature and low self-discharges [34].

3. Characteristic quantities of batteries

3.1 Capacity

The amount of energy that can be taken out from a fully charged battery till it reaches its empty level is called Capacity and is represented by the specific energy in ampere-hours (Ah). Ah is the current at which the battery can be discharged and will discharge for 1 hour. One can install a bigger or smaller battery and can still discharge at the same rate but will get longer or shorted usage time. Each battery with different capacity would generally come with a different charger, but a standard charger would just take longer or shorter time depending on the size/capacity of the battery. Capacity has different standards in different regions, such as, in Europe battery capacity is in Ah while in North America by Reserve Capacity (RC - time in minutes at a 25A discharge rate).

3.2 Résistance interne

The internal resistance of the battery is linked to the materials constituting the battery and the reactions within it. It depends on the charge/discharge regime, the temperature, the state of health and state of charge. It gives an indication of the energy efficiency of the battery. Indeed, with the resistance, the Joule effect losses increase which reduces the efficiency. It should be noted that the capacity and internal resistance of a battery are two particularly important data to quantify your state of health. They are also linked to the SOF function state (State Of Function) since the resistance is the image of the maximum available power and the capacity that of the maximum energy that can be exploited [35].

3.3 Open circuit voltage

This is the potential difference between the two electrodes when the battery is at rest. It depends directly on the activities of the state of charge and the temperature.

3.4 State of charge

The SOC (State Of Charge) is an expression of the available capacity of the battery at a given time expressed as a percentage of its maximum capacity. This quantity is generally calculated by integrating the current and thus following the evolution of the quantity of charging throughout the electrical stress of the battery.

3.5 State of Health

State of Health (SOH) is a quantity which quantifies the loss of performance due to battery degradation. It can be defined as the ratio between the total capacity current and the maximum capacity obtained when the battery was new.

4. Principle of Operation of a Li-ion Battery

Generally speaking, current is created by an overall movement of electrons. These move from the cathode (the positive electrode) to the anode (negative electrode) via a metal wire (conductor), to then power a motor, or a lamp for example. The ions resulting from this electron transfer pass through the electrolyte, starting from the cathode to reach the anode, like the electrons. This therefore happens when the battery discharges. When the battery is recharged, the electrons are returned from the cathode to the anode, as well as the lithium ions [36].

5. Lithium battery models

5.1 Simple model of an accumulator

The simplest model consists of an ideal voltage source V0 (open-circuit voltage) in series with an internal resistance. Where V1 is the terminal voltage across the accumulator.

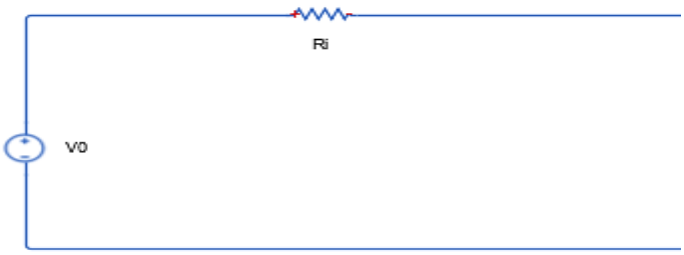

Figure 4.1: Simple model of an accumulator

$$V(t) = V0 - Ri^{*}Ib(t) \quad (4.1)$$

In this simple model, **Ri** and **V0** are considered constant. This model does not take into account the variation of the internal resistance of the accumulator as a function of the state of charge or temperature. This model can be applied if the dependence of the parameters on the state of charge and temperature can be neglected [37]

5.2 Thevenin Model

This model represented by the diagram below is often used. It consists of an ideal source V0, an internal resistance Ri, a capacitor that represents the polarization of the metallic plates of the accumulator, and an overvoltage resistance R which is due to the contact of the plates with the electrolyte.

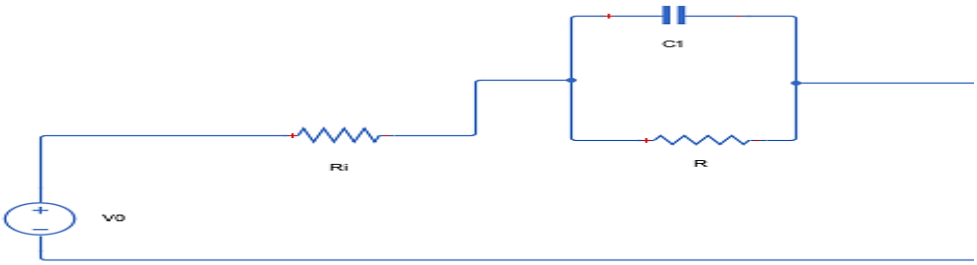

Figure 4.2 Thevenin Model of an Accumulator

In this model, all elements of the equivalent circuit are assumed to be constant and different during charging and discharging. However, in reality, these parameters also vary according to the state of charge and the discharge rate [38].

5.3 Nonlinear Dynamic Model:

This is a variant of the Thevenin model that takes into account the nonlinearity of the parameters. In this model, represented by the diagram below, the charging and discharging

processes are separated. Additionally, all parameters depend on the state of charge of the battery.

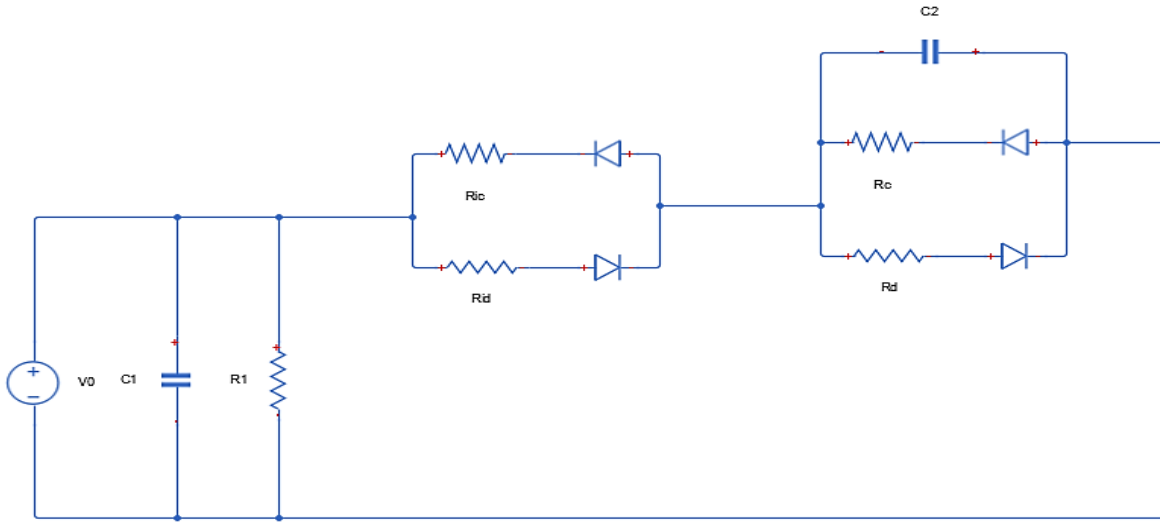

Figure 4.3 Nonlinear Model of the Accumulator

The model parameters are defined as follows:

- C1 : is accumulator capacity.
- R1 : is self-discharge resistance.
- R_{ic} and R_{id} : are represent the internal resistance due to the electrolyte and electrodes during charging and discharging, respectively.

The two RC circuits (R_cC_2 and R_dC_2) represent the overvoltage at the end of charging and the sudden voltage drop at the end of discharging, respectively. Since all the parameters of this model are variable (depending on the state of charge or open-circuit voltage), their identification is difficult [39].

5.4 Cauer and Foster Model

This type of model, illustrated in the diagram below, is similar to that of Thevenin. The difference between the two models lies in the addition of an impedance called Warburg impedance (Zw). In this model, Ri represents the internal resistance, the RC circuit, and the impedance Zw represent respectively the charge transfer phenomenon and the diffusion phenomenon that occur during the operation of the accumulator. Therefore, it is a fairly comprehensive model and represents the dynamics of the accumulator more accurately [39].

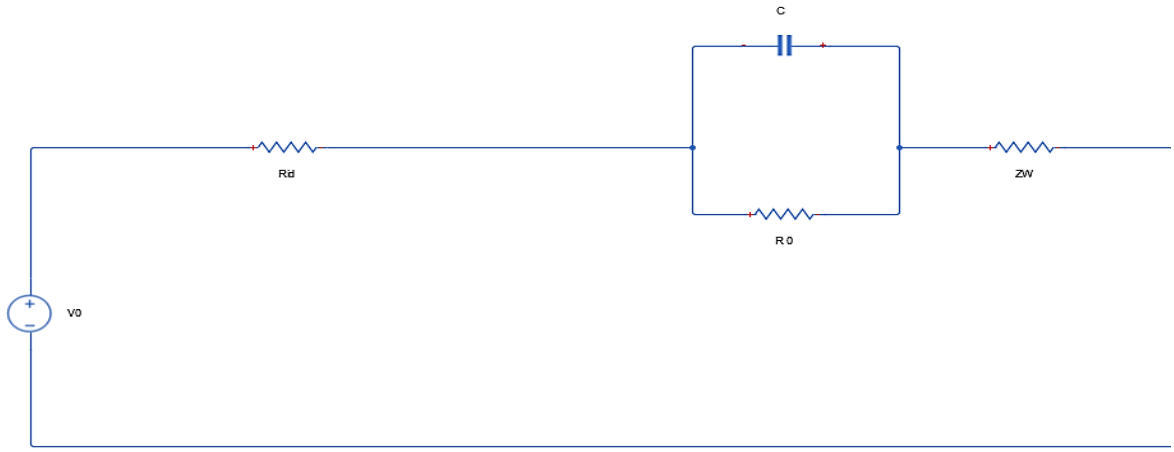

Figure 4.4 Cauer and Foster Model

The Warburg impedance has been modeled by two structures called: Cauer structure and Foster structure.

A. Cauer Structure:

The Warburg impedance is represented by four RC circuits as shown in the diagram below:

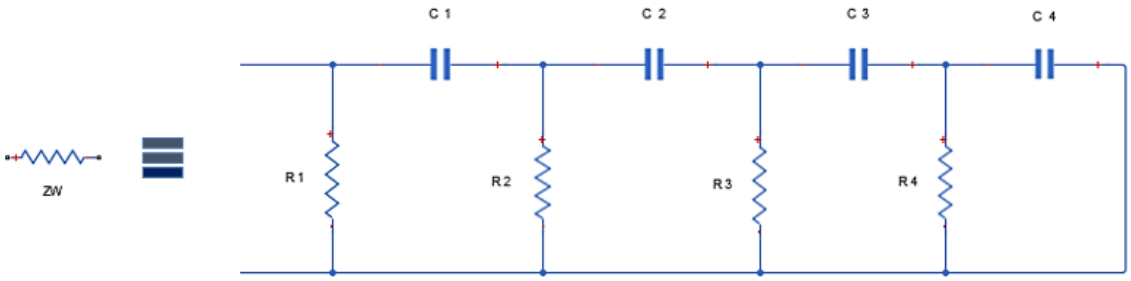

Figure 4.5 Cauer Structure

B. Foster Structure:

In this case, the impedance is simply a series of parallel RC circuits. Foster limited it to four RC circuits.

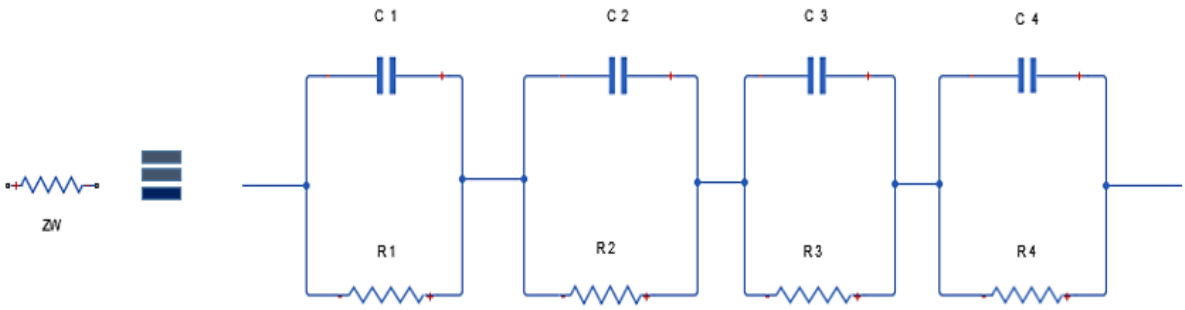

Figure 4.6: Foster Structure

For this type of model with both structures, the identification of parameters is carried out using an experimental electrochemical method called impedance spectroscopy, which is quite complex to implement. [40]

5.5 Shepherd Model:

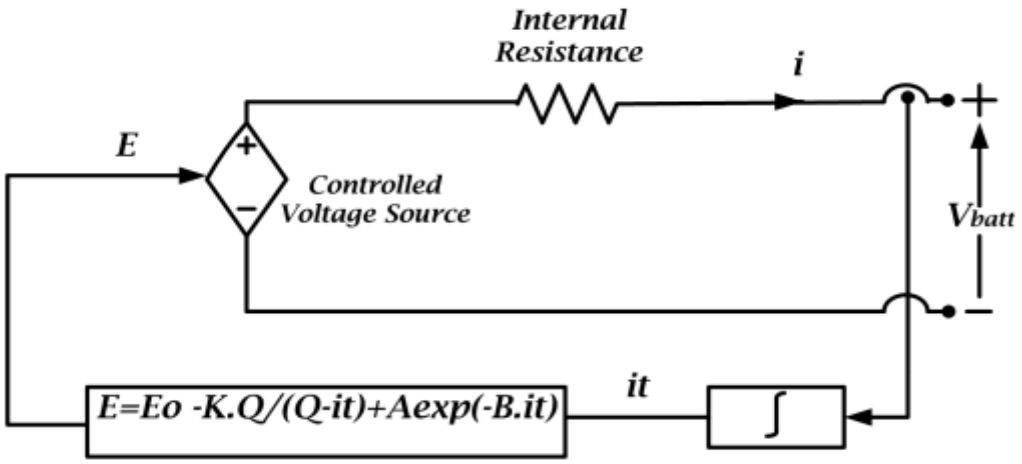

Figure 4.7: Shepherd Model

This model was presented by Shepherd. It assumes that the discharge current and the internal resistance are constant. This model is based on an equation that allows reproducing discharge curves for a significant number of accumulators. The parameters of this equation are calculated from a certain number of discretized points from a manufacturer's curve. This modelling does not take into account the temperature and the variation of the open-circuit voltage as a function of the state of charge. The terminal voltage at the terminals of the

accumulator in this model is expressed by the following equation:

$$V1 = V0 + K\frac{Q}{Q-Ib.t}Ib \quad (4.2)$$

By adding the ohmic voltage drop to this equation, we obtain:

$$V1 = V0 + K\frac{Q}{Q-Ib.t}Ib - Ri.Ib \quad (4.3)$$

This equation does not include the voltage drop at the beginning of the discharge. We can represent this part of the curve by adding an exponential function. The equation then becomes:

$$V1 = V0 + K\frac{Q}{Q-Ib.t}Ib - Ri.Ib + A.exp\left(-\frac{B}{Q}Ib.t\right) \quad (4.4)$$

In this equation, V0, K, Q, Ri, A, and B represent constant parameters to be determined graphically, which requires several points from the manufacturer's discharge curve. Additionally, Shepherd uses two discharge curves to determine the six parameters. Sometimes, the exponential part of the curve is difficult to observe because it is very short and can be neglected, and the discharge curve can be represented by the polarization zone. Shepherd's equation has been widely used and modified by other authors in the literature.

As observed, there are different models in the literature, each with its characteristics. The chosen model depends on the application; if more precision is required, then a more detailed model is needed, taking into account all parameters that can affect the performance of accumulators. The nonlinear dynamic model is very interesting because it presents a charging and discharging circuit, and all parameters are a function of the state of charge. The Cauer and Foster model (inspired by Thevenin's) is used more to represent the charge transfer phenomenon and diffusion (chemical phenomena) [41].

6. Battery State of Charge Calculation for LI-ION:

State of charge is the amount of charge available in the battery at a given moment relative to its maximum capacity. In most applications involving an energy storage system, knowing the state of charge of the battery is crucial. It's akin to a fuel gauge for a regular car. In the case of an electric vehicle, this information helps the driver know the remaining distance before the battery runs out. Moreover, this indication helps us avoid deep discharge or excessive charging of the battery. Thus, the battery's lifespan will be longer. The problem often reported in the literature is that the state of charge cannot be directly measured using sensors like in the case of a regular car where we can measure the fuel level in the tank using a fuel gauge. Therefore, to address this problem, several methods have been developed to estimate the state of charge.These methods are applicable to most batteries. They are based on the measurement

of electrical parameters such as voltage, current, and internal resistance. Among these methods, we will mention two that will be used in the two battery models under study**.**

6.1 Calculation by Current Integration Method:

This is the most common method for calculating the state of charge since charging and discharging are directly related to the current supplied or withdrawn from the battery. If the initial state of charge SOC0 is known, the value of the current integral is an indicator of the state of charge SOC. The state of charge can be defined by the following equation:

$$SOC(t) = SOC0 - \frac{\int_{t0}^{t} Ibdt}{Q} \quad (4.5)$$

With:

SOC(t) : is state of charge of the battery at time t.

SOC0: is initial state of charge.

I_b: is battery discharge current.

Q: is nominal capacity of the battery.

$\int_{t0}^{t} Ib\, dt$: represents the charge delivered by the battery at time t (current charge). [42], [43]

7. Advantages and disadvantages of various battery technologies

Following table shows the advantages and disadvantages of various battery technologies and applications [35] [36],

Battery type	Lead–Acid	Ni–Cd	Ni–MH	Ni–Zn	Li-Ion
Energy density (W h/kg)	20-100	40-60	50-80	55-75	90-200
Power density (W/kg)	50-400	80-350	80-300	150-300	500-2000
Cycles	500-2000	600-3000	600-2000	600-1200	800-3000
Advantages	Low cost, mature technology, high specific power	High specific energy, no degradation for deep charge/ discharge	High specific energy, large temperature ranges, safety, long service life	High specific energy, no degradation for deep charge/discharge, high peak power	High specific energy, high voltage operation
Disadvantages	Low specific energy, short service life	High cost cadmium toxicity, recycling issues	High cost, high self - discharge, memory effect	High cost, life shorten by fast growth of dendrites	High cost, life shorten by deep discharges, affected by temperature, fragile
Application stage	Widely used	Some used	Rarely used	Research and development	Research and development

Table 4.1 Advantages and disadvantages of different Battery

7.1 Advantages and Disadvantages of Lithium-Ion Batteries

Advantages:

- Very high energy density
- Very low self-discharge (1% per month)
- Relatively low internal resistance and capability to provide moderate to high currents
- Reduced weight
- No memory effect
- They require no maintenance

Disadvantages:

- Special charger required
- Risk of explosion in case of short circuit or overcharge (Hydrogen production!)
- Need to charge each cell in a pack separately; otherwise, there is a risk of voltage imbalance
- Depth of discharge: these batteries age more slowly when recharged every 10% compared to every 80%
- Risk of explosion if all safety conditions are not met
- The use of a liquid electrolyte presents dangers if a leak occurs and it comes into contact with air or water (transforming into a corrosive liquid: lithium hydroxide)

8. Topology of Electric Vehicle Charger

Figure (4.8) shows the overall configuration of Direct Power Control for a three-phase PWM rectifier.

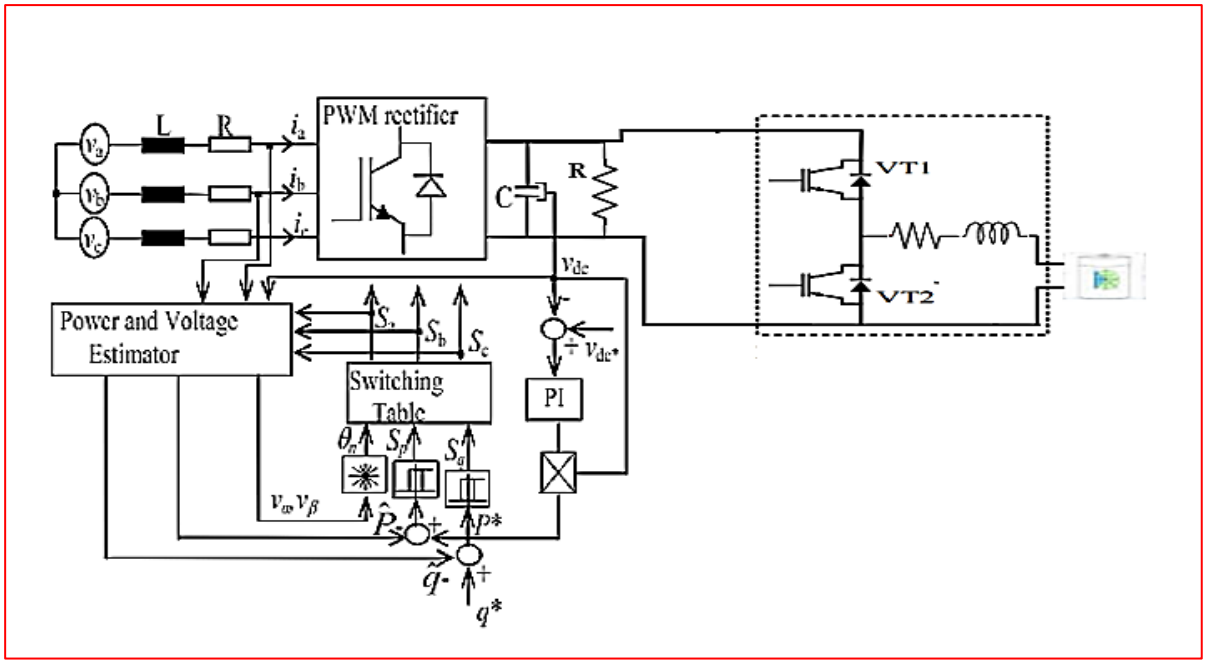

Figure 4.8 Topology of Electric Vehicle Charger Using DPC control for PWM Rectifier

9. Results and discussions

Simulation is conducted to test the performance of DPC-PWM rectifier control connected to Grid to battery charger. The battery initial SOC is set to 10%. Figure 4.9 present the simulation results of proposed system.

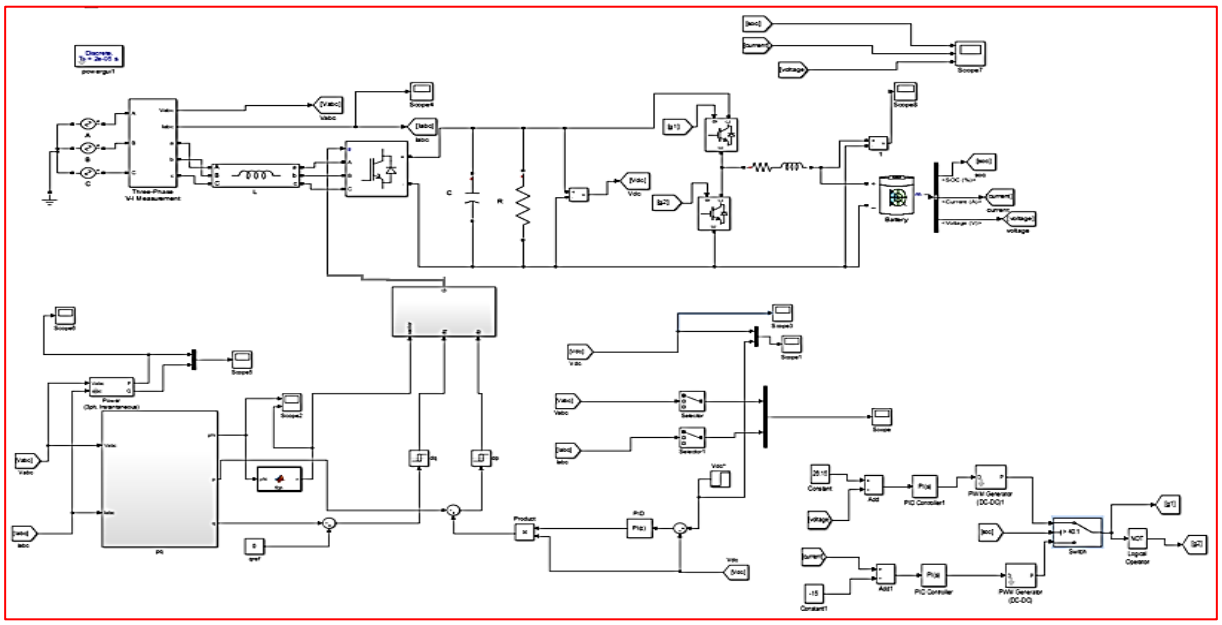

Figure 4.9 Charger battery vehicle connected to PWM rectifier Using DPC Control

9.1 First case: battery charging

In this case, figure 4.10 illustrate de input current of PWM rectifier, we can see in this figure that the waveform of the currents are sinusoidal.

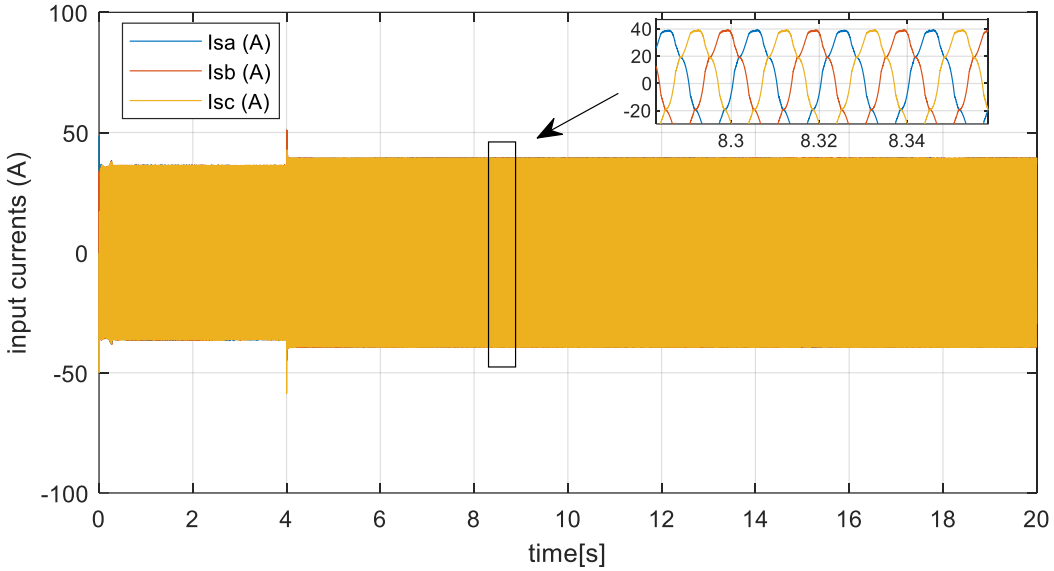

Figure 4.10 Input currents of PWM rectifier connected to battery

Figure 4.11 show de output DC voltage of PWM rectifier, we can see in this figure that the output dc voltage follows up its reference in 600 and 650 at 4s. figure 4.12 show the constant output DC voltage of DC-DC Converter connected to the battery.

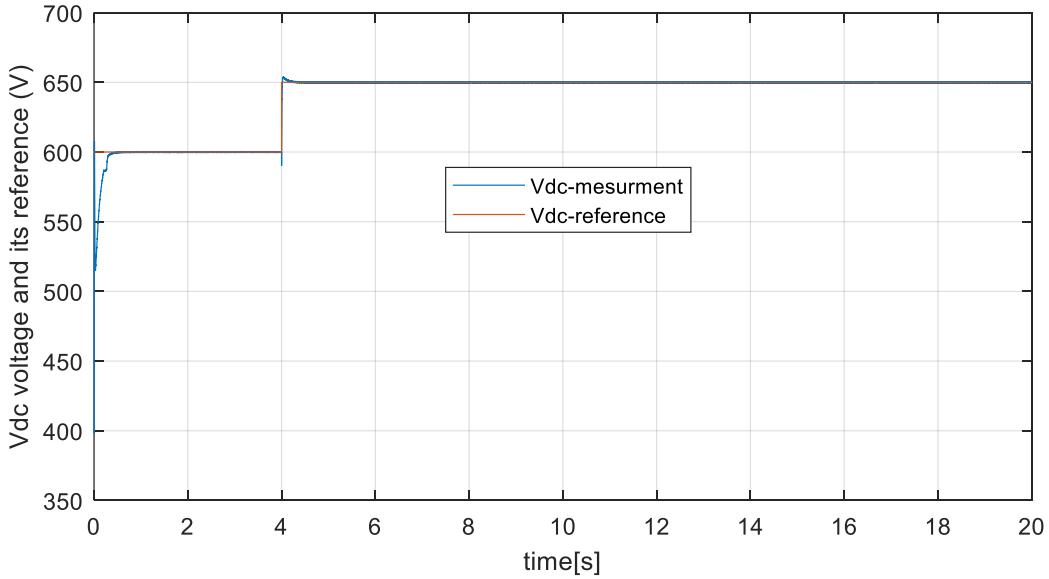

Figure 4.11 Vdc voltages and its reference of PWM rectifier

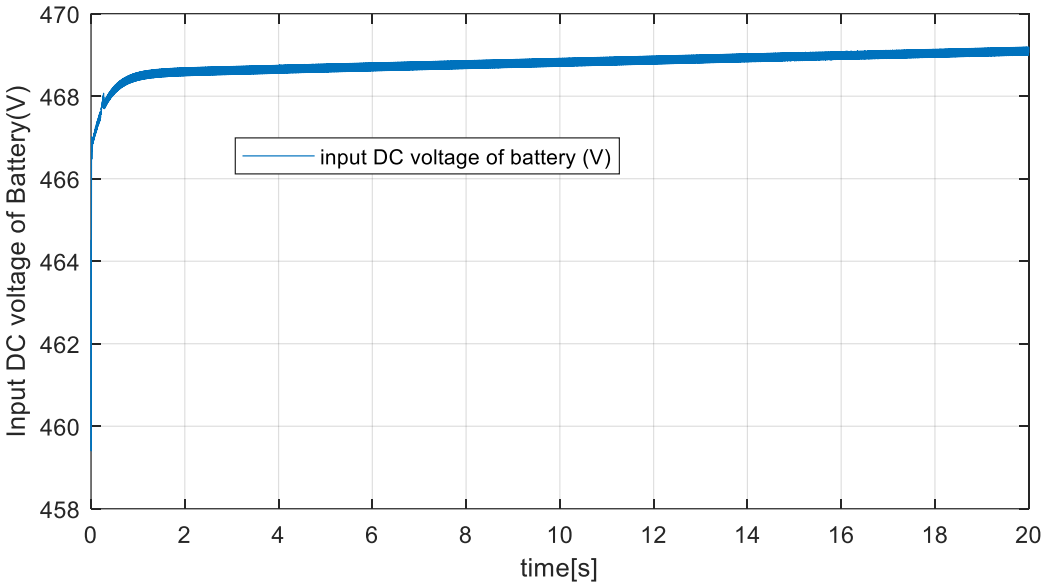

Figure 4.12 Input DC voltage of DC-DC converter

Interne Characteristics of battery about SOC, current and voltage are presented in figures bellows, we can see in figure 4.11 the DC voltage of battery which is constant value. In this type of model the SOC of battery is obtained using the method based on current integration and it was assumed that the initial state of charge SOC0=10% is given in figure 4.13.

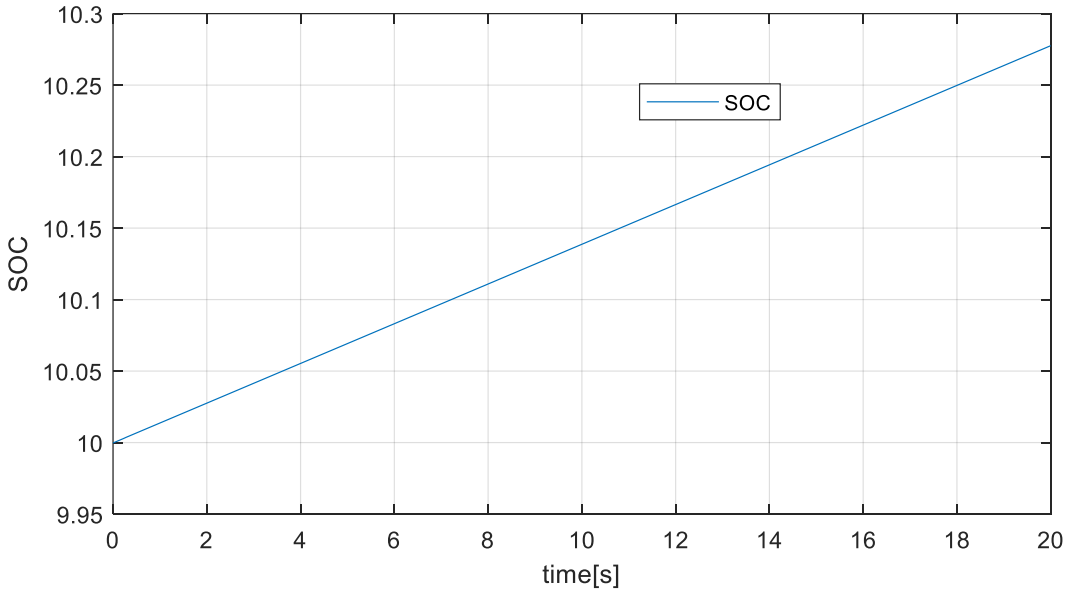

Figure 4.13 SOC of battery

The battery charging current is represented by figure 4.14, we notice in this figure that the current value is -20A, this value was imposed by the control and command system of the DC/DC converter associated between the battery and the PWM. for the dc voltage of battery is given in figure 4.15, we can see in this figure that the voltage remains constant.

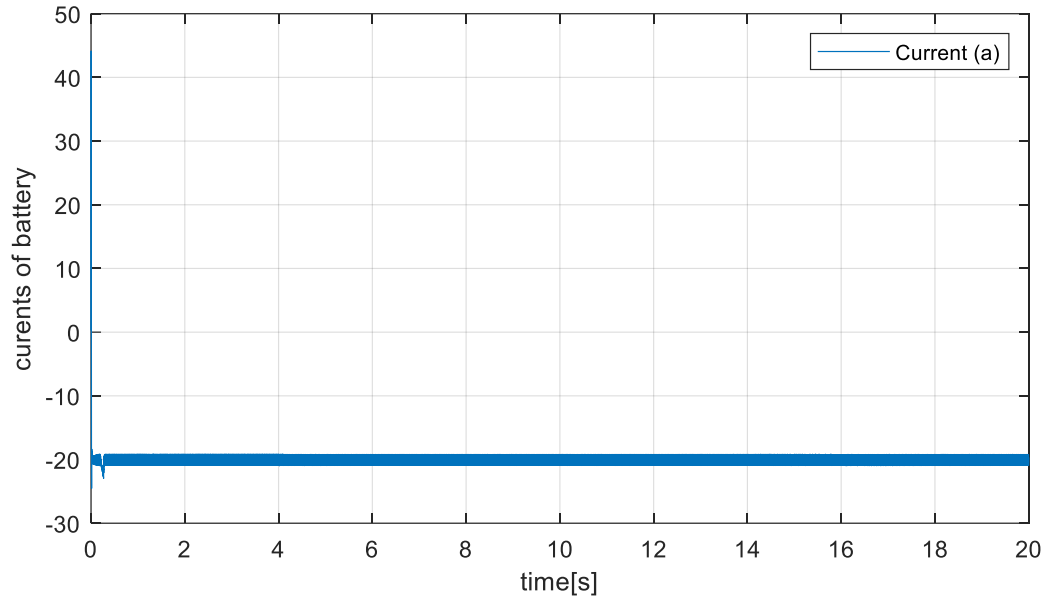

Figure 4.14 Currents of battery

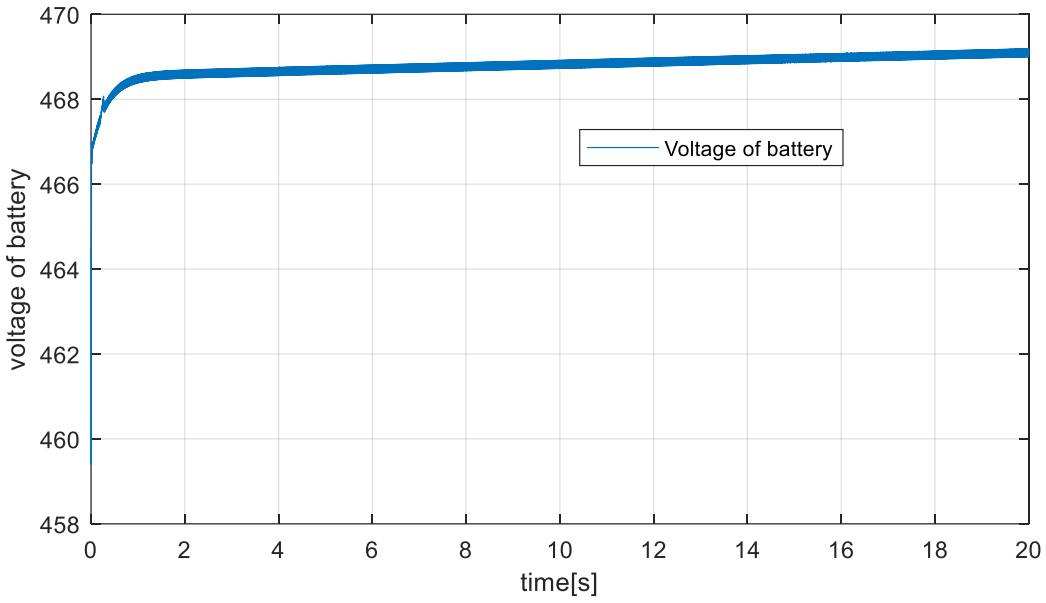

Figure 4.15 Voltage of battery

9.2 Second case: battery charging and discharging battery

Figures 4.16, 4.17 and 4.18 give the shapes of SOC in the case of battery charging and discharging as well as in the shape of the battery current and voltage, it is noted in this case that the internal characteristics of the battery vary depending on the state of charge of the battery.

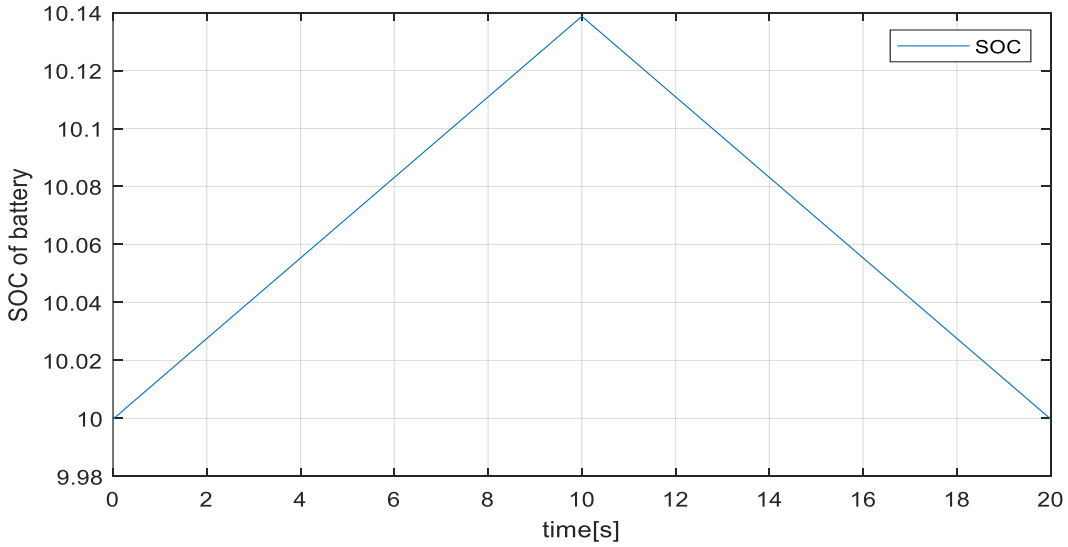

Figure 4.16 Voltage of battery in the charging and discharging battery

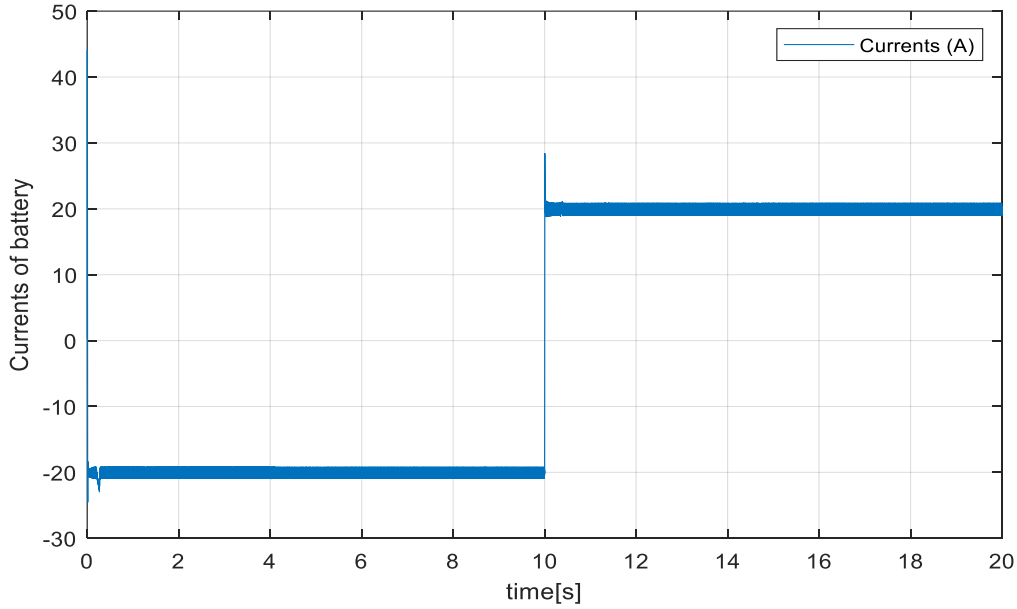

Figure 4.17 Currents of battery in the charging and discharging battery

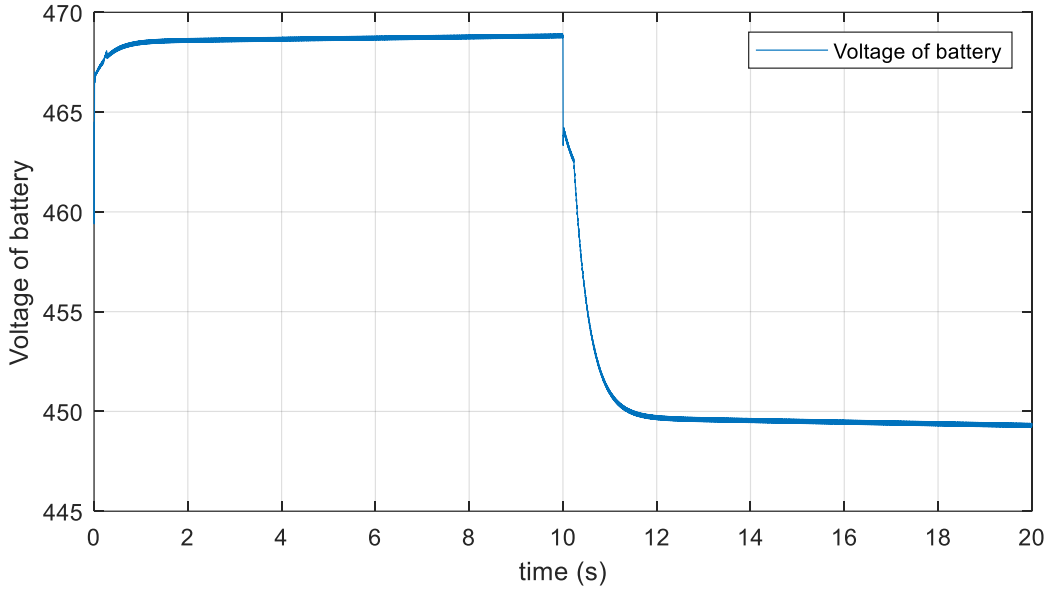

Figure 4.18 Currents of battery in the charging and discharging battery

10. Conclusion

In this chapter we presented a state of charge of the battery for different cases, To achieve this goal we talked about different battery simulation models, then we presented a battery simulation model powered by a DPC controlled PWM rectifier, results are presented and discussed, these show the efficiency and importance of battery charging and discharging, especially for electric vehicle charging.

GENERAL CONCLUSION

In this thesis, the modeling and simulation of a PWM rectifier using different control techniques are presented, hysteresis and DPC control are used to control PWM rectifier. This converter is particularly used for harmonic compensation and to replacing the diode rectifier bridge in various applications.

Several advantages of PWM rectifier have been recorded. Its two-level structure reduces voltage stress on power switches, regulates the output DC bus capacitor voltage, and decreases harmonic distortion, improving the power factor of the power supply while exploiting relatively significant active power.

In this work, the first chapter discusses various disturbances in electrical networks, particularly harmonic-related disturbances, and the proposed solutions to remedy them. This chapter concludes with a review of the different passive and active compensators proposed in the literature.

In the second chapter, we present a theoretical and simulation study demonstrating the operating principle of the PWM rectifier with its control part using the hysteresis control technique equipped with a PI controller. The obtained simulation results showed that the proposed control technique offers high efficiency. This converter provides a stable DC voltage with a unity power factor and purely sinusoidal input currents with a very low THD value of 0.16%.

In the third chapter, we presented a simulation study of a PWM rectifier with DPC control. A theoretical reminder of the DPC control principle was given, followed by simulation results. These results show that the rectifier provides a stable DC voltage with a unity power factor and purely sinusoidal currents with a very low THD value of 2.78%.

Finally, in the last chapter, we presented a study of the association of the PWM rectifier using DPC-control equipped with a PI regulator connected to a battery. This conversion chain is generally used for charging electric vehicle battery and renewable energy.

In the future, we hope that our work can be extended to:

- Conduct experimental tests to validate the obtained simulation results.
- Use other control techniques with advanced controllers such as fuzzy logic and neural networks.
- Renewable energy conversion system and electrical vehicle charging.

Appendix A:

Transformation Matrices:

The conversion of three-phase line-to-neutral voltages (e_a, e_b, e_c) to two-phase voltages (e_α, e_β) is performed using the following matrix:

$$\begin{bmatrix} e_\alpha \\ e_\beta \end{bmatrix} = \sqrt{\frac{2}{3}} \begin{bmatrix} 1 & -1/2 & -1/2 \\ 0 & \sqrt{3}/2 & -\sqrt{3}/2 \end{bmatrix} \begin{bmatrix} e_a \\ e_b \\ e_c \end{bmatrix}$$

This conversion can be performed based on the two line-to-line voltages e_{ab} and e_{ca} using the following matrix:

$$\begin{bmatrix} e_\alpha \\ e_\beta \end{bmatrix} = \sqrt{\frac{2}{3}} \begin{bmatrix} 1/2 & -1/2 \\ -\sqrt{3}/2 & -\sqrt{3}/2 \end{bmatrix} \begin{bmatrix} e_{ab} \\ e_{ca} \end{bmatrix}$$

On the other hand, the conversion from (α_β) coordinates to (d_q) coordinates is performed using the following matrix:

$$\begin{bmatrix} e_d \\ e_q \end{bmatrix} = \begin{bmatrix} \sin(\omega t) & -\cos(\omega t) \\ \cos(\omega t) & \sin(\omega t) \end{bmatrix} \begin{bmatrix} e_\alpha \\ e_\beta \end{bmatrix}$$

The inverse conversion is expressed by:

$$\begin{bmatrix} e_\alpha \\ e_\beta \end{bmatrix} = \begin{bmatrix} \sin(\omega t) & \cos(\omega t) \\ -\cos(\omega t) & \sin(\omega t) \end{bmatrix} \begin{bmatrix} e_d \\ e_q \end{bmatrix}$$

The direct conversion from three-phase line-to-neutral voltages (e_a, e_b, e_c) to two-phase voltages in the rotating reference frame (e_d, e_q) is performed using the following matrix:

$$\begin{bmatrix} e_d \\ e_q \end{bmatrix} = \sqrt{\frac{2}{3}} \begin{bmatrix} \sin(\omega t) & \sin(\omega t - 2\pi/3) & \sin(\omega t - 4\pi/3) \\ \cos(\omega t) & \cos(\omega t - 2\pi/3) & \cos(\omega t - 4\pi/3) \end{bmatrix} \begin{bmatrix} e_a \\ e_b \\ e_c \end{bmatrix}$$

This conversion can also be expressed based on the compound voltages in the following form:

$$\begin{bmatrix} e_d \\ e_q \end{bmatrix} = \sqrt{\frac{2}{3}} \begin{bmatrix} \sin(\omega t + \pi/3) & -\sin(\omega t - \pi/3) \\ \cos(\omega t + \pi/3) & -\cos(\omega t - \pi/3) \end{bmatrix} \begin{bmatrix} e_{ab} \\ e_{ca} \end{bmatrix}$$

Appendix B:

The block diagram in Figure (A.1) shows two two-level hysteresis controllers. These controllers are designed to regulate both active and reactive powers. One controller is affected by the error($\Delta_P = P_{ref} - P$) for active power regulation, while the other is influenced by the error $(\Delta_q = q_{ref} - q)$ for reactive power regulation.

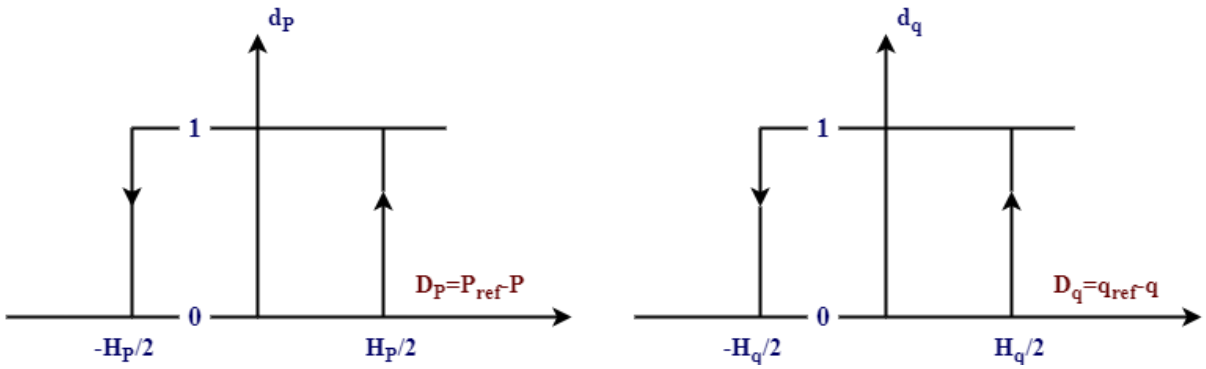

Figure A.1: Characteristics of two-level hysteresis controllers.

The width of the hysteresis band has an influence on the performance of the rectifier, particularly on harmonic current distortion and average switching frequency.

The two-level hysteresis regulator for instantaneous reactive power can be described as:

$$\begin{cases} \Delta_q > H_q \quad so \quad d_q = 1 \\ -H_q \le \Delta_q \le H_q \quad and \quad \dfrac{d\Delta_q}{dt} > 0 \quad so \quad d_q = 0 \\ -H_q \le \Delta_q \le H_q \quad and \quad \dfrac{d\Delta_q}{dt} < 0 \quad so \quad d_q = 1 \\ \Delta_q < -H_q \quad so \quad d_q = 0 \end{cases}$$

And similarly for the two-level hysteresis regulator for active power:

$$\begin{cases} \Delta_P > H_P \quad so \quad d_P = 1 \\ -H_P \le \Delta_P \le H_P \quad and \quad \dfrac{d\Delta_P}{dt} > 0 \quad so \quad d_P = 0 \\ -H_P \le \Delta_P \le H_P \quad and \quad \dfrac{d\Delta_P}{dt} < 0 \quad so \quad d_P = 1 \\ \Delta_P < -H_P \quad so \quad d_P = 0 \end{cases}$$

Appendix C :

Synthesis of the commutation table:

The synthesis of the commutation table is based on the signs of the derivatives of active and reactive powers in each sector. For each sector, the change in reactive power is positive for three vectors, negative for three vectors, and zero for V_0, V_7.. The sign of the change in active power is positive for four vectors, negative for two or three vectors.

Sector 01:

$\hat{P} > 0$	$\hat{P} < 0$	$\hat{q} > 0$	$\hat{q} < 0$	$\hat{P} = 0$
V_3, V_4, V_5, V_0	V_1, V_6	V_1, V_2, V_3	V_4, V_5, V_6	V_0, V_7

For each combination of hysteresis output signals, S_P and S_q, the selected voltage vectors for sector θ_1 are shown in the following table:

Sector 01:		$\hat{q}$	
		$> 0\ SO\ S_q = 1$	$< 0\ SO\ S_q = 0$
$\hat{P}$	>0 SO $S_P=1$	V_3	V_4, V_5
	$< 0\ SO\ S_P = 0$	V_1	V_6

Sector 02:

$\hat{P} > 0$	$\hat{P} < 0$	$\hat{q} > 0$	$\hat{q} < 0$	$\hat{P} = 0$
V_3, V_4, V_5, V_0	V_1, V_2	V_2, V_3, V_4	V_1, V_5, V_6	V_0, V_7

For each combination of hysteresis output signals, S_P and S_q, the selected voltage vectors for sector θ_2, are shown in the following table:

Sector 02:		$\hat{q}$	
		$> 0\ SO\ S_q = 1$	$< 0\ SO\ S_q = 0$
$\hat{P}$	$> 0\ SO\ S_P = 1$	V_3, V_4	V_5
	$< 0\ SO\ S_P = 0$	V_2	V_1

Sector 03:

$\widehat{P} > 0$	$\widehat{P} < 0$	$\hat{q} > 0$	$\hat{q} < 0$	$\widehat{P} = 0$
V_4, V_5, V_6, V_0	V_1, V_2	V_2, V_3, V_4	V_1, V_5, V_6	V_0, V_7

The selected voltage vectors for sector $\theta_3$are shown in the following table:

Sector 03:		$\hat{q}$	
		$> 0\ SO\ S_q = 1$	$< 0\ SO\ S_q = 0$
$\widehat{P}$	$> 0\ SO\ S_P = 1$	V_4	V_5, V_6
	$< 0\ SO\ S_{P=0}$	V_2	V_1

Sector 04:

$\widehat{P} > 0$	$\widehat{P} < 0$	$\hat{q} > 0$	$\hat{q} < 0$	$\widehat{P} = 0$
V_4, V_5, V_6, V_0	V_2, V_3	V_3, V_4, V_5	V_1, V_2, V_6	V_0, V_7

The selected voltage vectors for sector θ_4 are shown in the table below:

Sector 04:		$\hat{q}$	
		$> 0\ SO\ \ S_q = 1$	$< 0\ SO\ \ S_q = 0$
$\widehat{P}$	$> 0\ SO\ S_P = 1$	V_4, V_5	V_6
	$< 0\ SO\ \ S_P = 0$	V_3	V_2

Sector 05:

$\widehat{P} > 0$	$\widehat{P} < 0$	$\hat{q} > 0$	$\hat{q} < 0$	$\widehat{P} = 0$
V_1, V_5, V_6, V_0	V_2, V_3	V_3, V_4, V_5	V_1, V_2, V_6	V_0, V_7

The selected voltage vectors for sector θ_5, are shown in the table below:

	$\hat{q}$

Sector 05:		$> 0\ SO\ \ S_q = 1$	$< 0\ SO\ \ S_q = 0$
$\widehat{P}$	$> 0\ SO\ S_P = 1$	V_5	V_6, V_1
	$< 0\ SO\ \ S_P = 0$	V_3	V_2

Sector 06:

$\widehat{P} > 0$	$\widehat{P} < 0$	$\hat{q} > 0$	$\hat{q} < 0$	$\widehat{P} = 0$
V_1, V_5, V_6, V_0	V_2, V_4	V_6, V_4, V_5	V_1, V_2, V_3	V_0, V_7

The selected voltage vectors for sector θ_6, are shown in the table below:

Sector 06:		$\hat{q}$	
		$> 0\ SO\ \ S_q = 1$	$< 0\ SO\ \ S_q = 0$
$\widehat{P}$	$> 0\ SO\ \ S_P = 1$	V_5, V_6	V_1
	$< 0\ SO\ S_P = 0$	V_4	V_3

Sector 07:

$\widehat{P} > 0$	$\widehat{P} < 0$	$\hat{q} > 0$	$\hat{q} < 0$	$\widehat{P} = 0$
V_1, V_2, V_6, V_0	V_3, V_4	V_4, V_6, V_5	V_1, V_2, V_3	V_0, V_7

The selected voltage vectors for sector θ_7, are shown in the table below:

Sector 07:		$\hat{q}$	
		$> 0\ SO\ S_q = 1$	$< 0\ SO\ \ S_q = 0$
$\widehat{P}$	$> 0\ SO\ \ S_P = 1$	V_6	V_1, V_2
	$< 0\ SO\ S_P = 0$	V_4	V_3

Sector 08:

$\hat{P} > 0$	$\hat{P} < 0$	$\hat{q} > 0$	$\hat{q} < 0$	$\hat{P} = 0$
V_1, V_2, V_6, V_0	V_5, V_4	V_1, V_5, V_6	V_2, V_3, V_4	V_0, V_7

The selected voltage vectors for sector θ_8, are shown in the table below:

Sector 08:		$\hat{q}$	
		$> 0\ SO\ S_q = 1$	$< 0\ SO\ S_q = 0$
$\hat{P}$	$> 0\ SO\ S_P = 1$	V_1, V_6	V_2
	$< 0\ SO\ S_P = 0$	V_5	V_4

Sector 09:

$\hat{P} > 0$	$\hat{P} < 0$	$\hat{q} > 0$	$\hat{q} < 0$	$\hat{P} = 0$
V_1, V_2, V_3, V_0	V_5, V_4	V_1, V_5, V_6	V_2, V_3, V_4	V_0, V_7

The selected voltage vectors for sector θ_9, are shown in the table below:

Sector 09:		$\hat{q}$	
		$> 0\ SO\ S_q = 1$	$< 0\ SO\ S_q = 0$
$\hat{P}$	$> 0\ SO\ S_P = 1$	V_1	V_3, V_2
	$< 0\ SO\ S_P = 0$	V_5	V_4

Sector 10:

$\hat{P} > 0$	$\hat{P} < 0$	$\hat{q} > 0$	$\hat{q} < 0$	$\hat{P} = 0$
V_1, V_2, V_3, V_0	V_5, V_4	V_1, V_5, V_6	V_2, V_3, V_4	V_0, V_7

The selected voltage vectors for sector θ_{10}, are shown in the table below:

	$\hat{q}$

Sector 10:		$> 0\ SO\ \ S_q = 1$	$< 0\ SO\ S_q = 0$
$\hat{P}$	$> 0\ SO\ \ S_P = 1$	V_1	V_3, V_2
	$< 0\ SO\ \ S_P = 0$	V_5	V_4

Sector 11:

$\hat{P} > 0$	$\hat{P} < 0$	$\hat{q} > 0$	$\hat{q} < 0$	$\hat{P} = 0$
V_4, V_2, V_3, V_0	V_5, V_6	V_1, V_2, V_6	V_5, V_3, V_4	V_0, V_7

The selected voltage vectors for sector θ_{11}, are shown in the table below:

Sector 11:		$\hat{q}$	
		$> 0\ donc\ S_q = 1$	$< 0\ donc\ S_q = 1$
$\hat{P}$	$> 0\ donc\ S_P = 1$	V_2	V_3, V_4
	$< 0\ donc\ S_P = 0$	V_6	V_5

Sector 12:

$\hat{P} > 0$	$\hat{P} < 0$	$\hat{q} > 0$	$\hat{q} < 0$	$\hat{P} = 0$
V_4, V_2, V_3, V_0	V_1, V_6	V_1, V_2, V_3	V_4, V_5, V_6	V_0, V_7

The selected voltage vectors for sector θ_{12}, are shown in the table below:

Sector 12:		$\hat{q}$	
		$> 0\ SO\ S_q = 1$	$< 0\ SO\ S_q = 0$
$\hat{P}$	$> 0\ SO\ S_P = 1$	V_2, V_3	V_4
	$< 0\ SO\ S_P = 0$	V_1	V_6

Bibliographic References :

[1] CHEBABI KAMILIA, «Etude d'une loi de commande en courant par hystérésis à bande adaptative pour un onduleur de tension», Mémoire de master, Université Mohamed Khider de Biskra, Dimanche 07 juillet 2019.

[2] M. SHAFIEE KHOOR, « Amélioration de la qualité de l'énergie à l'aide de compensateurs actifs : série, parallèle ou conditionneurs unifiés de réseaux électriques», Thèse de doctorat de l'école Polytechnique, Université de Nantes, Nantes, 2006.

[3] M.KAHIA BILLEL, « Commande MLI Vectorielle d'un Redresseur Triphasé à Trois Niveaux», Mémoire de Master, **U**niversité **S**étif, 2013.

[4] B. CHARIER, « La qualité de l'énergie électrique: critères et définitions », Revue de Technologie, 2009.

[5] DJAFFAR OULD ABDESL AM, «Techniques neuromimétiques pour la commande dans les systèmes électriques : application au filtrage actif parallèle dans les réseaux électriques basse tension», thèse de doctorat, Université de Haut-Alsace 08 décembre, 2005.

[6] YOUSFI ABDELKADER, « Amélioration de la qualité d'énergie électrique en utilisant un onduleur de tension à cinq niveaux», Mémoire de magister en électrotechnique, université de Chleff ,2008.

[7] V. IGNATOVA, « Méthodes d'analyse de la qualité de l'énergie électrique Application aux creux de tension et à la pollution harmonique », Thèse de Doctorat, Université de Grenoble, 2006.

[8] Amara & A. Bengana : « Etude et simulation d'un circuit de commande pour un filtre actif de puissance parallèle à deux bras à point milieu pour un réseau électrique à trois fils ». Mémoire de fin de master, Université de Tlemcen, 25 Juin 2015.

[9] M. M. ABDUSALAM, « Structures et stratégies de commande des filtres actifs parallèle et hybride avec validations expérimentales», Thèse de doctorat, Université de Nancy, France, 2008.

[10] BOUKADOUM AZIZ, « Contribution à l'étude des stratégies d'identification harmoniques et de commande basées sur les techniques avancées pour les compensateurs actifs des réseaux électriques», Thèse de doctorat, Université BADJI MOKHTAR Annaba

[11] L. ZARRI, « Control of Matrix Converters », thèse de doctorat, université de Bologne, 2010.

[12] A.MOHAMED MUFTAH, «Structures et stratégie de commande des filtres actifs parallèle et hybride avec validations expérimentales» Thèse de Doctorat, Université Henri Poincaré, Nancy-I, Mai 2008.

[13] A.BOULAHIA, « Etude des convertisseurs statique destinés à la qualité d'énergie électrique» thèse de Magistère en Electrotechnique, Université de Constantine, Avril 2009.

[14] H. MARKIEWICZ, A. KLAJN, « Caractéristiques de la tension dans les réseaux publics de Distribution, Norme EN 50160 », Université de technologie de Wroclaw, Juillet 2004.

[15] ABDELMALEK.B, «Etude des Convertisseurs Statiques destinés à la Qualité de l'Energie Electrique», mémoire de magister, Université de Constantine, 2009.

[16] KEDDARI.B et KOT.Y, «Modélisation et Simulation D'un Convertisseur AC/DC triphasé», mémoire de master, Université d'EL-Oued, 2014.

[17] A. BOUKADOUM, T. BAHI, « Compensation Harmonic Based on Fuzzy Logic Controller For Shunt Active Power Filter to improve power quality » 2nd International Conference On Electrical Energy and Systems, October 28-30, 2014, Annaba, Algeria.

[18] MEGHERBI HICHAM HAMRI SOFIANE, «Etude et modélisation des convertisseurs statiques destinés à améliorer la qualité de l'énergie électrique »,mémoire de master, Université Dr. Tahar Moulay de Saida, 2016.

[19] BELHAOUCHET NOURI, «Fonctionnement à Fréquence de Commutation Constante des Convertisseurs de Puissance en Utilisant des Techniques de Commande Avancées Application : Amélioration de la Qualité de l'Energie », Thèse doctorat, 2011, Université FERHAT ABBAS – SETIF, Algérie.

[20] N. VASQUEZ, H. RODRIGUEZ, C. HERNANDEZ, E. RODRIGUEZ AND J. ARAU, «Three-phase rectifier with active current injection and efficiency», IEEE Trans. On Industrial Electronics, vol. 56, no. 1, pp. 110-119, Jan. 2009.

[21] L. MARROYO, «Contribution à l'étude des redresseurs triphasés à absorption de courants sinusoïdaux», Thèse de docteur, Institut National Polytechnique de Toulouse (INPT), Toulouse, 1999.

[22] T. Benmilou et A. Omari, " Régulation de la tension d'alimentation du filtre actif parallèle par PI adaptatif ", 4 th International Conference on Computer Integrated Manufacturing CIP'2007, Sétif, Algérie, November 2007.

[23] Mohamed Muftah Abdusalam, "Structures et stratégies de commande des filtres actifs parallèle et hybride avec validations expérimentales", Thèse de doctorat, Université Henri Poincaré, Nancy-I, 29 mai 2008.

[24] A.BELAOURA.I.BOUSSAID, «Contrôle directe de puissance avec modulateur vectoriel (DPC_SVM) d'un redresseur PWM triphasé», Mémoire Master, Université d'Adrar, Mai 2017.

[25] A. BOUKADOUM, T. BAHI « Harmonic current suppression by shunt active power filter using fuzzy logic controller», Journal of Theoretical and Applied Information Technology , Vol. 68, N°3, pp 651-656, 2014.

[26] BOUAFIA ABDELOUAHAB, « techniques de commande prédictive et floue pour les systèmes d'électronique de puissance: application aux redresseurs a mli», Thèse de doctorat en sciences, Université Ferhat Abbas – Sétif Ufas (Algérie), 2010.

[27] BENGANA.S, «Stratégies de Contrôle Direct de Puissance d'un Redresseur PWM Triphasé», mémoire de master, Université KASDI – Ouargla, 2013.

[28] Abdelmalek. B, «Filtrage actif d'un réseau Électrique», mémoire de master, Université Mohamed Khider Biskra, 2014.

[29] L. BELHADJI, « Commande Directe de Puissance Basée sur le Flux Virtuel d'un Convertisseur AC/DC Triphasé sans Capteur de Tension » Mémoire de Magister, Ecole Militaire poly technique (EMP), Alger, 2007.

[30] M. Malinowski, M. P. Kazmierkowski, S. Hansen, F Blaabjerg, and G.D Marques, "Virtual flux based direct power controle of three-phase PWM rectifiers", IEEE Trans. Ind. Applicat, vol 37, 2001, pp. 1019–1027, July/Aug.

[31] M. Sc. Mariusz Malinowski, " Sensorless Control Strategies for Three - Phase PWM Rectifiers ", Ph.D. Thesis warsaw university of technology faculty of electrical engineering institute of control and industrial electronics. Warsaw, Poland – 2001.

[32] T. Nogochi, H. Tomoki, S. Kondo et I. Takahashi , " Direct power control of PWM converter without power-source voltage sensors ", IEEE, Mai, Juin 1998, Transactions on industry application, Vol 34, N°3

[33] Abdelouahab Bouafia , Fateh Krim , Jean-Paul Gaubert , " Design and implementation of high performance direct power control of three-phase PWM rectifier, via fuzzy and PI controller for output voltage regulation ", laboratoire d'automatique et d'informatique industrielle (LAII), ESIP, université de poitiers, france

[34] Joseph A, Shahidehpour M. Battery storage systems in electric power systems. In: Proceedings of IEEE power engineering society general meeting. 2006. p. 1–8

[35] I. Hadjipaschalis, A. Poullikkas, V. Efthimiou, Overview of current and future energy storage technologies for electric power application, Renew Sustain Energy Rev, 13 (2009), pp. 1513-1522,

[36] A. Khaligh, Z. Li, Battery, ultra capacitor, fuel cell, and hybrid energy storage systems for electric, hybrid electric, fuel cell, and plug-in hybrid electric vehicles: state of the art, IEEE Trans Veh Technol, 59 (6) (2010), pp. 2806-2814,

[37] Durr, M. Cruden, S. & McDonald, J.R. Oct 27, 2006.Dynamic model of a lead acid battery for use in a domestic fuel cell System. Journal of Power Sources, "Volume 161, Numéro 2. p 1400-1411.

[38] Paganelli, G. Guezennec, Y.G. Hansung, K. & Avra. B.2001. Battery dynamic modeling and real-timestate-of-chargeestimation in hybrid electric vehicle application. ASME International Mechanical Engineering Congress and Exposition, Proceedings, 'Volume 2, p 1101-1107.

[39] Kuhn, E., Forgez. C. Lagonotte, P & Friedrich, G. Aug 25, 2006. Modelling Ni-Mh battery using Cauer and Foster structures. Journal of PoM'er Sources. "Volume 158, Numéro 2, p 1490- 1497.

[40] Mauracher, P. & Karden. E.1997.Dynamic modelling of lead-acid batteries using impédance spectroscopy for parameter idenficatton. Journal of Power Source, Volume 67, p 69-84.

[41] Shepherd. C.M.July, 1965.Design of Primary and Secondary Cells - Part 2. An équation describing battery discharge. Journal of Electrochemical Society. Volume 112.p 657-664.

[42] Piller S., Perrin M., Jossen A. June 2001.Methods for state-of-charge détermination and their applications. Journal of Power Sources, Volume 96, Numéro 1, p 113-120.

[43] Feng Pei, Kegang Zhao, Yutao Luo & Xiangdong Huang. June 21 - 23, 2006. Battery Variable Current-discharge Résistance Characteristics and State of Charge Estimation of Electric Vehicle, Proceedings of the 6th World Congress on Intelligent Control and Automation, Dalian, China

Résumé :

Dans ce travail, nous avons étudié une la modélisation et la simulation d'un redresseur PWM connecté à une batterie, la régulation de la tension du bus continu de sortie à l'aide d'un régulateur PI, dont l'objectif est de diminuer les distordions harmoniques à l'entrée et par conséquent obtenir des courants sinusoïdaux à l'entré du convertisseur avec un zéro de consommation de la puissance réactive, ce qui permet d'améliorer le facteur de puissance de la source d'alimentation. La commande de ce convertisseur est assurée par des différentes techniques telles que la commande hystérésis et la commande DPC. La batterie est présentée avec différentes modèles et en suite connectée avec un redresseur à MLI à commande DPC qui peuvent être utilisée pour un système de chargement des véhicules électriques et des énergies renouvelables. Les performances et les caractéristiques de la batterie sont présentées et interprétés pour les deux cas chargement et déchargement de la batterie. Les résultats de simulation sous Matlab/Simulink montrent que le redresseur fonctionnant à un facteur de puissance unitaire et permet de fournir une tension continue stable et des courants sinusoïdaux à l'entré du convertisseur avec un faible THD.

Mots clés :

Redresseur a MLI, commande hystérésis, Commande DPC, régulateur PI, batterie, chargement, performances.

Abstract :

In this work, we studied the modeling and simulation of a PWM rectifier connected to a battery, the regulation of the output DC bus voltage using a PI controller, the objective of this work is to reduce harmonic distortions at the input and to obtain sinusoidal input currents with zero consumption of reactive power, which improves the power factor of the power source. The control of the converter is provided by different techniques such as hysteresis and DPC controls. The battery is presented with different models and then connected with a PWM rectifier using DPC control that can be used for a charging system for electric vehicles and renewable energies. Battery performance and characteristics are presented and interpreted for charging and discharging battery cases. The simulation results under Matlab / Simulink show that the PWM rectifier operating at a unit power factor and can provide a stable DC voltage and sinusoidal input currents at with a low THD.

Keywords:

PWM rectifier; hysteresis control; DPC control; PI controller; battery; charging; performances.